CHALMERS

Rate-dependent response of excavations in soft clays

JOHANNES TORNBORG

TECHNICAL REPORT FOR MID-TERM SEMINAR

Rate-dependent response of excavations in soft clays

JOHANNES TORNBORG

Rate-dependent response of excavations in soft clays
JOHANNES TORNBORG

Cover:
Excavation works at the instrumented site, a part of the Hisings bridge project in Gothenburg. Photo from Skanska's drone on 2019-06-26.

Rate-dependent response of excavations in soft clays

Technical report for mid-term seminar
JOHANNES TORNBORG
Department of Architecture and Civil Engineering
Division of Geology and Geotechnics
Chalmers University of Technology

ABSTRACT

The stress state of the soil influences the actions against underground structures. As unloading in the form of excavations in soft clay may significantly affect the stress state, it is crucial to consider the impact of the construction phase (short-term) on the long-term response and permanent structure. The aim of this report is to study the rate-dependent response of excavations in soft clay and its impact on the actions against underground structures. Hence measurement data from a previous excavation in soft clay have been revisited in order to benchmark a constitutive soil model for studies of excavation problems. Additionally, new measurements have been carried out to study the development of earth pressures under a permanent structure in soft clay.

The validation of the constitutive soil model was performed against measurement data from a well instrumented cross section of the Göta Tunnel excavation in Gothenburg. This part of the study validates the Creep-SCLAY1S model for simulation of excavations. In particular the model enables predictions of the short- and long-term performance in areas with on-going background creep settlements, as the model incorporates the viscous, rate-dependent, behaviour of soft clay.

Additionally, a construction site with soft sensitive clay was selected in order to study the development of earth pressures under a permanent structure. An extensive laboratory testing program was conducted for soil characterisation. The instrumentation of the excavation comprised inclinometers, bellow-hose, piezometers in addition to an extensometer and total pressure cells beneath the slab. Total pressure cells were installed to measure both the vertical and horizontal stresses. The pouring of the wet concrete for the slab provided an indication of a satisfactory performance of the sensors installed in the clay under the slab. Measurement data so far show, for example, that the stress path in the centreline of the excavation approximately follow the relationship of horizontal to vertical effective stresses according to Schmidt (1966). Also, the increase in vertical effective stresses after casting of the slab indicate an upwards effective (heave) pressure in the order of magnitude 0.2-0.3 times the in-situ vertical effective stress at foundation level (before excavation works). The on-going measurements are indented for long-term monitoring and are considered to add valuable and novel data on the rate-dependent response and influence of excavations on the permanent structure.

Keywords: soft clay, excavations, rate-dependency, instrumentation, heave, earth pressure, numerical modelling.

Preface

The work presented in this report was carried out at the Geotechnical research group at Chalmers University of Technology. First of all, I would like to thank my main supervisor Professor Minna Karstunen, co-supervisor Mats Karlsson and industry supervisor Anders Kullingsjö for their great guidance, teaching and continuous support during this work. I am also grateful to Professor Jelke Dijkstra at Chalmers for providing great knowledge, discussions and feedback on instrumentation and scope of work throughout the project. The technicians at Chalmers geotechnical laboratory, Georgios Birmpilis and Anders Karlsson, enabled the work thanks to their support and knowledge during laboratory testing and preparations for the field instrumentation. Jorge Yannie and Anders Bergström at NCC put forward the data logger for the field monitoring, in addition to continuous encouragement and support, for that I am very grateful. I would like to thank all my colleagues at Chalmers and Skanska's geotechnical groups for their support and friendship. In short, it is a privilege to work with people who share the same interest and passion for geotechnical engineering and soft soils.

I would also like to thank Skanska for generous financial support and practical assistance during measurements and installations of sensors in the field. It has been a good learning experience and great fun to work along with the crew at the Hisings Bridge site. The topic of rate-dependent response of excavations and its impact on the permanent structure was raised in 2015, during Skanska's tender design for a major infrastructure project in Gothenburg. The idea for the prestudy to this research project was raised by Sven Liedberg together with Torbjörn Edstam and Anders Kullingsjö (all at Skanska). I am grateful for having these people as my colleagues and being able to define the project idea for this research project together with them.

A reference group have been supporting the work continuously and for that I am grateful. During our meetings there are always some important aspects or questions put on the table. I would especially like to express my gratitude to Professor Claes Alén, Leif Jendeby and Tara Wood for their support and encouragement in this project as well as during the prestudy. For discussions on various geotechnical aspects I have turned to Professor Göran Sällfors throughout my "geotechnical lifetime" and his teaching and our discussions always brings me great value.

Last, and most importantly, I want to thank my family Maja and Ella for their love and patience throughout this work.

Nomenclature

Abbreviations

CAD	Anisotropically consolidated drained triaxial test
CAU	Anisotropically consolidated undrained triaxial test
CF	Calibration factor
CFT_{cell}	Total pressure cell body temperature correction factor
CFT_{vw}	VW sensor temperature correction factor (piezometers and total pressure cells)
CID	Isotropically consolidated drained triaxial test
CRS	Constant rate of strain oedometer test
DSS	Direct simple shear test
EHP	Effective heave pressure
EOP	End of primary consolidation
FoS	Factor of safety
GWL	Ground water level
IL	Incremental loading oedometer test
k, k_0	Permeability, in-situ permeability
OCR	Overconsolidation ratio
OCR^*	Isotropic overconsolidation ratio
SPW	Sheet pile wall

Greek symbols

β_k	Permeability change index $= \Delta \log k / \Delta \varepsilon$
Δu	Excess pore water pressure
$\dot{\varepsilon}$	Strain rate
ν'_0	Poisson's ratio for drained small strain stress increment
ϕ'	Friction angle
ϕ'_{cs}	Critical state friction angle
$\sigma'_{v,ehp}$	Effective heave pressure
$\sigma'_{v0}, \sigma'_{h0}$	Initial vertical and horizontal effective stress
$\sigma'_{vc}, \sigma'_{hc}$	Vertical and horizontal preconsolidation pressure
τ	Shear stress
ε	Strain (engineering strain $= \Delta l / l_0$)

Roman letters

C_α	Creep index
C_c	Compression index
C_k	Permeability change index $= \Delta e / \Delta \log k$
C_p	Preconsolidation index
C_r	Re-compression index
c_u	Undrained shear strength
c_v, c_h	Coefficient of consolidation in vertical and horizontal direction
$c_{u,corr.}$	Undrained shear strength corrected w.r.t. liquid limit
e_0	Initial void ratio
I_p	Plasticity index
K	Specific permeability
k	Permeability (hydraulic conductivity)
K_0	Coefficient of earth pressure $= \sigma'_h / \sigma'_v$
$K_0^{in-situ}$	Coefficient of earth pressure at rest in-situ
K_0^{nc}	Coefficient of earth pressure during primary loading
K_0^{yield}	Ratio of horizontal and vertical preconsolidation pressures
M_{ul}	Unloading modulus
N	Stability number

N_c	Critical stability number		stress
N_{cb}	Critical stability number w.r.t. bottom heave	p'_m	Equivalent (isotropic) mean effective preconsolidation stress
p'	Mean effective stress	w_L	Liquid limit
p'_0	Initial mean effective stress	w_N	Natural water content
p'_{eq}	Equivalent (isotropic) mean effective	w_P	Plastic limit

Contents

List of Figures

List of Tables

1 Introduction

1.1 Background & Motivation

The transition into sustainable development requires a shift to sustainable transportation systems, relating to UN sustainable development goals (SDGs) 9 and 11 (UN 2020). Such transportation systems may include railway transportation, which is in urban areas most often placed underground to accommodate for land-use and recreational areas above ground. Examples of some major infrastructure projects can be found in Boston (Central Artery/Tunnel Project "Big Dig"), Oslo (Bjørvika Tunnel), Los Angeles (Regional Connector project), Gothenburg (Göta Tunnel). Also, due to climate change stressors, such as e.g. increased rainfall intensity, there is an increased necessity for underground infrastructure systems such as e.g. storm water retention systems in order to achieve resilient cities (part of UN SDG 11).

As cities expand, the depth and extent of excavations and underground structures in urban areas will likely increase. Associated with the increase in depth and extent of excavations in urban areas, there are strict regulations for the allowable deformations to the (often historic) surroundings and existing infrastructure. However, minimising the deformations during the construction phase not only affects the earth pressures in the short-term, but also may affect the long-term earth pressures against the permanent structures (e.g. Carder and Darley 1998; Richards et al. 2007). Therefore, as limits are extended and strict regulations on deformations are imposed, reliable predictions of e.g. earth pressures acting on retaining and underground structures are needed both for the construction period (short-term) as well as the long-term (the design lifetime of underground structures in Sweden typically being 100-120 years). The predictions need to consider relevant features of soil behaviour, e.g. by numerical analyses, incorporating advanced constitutive soil models fit for the purpose. Failure to do so may not only result in overdesign and additional monetary or environmental impact of the construction itself, but conversely potentially in failure (exemplified by e.g. Magnus et al. 2005). Research is thus required to develop and verify new, adequate, methods for reliable predictions of actions on underground structures, and possibly review existing calculation methods and guidelines. Knowledge and reliable predictions leads to optimisation of structures as uncertainties are reduced. This further aids the transition to sustainable development and supports the Swedish construction industry in reaching the goal of net zero greenhouse gas emissions in 2045 (Fossil Free Sweden 2020).

During excavation and foundation works changes in the effective stress state in the soil will occur. Due to the hydro-mechanical properties of soft soil, the changes of effective stresses are rate-dependent[1] and may develop under a considerable amount of time in low permeable clays. Moreover, the rate-dependent response of soft clay is effected by the viscous nature of the material, and the estimations of long-term deformations and

---

[1]In this report rate-dependent is referring to effects of consolidation as well as viscous material behaviour. Rate-dependent is used since imposed loading rate (e.g. excavation rate) is affecting both the development and dissipation of excess pore pressures (consolidation) as well as the viscous response (e.g. resulting in creep settlements).

earth pressures against structures therefore need to consider effects of for example on-going background creep settlements. However, current practice in geotechnical design of excavations in soft Swedish clays, is in general based on undrained analyses. Such analyses are characterised by the use of a fixed value for the undrained shear strength, which except for short-term situations will be non-conservative for excavation problems. The rate-dependent, transient, response is rarely incorporated into design, and thus only the theoretical limiting cases of undrained or drained are considered in practice (Fredriksson et al. 2018).

Arising from a pre-study that looked into heave pressure in soft clay, and an identified industry need to study the short- and long-term earth pressures, e.g. by taking the time of construction and background creep into account, this thesis will focus on rate-dependent response on the forces acting upon permanent structures in soft clay. Considering that 1) the construction industry is extending the limits for excavation depths and proximity to existing structures and 2) the impact of rate-dependent response of excavations in clay (combination of consolidation process and viscous rate-dependent behaviour of soft clay) is not fully analysed and at best rudimentary accounted for in design practice - the following general questions were raised when initiating this research project:

- What is the magnitude of earth pressures (horizontal and vertical) acting against underground structures and how do they vary over the design lifetime of the structure?
- What are the governing factors that influence these earth pressures in the transient state? That is during the construction period and over the design lifetime.
- Are the current semi-empirical design guidelines applicable when the excavation and foundation depths exceed previous maximum depths of approximately 10 m in Swedish soft clay? Is there a need to update the guidelines to avoid failures or design based on over conservative simplified assumptions?

The research is motivated in order to develop and possibly review existing calculation methods and guidelines. This in order to maintain safety and optimisation as society and industry is pushing the limits for underground structures into "new" territory. Furthermore, optimisation is becoming increasingly important in order to build cost-effective construction works with minimised environmental impact.

This report presents the results of a case study of an excavation in soft clay (Göta Tunnel) that was extensively instrumented over a period of ca 3 years during the construction stage. Also presented is the setup and instrumentation for new field measurements, performed in order to study both the short- and long-term response of earth pressures under a permanent structure in soft clay. Vertical and horizontal earth pressures, as well as pore pressures, have been measured under the concrete slab in addition to the relative displacements of the clay-slab interface.

1.2 Aims and objectives

The aim of this project is to study the rate-dependent response of excavations in soft clay, and the resulting impact this has on the earth pressures forming against the permanent underground structure over time. The main objectives that together comprise the scope of work for this mid-term report are:

- Review of previous research related to rate-dependent response of excavations in soft clay, including previous measurements of vertical and horizontal earth pressures against underground structures.
- Identify relevant previous projects and perform case study analyses on well documented excavation(s) in soft clay. The purpose being benchmark a material model, that accounts for rate-dependent response, against the soil-structure response at field scale.
- Identify and select site for instrumentation and long-term monitoring of earth pressures. Carry out site characterisation (sampling and laboratory testing, analyses of e.g. InSAR satellite data).
- Design field monitoring programme. Carry out field measurements on site, including installation of sensors in the clay for automatic data collection.
- Collect, compile and present the monitoring data, including qualitative interpretation of results.

1.3 Research questions

The following questions were raised during the pre-study phase (initiation) of this project:

- How do the effective stresses in the soil develop during the construction and design lifetime?
- How do the horizontal earth pressures develop with time against the underground structure?
- What is the effect of rate-dependency on the emerging soil strength? Normally design is carried out for the (theoretical) extreme cases of undrained and/or drained analysis. Rate-dependent analysis, taking the transient processes into account, can possibly result in optimisation of the retaining as well as the permanent structure.
- Will effective heave pressures ("locked-in" heave) develop against structures in the short- and/or long-term due to the rate-dependent response of excavations?
- How do the excavation and/or underground structure effect the settlements in adjacent ground and structures in the long-term?
- How do on-going background creep settlements influence the questions raised above?

1.4 Limitations

Initially, three Swedish projects were identified for case study analyses. These were the excavations for Göta and Marieholm Tunnels in Gothenburg, and an excavation including

the installation and monitoring of a permanent sheet pile wall in Uppsala. Within the scope of this mid-term report it was decided to limit the analyses to the case of Göta Tunnel. Geotechnical site characterisation reports and measurement data (spanning from 2015 up to this date) have been collected for the Uppsala project. However, these results will be reported in a forthcoming separate report.

The work in this report does not incorporate studies on the effects of expansive clays. Thus, this study is limited to and focused on the potential change in the material properties and the response of clays due to pure unloading effects. Hence, the following mechanisms (as discussed by e.g. Leroueil 2001) are not included: destructuration and swelling caused by drying-wetting cycles or expansive clay minerals, as well as the change in the pore-water composition, for example decrease in salinity in marine clays.

The design of underground structures in practice requires competence from Geotechnical as well as Structural Engineering. This mid-term report focuses on the rate-dependent response of soft clays in excavation problems and the resulting earth pressures on underground structures. The load-deformation response (stiffness) of the permanent underground structure itself will not be studied in detail at this stage, and have hence been implemented in the analyses in a rudimentary manner (such as e.g. linear-elastic material).

1.5   Outline of the report

The outline of the report is presented below:

- Chapter 2: *Excavations in soft clays - a literature review.* Covering the general background related to excavations and retaining structures. Also, aspects of soil behaviour related to excavations in soft sensitive clay is reviewed. Previous studies and field measurements are reviewed focusing on long-term measurements of earth pressures. A description of the constitutive soil model Creep-SCLAY1S model, used for numerical modelling, is included. Finally, the initial research questions are revisited in light of the literature review.
- Chapter 3: *Case study analyses of a deep excavation, Göta Tunnel J2.* Measurement data from an extensively instrumented and well documented section of the Göta Tunnel excavation are revisited. The motivation being to benchmark the Creep-SCLAY1S model for further studies and design of excavations.
- Chapter 4: *Instrumented site: conditions, soil properties and sensor installation.* Description and characterisation of site that have been instrumented primarily for long-term monitoring of earth pressures. Experimental methodology is explained as well as detailed methodology for installation of sensors in the field.
- Chapter 5: *Instrumented site: results and discussion.* Presentation and analyses of monitoring data of key results such as e.g. vertical and horizontal effective stresses under the permanent structure at the site. Preliminary comparison of measured vertical effective stresses and numerical model simulations.
- Chapter 6: *Conclusions and recommendations for future work.*

2 Excavations in soft clays - a literature review

This chapter consists of a literature review which is divided into four main sections. The first section covers a general description of earth retaining structures, and some previous major studies that lead to the development of semi-empirical design procedures. The first section also includes a short description of the background to the design procedures in Swedish guidelines. The second section discusses soil behaviour related to excavations and underground structures in soft clay. The third section presents a review of previous field measurements of earth pressures. The fourth section includes a brief description of the Creep-SCLAY1S constitutive soil model. Finally, the chapter includes a review of the research questions with respect to the literature review as well as an outlook for additional research.

2.1 Retaining structures; semi-empirical methods and design principles

2.1.1 Introduction to retaining structures in soft clays

Numerous options are available regarding the choice of retaining structures for the design of excavations in soft clay. As the depth and extent of excavations increase in urban areas, construction work measures will have to adopt in order to maintain a set safety level and minimise deformations. Some design options related to retaining and permanent underground structures and measures which can be taken for optimisation are:

- Intended use of retaining wall: for excavation stage only and/or part of the permanent structure.
- Material and type of retaining wall: e.g. steel sheet pile profiles, combined walls, cast in place walls (diapraghm walls) or piles (secant piles), soldier-pile walls, interlocked large diameter pipes.
- Support of retaining structure: e.g. struts or tie-back anchors.
- Construction process: top-down or bottom-up methods, underwater excavation, sequential excavation and casting of working platform and/or ground improvement by deep mixing (e.g. lime-cement columns) or jet-grouting.

For a more complete description of wall and bracing systems, refer to e.g. Fang (1991).

The interaction of soil and structural behaviour on the overall performance of underground structures can be illustrated as e.g. in Figure 2.1. This figure highlights the importance of considering both soil behaviour (creep and relaxation, which are both arising from the viscous response of clay) as well as structural stiffness.
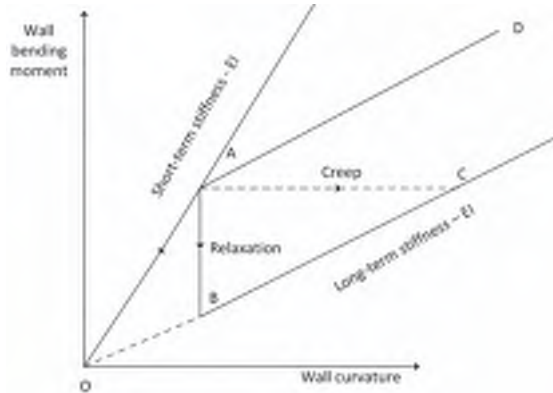
Figure 2.1: *Example of soil-structure interaction. From CIRIA guidelines (Gaba, Hardy, et al. 2017). Path OA idealises the short-term response. Path AB and AC idealise stress relaxation (constant strain) and creep (constant effective stress), respectively, under structural degradation to long-term stiffness. Path AD idealises no creep or relaxation, only change in structural stiffness considered.*

2.1.2 Factors affecting the response of earth retaining and underground structures

As fundamental it is to comply to the concept of safety for the design of excavations, deep excavations in urban areas, in close proximity to existing infrastructure, are also imposed with strict regulations on the allowable deformations. Consequently, special assessments are required regarding how such restrictions effect the earth pressures acting on the retaining structures in the short-term, as well as the long-term (including the permanent structure). The increase in the forces acting on the retaining system, and the support measures needed for deep excavations in urban areas is thus most likely not linearly correlated with the excavation depth. In fact, a number of factors may influence (Gebreselassie 2003) the short- and long-term earth pressures as illustrated in Figure 2.2.
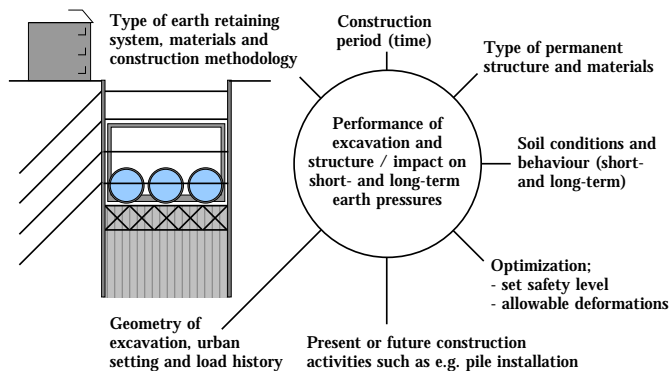
Figure 2.2: *Factors that may influence short- and long-term earth pressures against earth retaining and permanent structures in urban areas. Inspired by Gebreselassie (2003).*

2.1.3   Classical analysis of limiting earth pressures

This section and section 2.1.4 review the development of analytical and semi-empirical methods for estimation of earth pressures.

Methods for calculation of earth pressure against retaining structures were originally developed by Coulomb (1776) and Rankine (1857). Rankine assumed the soil behind the wall to be in plastic equilibrium, thus the Rankine active and passive earth pressure coefficients (eqs. 2.1), relating vertical stresses to horizontal stresses, are limiting values at failure according to:

$$\left. \begin{aligned} K_a &= \frac{1 - sin\phi'}{1 + sin\phi'} = \tan^2(45° - \phi'/2) \\ K_p &= \frac{1 + sin\phi'}{1 - sin\phi'} = \tan^2(45° + \phi'/2) \end{aligned} \right\} \tag{2.1}$$

where K_a and K_p are Rankine's active and passive earth pressure coefficients and ϕ' friction angle of the soil. For an ideal purely cohesive soil with undrained shear strength, c_u, ($\phi'=0$) the active and passive earth pressures at a depth H below ground surface corresponds to (Terzaghi 1943):

$$\left. \begin{aligned} \sigma_a &= \gamma H - 2c_u \\ \sigma_p &= \gamma H + 2c_u \end{aligned} \right\} \tag{2.2}$$

As stressed in the previous section, the earth pressures that mobilise against a structure will depend, among others, on the relative movements and the interaction of the structure and the soil. This was discussed by Terzaghi (1936), even suggesting that the earth pressure theory by Rankine should be "discontinued" since it did not consider the stress-strain dependence of soil behaviour, as illustrated in Figure 2.3. From the figure it is clear that the level and direction of strain greatly influence the mobilising earth pressures on both sides of a retaining structure.
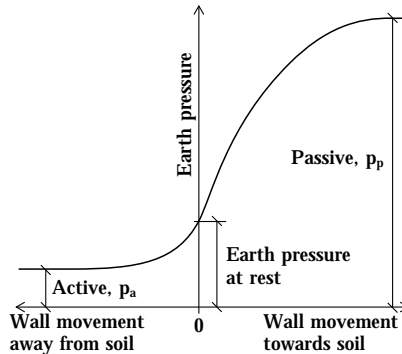
Figure 2.3: *Earth pressure as a function of relative movement of soil and wall (after Janbu et al. 1956).*

Terzaghi (1936) noted that: 1) the lateral movement required to obtain the reduction from lateral earth pressure at rest to active Rankine state (or increase to passive) earth pressure could be calculated from the relation between stress and strain in the soil, and 2) to mobilise a theoretical limiting pressure distribution against the back of a retaining structure require a certain minimum strain (potentially caused by yielding of the earth retaining structure) and 3) the practical importance of considering non-hydrostatic lateral earth pressure distributions for earth retaining structures with limited yielding. The aspect of potential non-hydrostatical earth pressure was described further in the work by Terzaghi (1943). However, the knowledge of actual earth pressure distributions behind retaining walls were lacking at the time. Terzaghi therefore suggested that the effect of non-hydrostatic pressure should be estimated based on empirical knowledge, as described in Section 2.1.4.

2.1.4 Semi-empirical earth pressure diagrams for computation of strut loads

In order to take the stress-strain dependency of soil behaviour into account in the development of earth pressures, semi-empirical methods were developed in the 1940s in order to estimate the earth pressures for computation of strut loads in braced excavations. Semi-empirical is here referred to as the use of measurement data of earth pressures and strut loads to correct or improve underlying theoretical assumptions. For example, Terzaghi, Peck, and Mesri (1996) (3rd edition, 1st edition in 1948) presented so called apparent lateral earth pressure diagrams based in part of field measurements on the excavation for the Chicago subway, as described and summarised by Peck (1943). The data on earth pressures at the time was mostly inferred from measurements of strut loads, since direct measurements of earth pressures against retaining walls were scarce. It should also be noted that the values obtained through strut forces thus reflect the values that would be obtained for tie-back walls *without* pre-stressing. Some apparent earth pressure diagrams given by various authors are summarised in Table 2.1.

It should be noted that Peck (1969) emphasised that the apparent earth pressure diagrams do not represent real distribution of earth pressures. They were intended to be used for computation of the maximum strut loads, this was the reason referring to these artificial pressure diagrams as the *apparent* earth pressures.

Based on additional measurement data e.g. from the Oslo subway excavations, Peck (1969) in a state-of-the art report concluded that the response of the soil retaining structure depended on a stability number, $N=\gamma H/s_u$, of an excavation (at different stages), upon which recommendations were presented for the value of a correction factor, m (see Table 2.1). As an example, for $N>6$ $m=1$ if a stiff layer is located near the excavation bottom, and $m=0.4$ if the depth to firm bottom is large. It should be noted that N according to Peck should be estimated based on a s_u representative of a general failure of the excavation, i.e. an average s_u for a soil volume beside and below the excavation. Therefore, N becomes a measure of the degree of mobilisation of the entire soil volume involved around the excavation. By using N as a measure, Peck took into account the degree of mobilisation for the estimation of strut loads in a way that today commonly is accounted for using

Table 2.1: Examples of empirical apparent lateral earth pressure diagrams for estimation of strut loads for braced excavations in clays.

Reference and notes	Apparent earth pressure
Peck (1943) for clays K_a=1.2(1-2$q_a/\gamma_a H$) where q_a=0.75q_c, q_c specified as the average unconfined compression strength of the clay (i.e. 2c_u) and γ_a the average unit weight, both from surface to depth H. The factor 1.2 was designated in order to account for scatter in the measurement data. Beside of this factor, the coefficient for K_a thus represented the Rankine equation for active earth pressure in clay (ϕ'=0).	
Tschebotarioff (1951) for stiff clay, for soft clay d=0. Author considered apparent earth pressure to be derived based on at rest earth pressures, therefore specified K_γ=0.5.	
Terzaghi and Peck (1967) (2nd edition) for soft-medium clays. K_a=1-m4$s_u/\gamma H$, s_u specified as the average undrained shearing resistance of the clay and γ the average unit weight, both from surface to depth H. m is a reduction factor depending on the stability number of the excavation or rather excavation stage, $N=\gamma H/s_u$. Peck (1969) gave revised recommendations on m-values.	
Karlsrud and Andresen (2005) results from parametric finite element analyses of excavation in soft clay illustrating the effect of factor of safety (FoS) against bottom heave failure on apparent earth pressure diagram. FoS for case A1, A2, A3 specified as 0.93, 1.10 and 1.30 resulting (only) from varying the undrained shear strength.	
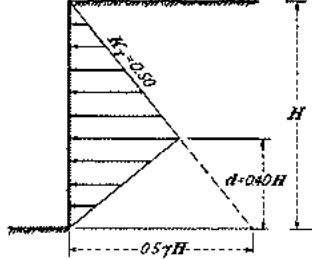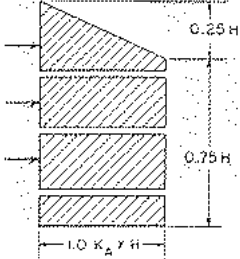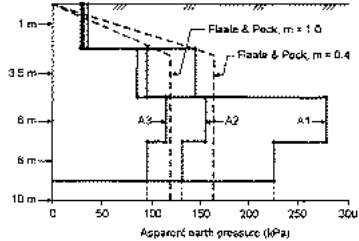
FE analysis. This becomes increasingly important as the restrictions on deformations around excavations increase, and thereby the earth pressures are more in the working range of earth pressures at rest, rather than the limiting extreme active and passive earth pressures.

The method of estimating strut loads based on the stability number of an excavation (at various stages) was studied further by Stille (1976), who conducted studies of failures of anchored sheet pile walls in Sweden. The results in 1979 became the basis for guidelines for the design of sheet pile walls in Sweden (Sahlström and Stille 1979, *Förankrade sponter*).

2.1.5   Bottom heave stability

This section briefly covers methods to estimate the safety against bottom heave failure. For clarification, notations of the stability number, N, used in this report are given below as in line with notations used by Peck 1969.

- N: stability number based on the undrained shear strength of clay representative for the clay beside and below the excavation bottom (as defined by Peck (1969) for estimation of apparent earth pressures).
- N_b: stability number based on the undrained shear strength representative in "a zone underneath and immediately around the bottom of the excavation" as defined by Bjerrum and Eide (1956) in order to estimate the FoS against bottom heave failure.
- N_{cb}: critical stability number associated with bottom heave failure. Bjerrum and Eide (1956) used N_c as notation, the sub-script $_b$ is added here as in Peck (1969) for clarification, i.e. that it refers to a failure involving the soil below excavation level.

A method for calculating the stability of excavations was presented by Terzaghi (1943). The bearing capacity was considered at a plane equal to the excavation level. The bearing capacity was given as $q_f=5.7s_u$. The weight on the plane was reduced by the shear strength along the vertical plane extending from excavation level to the ground surface. Bjerrum and Eide (1956) found, based on test shafts and observed (partial and full) bottom heave failures arising during excavations for the Oslo subway, that the FoS against bottom heave failure according to Terzaghi's method was overestimated for deep excavations. They realised that for deep excavations, the shear strength from excavation level all the way to ground surface may not be fully mobilised, if the bottom heave failure initialises below excavation bottom. An illustration of such varying strain mobilisation is presented in Figure 2.4.

Therefore, Bjerrum and Eide (1956) looked at the analogous problem of calculation of the bearing capacity of foundations, which also enabled including the effect of the geometry of the excavation. Based on work by Skempton 1951, they proposed the critical depth with respect to bottom heave of an excavation, D_c, to be calculated as:

$$D_c = N_{cb}c_u/\gamma \tag{2.3}$$
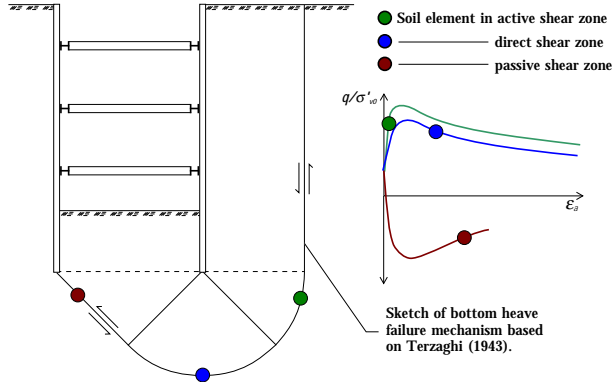
Figure 2.4: *Illustration of degree of mobilisation and importance of anisotropy and post-peak strain softening in deep excavations. Inspired by Bjerrum and Eide (1956), Aas (1984) and Wood (1990).*

where N_{cb} is critical stability number associated with bottom heave failure, c_u is undrained shear strength representative of "a zone underneath and immediately around the bottom of the excavation" and γ is the average unit weight of the soil above excavation level. The effect of wall embedment below excavation level was not included in this approach.

The Bjerrum and Eide (1956) diagram for the dimensionless N_{cb} factor and their equation for calculation of FoS is presented in Figure 2.5. This diagram is still used today in Sweden for the design of sheet pile walls in clay. It should be noted that the critical width, B, must be iterated, if the shear strength increases with depth, i.e. the average shear strength within a failure surface involving a smaller soil volume may decrease faster than the corresponding increase in $N_c b$. This was highlighted in a case study by Aas (1984), whom also exemplified the importance of considering the anisotropy in shear strength for the estimation of bottom heave failure.
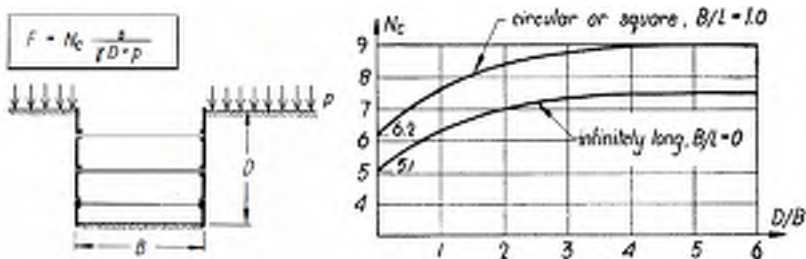
Figure 2.5: *Critical stability number, N_{cb}, associated with bottom heave failure. From Bjerrum and Eide (1956). Note: denoted N_c in the figure but in this report referred to as N_{cb} in line with Peck (1969).*

Bjerrum and Eide (1956) did not take into account the effect of time (or rather the viscous behaviour of clay), and later Bjerrum (1973) stated that the method from 1956 should

be corrected for rate effects in clays of medium and high plasticity, using the correction factors to vane strengths as proposed in his paper.

Following the work by Bjerrum and Eide, the effects of including for example the embedment depth and the wall stiffness on N_{cb}, as well as ground movements, have been studied by means of FE analyses adopting various constitutive soil models (e.g. Goh 1994; Hashash and Whittle 1996; Faheem et al. 2004).

2.1.6 Empirical estimations of deformations and pore pressure change

In addition to the safety concept and the estimation of structural forces, a major focus in the design of excavations concerns assessment of the ground movements. Peck (1969) presented empirical charts for the estimation of ground movements as a function of the excavation depth and distance from the excavation. The diagram, presented in Figure 2.6, was included in the Swedish guidelines for design of sheet pile walls (Sahlström and Stille 1979) and is still so today (Fredriksson et al. 2018). In a comprehensive database
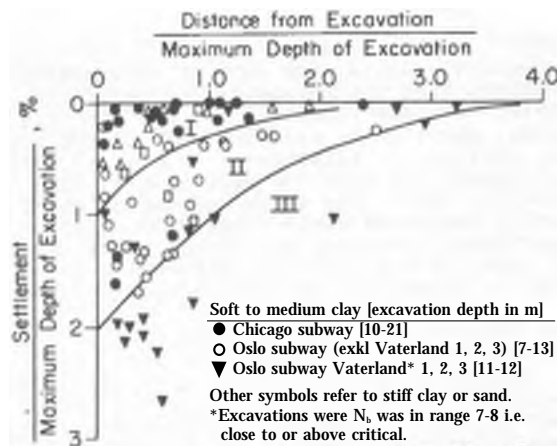
Figure 2.6: *Measurements of settlements adjacent to excavations. From Peck (1969). Zone I: Sand and soft to hard clay. Zone II: Very soft to soft clay with either limited depth of clay below bottom of excavation or $N_b < N_{cb}$. Zone III: very soft to soft clay extending to a significant depth below bottom and $N \geq N_{cb}$.*

compiled by Long (2001), containing 296 case studies, charts of measured settlements and lateral deflections of retaining structures were presented. For excavations with soft soil at the excavation level and a high factor of safety versus bottom heave failure, the trend of the data suggested decreasing movement for increasing excavation depth. The explanation given was that there is greater degree of control and workmanship in projects involving deep excavations. No major differences between anchored or propped excavations were found. Although it should be noted that the majority of the case records were propped walls and the comparison relating to anchored or propped is therefore rather

unrepresentative. The measured settlement and lateral movements in general were in the order of 1-2 % of the excavation depth for excavation depths up to 15 m, and 1 % for excavation depths >15 m (maximum 26 m). Excavations with a low FoS versus bottom heave failure were distinguished, see Figure 2.7. A database of 300 case histories (Wang
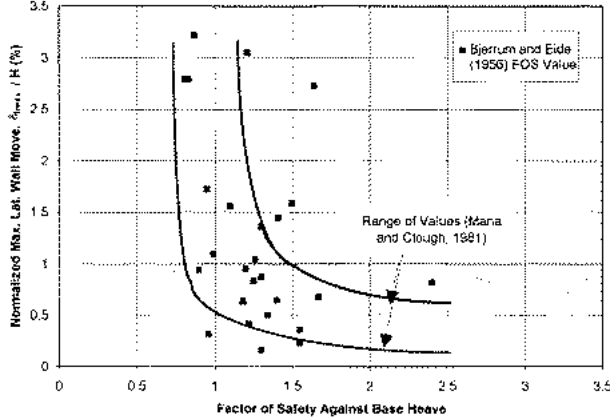
Figure 2.7: *Measurements of settlements and lateral wall deflections for excavations with low FoS against bottom heave failure (back-calculated by method of Bjerrum and Eide (1956)). From Long (2001).*

et al. 2010) of 3-25 m deep excavations in Shanghai (incorporating soft, silty and stiff clay layers) presented values of lateral wall movements over excavation depth, δ_{max}/H, of 0.1-0.6 % (top-down method), 0.1-1 % (bottom-up method including D-walls, pile walls and reinforced soil walls), 0.3-3 % (SPWs). Furthermore, a study of 18 excavations (depth 7-20 m in soft to medium stiff clay) in Vietnam (Hung and Phienwej 2016), δ_{max}/H ranged from 1-2.4 % for SPWs and bored pile walls and 0.15-1 % for D-walls. Thus, the stiffness of the retaining structure also affects the results.

2.1.6.1 Empirical estimations of heave

Relating to heave observed in excavation, Bjerrum (1973) reproduced an equation (based on previous work by Steinbrenner) in order to estimate the elastic heave (i.e. initial heave, immediately after excavation not including consolidation) in the centreline of an excavation. The equation is analogous to that of the immediate settlement of a loaded area (as described in 1934 by Steinbrenner and Terzaghi (1943)). An influence factor, I, was introduced to be dependent on the geometry of the excavation and the depth of the clay deposit.

$$\delta_h = qb\frac{1 - \nu^2}{E}I \tag{2.4}$$

where q is the total stress change, b the width of the excavation, ν Poisson's ratio, E Youngs modulus. Analogous to Steinbrenner $I = \Delta\sigma/q$, or in other words, the portion of q that results in immediate heave. Bjerrum described two case records of measured heave in shallow excavations, using E varying from 500-1000c_u for approximate match

13

(I and ν were not specified). The observed immediate heave ranged from 1.0-2.8 % of the excavation depths (2.25-3.0 m). In a large excavation in London clay (Simpson and Vardanega 2014), generalised the immediate heave during each excavation stage to 1 % (40 mm heave concentrated to 4 m depth below each excavation stage level). They further concluded that, owing to the relatively small lateral wall movements, it was mostly an effect of volumetric expansion of the clay. For a number of case studies of excavations in soft clay, Magnusson (1975), found that heave was primarily caused by volumetric expansion for stability numbers $N_b \leq 4$. For $N_b > 4$ the increasing mobilisation of shear strains caused increased heave. Thus, the magnitude of the heave is linked with the stability of the excavation and definitely a multi-dimensional problem.

2.1.6.2 Estimation of undrained pore pressure change

An observational quantity similar to the observed immediate heave and influence factors, is the measurement of the immediate pore pressure change as a response due to excavation. The immediate pore pressure change, Δu, is often related to the total stress change, $\Delta \sigma_v$, with the ratio of $\Delta u / \Delta \sigma_v$. Observed values from field measurements were reported e.g. by Lafleur et al. (1988a) to ca 0.5-0.6 for piezometers at the toe of a test excavation (values after entire test excavation completed) and ca 0.5 by McRostie et al. (1996), both for locations in Canada, and ca 0.8 for a 4.5 m deep and large excavation for a stadium in Gothenburg, Sweden (Alén and Jendeby 1996).

The concept of effective stress illustrate the impact of pore pressures on soil response (both in terms of strength and stiffness) (Mayne and Swanson 1981). Relating total stress change to pore pressure change is therefore important. The concept of pore pressure coefficients was proposed by Skempton (1954). He defined an equation which relates the change in total stress to the change in pore pressure according to:

$$\Delta u = B\left[\Delta \sigma_3 + A(\Delta \sigma_1 - \Delta \sigma_3)\right] \tag{2.5}$$

where parameters A and B are pore pressure coefficients which can be obtained from undrained triaxial tests. For fully saturated soil $B=1$. A can be back-calculated from field measurements of pore-pressure change and estimations of $\Delta \sigma_1$ and $\Delta \sigma_3$ (e.g. from theory of elasticity). The coefficient A by Skempton varies with the soil type, stresses and strains. Skempton's equation was further developed by Henkel & Wade in 1966, according to Leroueil (2001):

$$\Delta u = \beta(\Delta \sigma_1 + \Delta \sigma_2 + \Delta \sigma_3)/3 + \alpha\sqrt{(\Delta \sigma_1 - \Delta \sigma_2)^2 + (\Delta \sigma_2 - \Delta \sigma_3)^2 + (\Delta \sigma_3 - \Delta \sigma_1)^2} \tag{2.6}$$

where α and β are pore pressure parameters proposed by Henkel & Wade, which are related to Skempton's parameters A and B (in fact $\beta=B$). For the theoretical case of saturated linear-elastic soil under undrained conditions, the equation above reduces to (Leroueil 2001):

$$\Delta u = (\Delta \sigma_1 + \Delta \sigma_2 + \Delta \sigma_3)/3 \tag{2.7}$$

In tests presented by Larsson (1977), Skempton's A coefficient ranged from 0.75-0.81 for triaxial tests where the radial total stress was kept constant (tests with increasing as well as decreasing vertical total stress). However, it should be highlighted that the mode of stress change in the triaxial apparatus rarely resembles the field conditions. The influence of excavation geometry and wall type on excess pore pressures were illustrated by e.g. Callisto, Maltese, et al. (2014) and Bertoldo and Callisto (2016) using parametric FE-analyses. Results are included in Figure 2.8. Thus, in addition to the soil response,
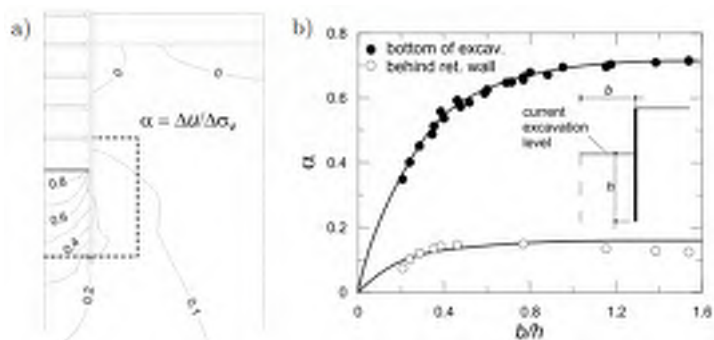
Figure 2.8: *Example of the effect of excavation geometry on the (undrained) pore pressure change. From Callisto, Maltese, et al. (2014). a) Contour lines of excess pore pressure ratio, including the zone for calculation of average α b) Average α values plotted versus ratio of width to embedment depth (total width of excavation = 2b).*

Δu and its dissipation with time depends on e.g. the geometry and size of the excavation, as well as the adopted earth retaining system and its stiffness. Such influencing factors were also noted in a comprehensive study of a deep excavation in Shanghai by Tan and Wang (2013).

2.1.7 Swedish design guidelines and regulations

This section briefly covers the general principles and background to the most common design principles and codes in Sweden for retaining and permanent structures in soft clay. The section is divided into short and long-term, referring to design of retaining structures via the use of undrained and drained analyses. The focus in the drained case will be on permanent earth pressures. The classification of soil response into these theoretical extreme cases, when dealing with excess pore pressures in soft clay, will be discussed further in Section 2.2.

2.1.7.1 Short term

As described in the guidelines for design of sheet pile walls (Sahlström and Stille 1979; Ryner et al. 1996; Fredriksson et al. 2018), the earth pressure against retaining structures in clay is based on limiting Rankine earth pressures. The guidelines from 1979 (Sahlström and Stille 1979) are influenced by work of Janbu (1972) and Stille (1976). The limiting active and passive earth pressures are used to calculate the net earth pressures below

the excavation bottom. As the corresponding earth pressure coefficients form the general basis for design in Sweden, the findings are described below.

Janbu (1972) presented analytical expressions for the active and passive earth pressure coefficients in clay ($\phi'=0$) taking into account the roughness and the (vertical) relative movement in the soil-wall interface. The diagram for the earth pressure coefficients are presented in Figure 2.9. The expressions for active and passive earth pressures coefficient for $\phi'=0$ ($p_a=\sigma_v$-$2c_u$ and $p_p=\sigma_v+2c_u$) were thus rewritten as $p_a=\sigma_v$-$N_a c_u$ and $p_p=\sigma_v$-$N_p c_u$ where $N_a=N_p=2\sqrt{1+r}$ (dashed line in Fig. 2.9). This expression is valid for small values of r ($r=c_u^{atwall}/c_u$) i.e. corresponding to approximately plane failure surfaces. For larger values of r the failure surfaces are curved (full lines in Fig. 2.9), resulting in a upper limit of $(\pi+2)/2=2.57$ for N_a and N_p (corresponding to a value of $N_{cb}=5.14$ and a value unmodified for geometry effects from the diagram in Figure 2.5). Setting $N_a=N_p=2\sqrt{1+2/3r}$ result in the blue line in Fig. 2.9 with an upper bound of 2.58. This expression has been included in Figure 2.9, since it is referred to in Swedish textbooks (e.g. Sällfors 2013).
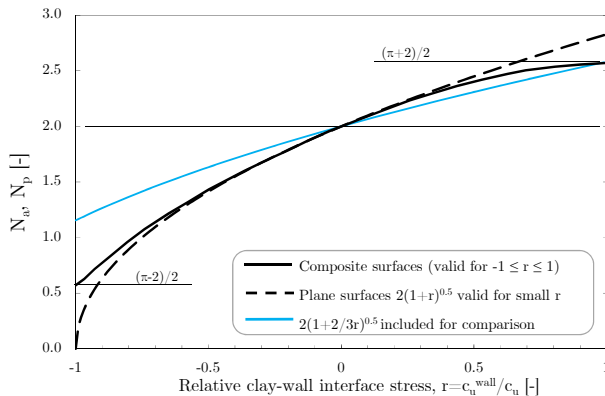
Figure 2.9: *Effect of the magnitude and direction of relative wall-soil interface shear stress on earth pressure coefficients. Adopted from Janbu (1972).*

Stille (1976) expanded on the work by Bjerrum and Eide (1956), Terzaghi and Peck (1967), and Janbu (1972). He studied a number of failures of tie-back sheet pile walls in Sweden, where the back-calculated bearing capacity factor had been estimated to be as low as approximately 4. The failures were found to be due to insufficient vertical support of the sheet pile walls with regard to the vertical component of the anchor force. In order to account for the effect of in-sufficient vertical support, or the disturbance due to construction activities, previous guidelines (Sahlström and Stille 1979) which followed on the work by Stille, recommended bearing capacity factors to be used for the calculation of net earth pressures. For example for SPWs with inadequate vertical support $N_c=4.1$ was recommended (likely a combination of $r_a=-0.5$ and $r_p=1$). This in order to account for example if a SPW were to exert downdrag on the soil. Specifying these values also cancelled out the possibility to account for an increase in N_{cb} values due to the geometry effects.

2.1.7.2 Reduction of passive earth pressure in short-term

In order to account for dissipation of negative (stabilising) excess pore pressures after excavation, i.e. moving from the theoretical undrained case, a gradual reduction of the passive (Rankine) resistance is recommended in the appendix of the current Swedish guideline for design of retaining structures (Fredriksson et al. 2018). The reduction is adopted from the British guidelines (Gaba, Hardy, et al. 2017) and compose of setting the passive resistance to zero at excavation bottom, with interpolation to the (undrained) Rankine earth pressure at a depth L below the excavation bottom:

$$L = \sqrt{12c_v t} \qquad (2.8)$$

where c_v is the coefficient of consolidation (m^2/day) and t is time (days). An example with c_v=1×10^{-6} m/s (corresponding to permeability, k=1×10^{-9} m/s and unloading modulus, M_{ul}=10 MPa) results in L=1.0 m after 1 day. A difficulty arises in e.g. the choice of unloading modulus, as this is depending on effective stress level, which is transient during the consolidation process (Section 2.2). The rate at which L increases will, therefore, slow down with time as the modulus decreases with decreasing effective stress. Different combinations of $c_v(k,M_{ul})$ are plotted versus time in Figure 2.10 which also illustrates the relative importance of the permeability versus modulus. The guidelines does not explicitly
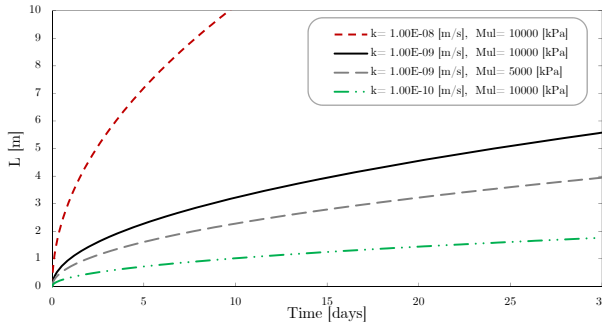
Figure 2.10: *Depth below excavation bottom, defined as L, for reduction of undrained passive earth pressure according to current Swedish guidelines (Fredriksson et al. 2018).*

describe if, and how, to consider effects of the viscous behaviour of clay. The consideration of shear strain rate in laboratory tests versus expected strain rate, or time to failure in the field, is thus not taken into account. This can be both conservative (if an excavation is only at a critical stage for a short time) or on the unsafe side, if an excavation is designed by means of undrained parameters determined from laboratory tests at standard strain rate. In the field, with construction sequence resembling that of "incremental loading", it can take considerably longer time to reach the "critical shear strain level" described by Bjerrum (1973). Instead, the viscous behaviour of clay is (rather implicitly) taken into design consideration by the reduction factor, μ. However this correction factor is only applied to shear strengths determined by field vane and fall cone tests, and applied independently of imposed mode of loading and duration. Shear strengths determined by

e.g. direct simple shear or triaxial tests are not corrected for strain-rate-effects. This emphasises the need for constitutive soil models taking viscous (rate-dependent) behaviour of clay into account both with respect to optimisation and safety.

2.1.7.3 Long-term - review of current guidelines

The current Swedish guidelines (Fredriksson et al. 2018) do not specify methods or values for the design of permanent underground structures (including retaining structures such as e.g. sheet pile, diaphragm or secant pile walls). The regulations specified by the Swedish Transport Administration specify to some extent earth pressures against permanent underground structures. The relevant regulation, including the references, are summarised below:

1. "Krav Tunnelbyggande" TDOK 2016:0231 ver 1.0 (Trafikverket 2016b) for tunnels:

   (a) For permanent load situations, earth pressure at rest shall be assumed.

   (b) Lateral earth pressures against tunnels shall be determined according to TDOK 2016:0204.

   (c) The above items are not fixed, as the code states that it is possible to add or adjust the demands of the code in consultation with the client (i.e. in Swedish "Objektspecifika byggherreval").

   (d) Water pressure shall be considered as a permanent load with min and max values corresponding to lower low water level (LLW) and higher high water level (HHW)[1].

2. "Krav brobyggande" TDOK 2016:0204 ver. 3.0 (Trafikverket 2016a) for bridges:

   (a) Bridges (and tunnels due to the cross-reference in "Krav Tunnelbyggande"), shall be designed for earth pressure at rest. Earth pressures are to be determined according to TDOK 2013:0667 "TK Geo 13" (Trafikverket 2014).

   (b) Permanent sheet pile walls shall be designed for earth pressure at rest.

   (c) Diaphragm and secant pile walls are to be designed for earth pressures according to TK Geo 13 (Trafikverket 2014).

   (d) For diapraghm or secant pile walls that are part of tunnel structures the requirements for tunnels "Krav Tunnelbyggande" TDOK 2016:0231 shall apply.

3. "TK Geo 13" TDOK 2013:0667 ver. 1.0 (Trafikverket 2014) for geotechnical design:

   (a) Only specifies, for diaphragm and secant pile walls, that the relative deformations of soil-structure is to be considered for the calculation of earth pressures.

---

[1]According to the Swedish Meteorological and Hydrological Institute defined as the lowest and highest recorded or calculated water levels (Swedish Meteorological and Hydrological Institute 2020b)

4. "TR Geo 13" TDOK 2013:0668 ver. 2.0 (Trafikverket 2016c) advise for geotechnical design:

    (a) Earth pressures can be calculated according to appendix C in SS-EN 1997-1. For normally consolidated soil the earth pressure at rest can be estimated according:

        i. Friction material and silt: 1-$\sin\phi'$

        ii. Clay: 0.31+0.71(w_L-0.2), were w_L is the liquid limit.

        iii. Varved clay and silt soils: 0.5

        iv. Organic soil (gyttja): 0.6

    (b) For clay, the overconsolidation ratio, OCR, is taken into account by $K_0 OCR^{0.55}$.

Regarding item 4(b); the text above is as stated in the document, but it should rather say that K_0^{nc} should be adjusted according to OCR, as intended by Schmidt (1966) i.e. $K_0 = K_0^{nc} OCR^{sin(1.2\phi')}$ (eq. 2.28). The misprint possibly arise from Larsson (1977) referring to the empirical estimate of $K_0^{in-situ}$ according to 0.31+0.71(w_L-0.2) as K_0^{nc}. Definitions for K_0 are reviewed in section 2.2.7.

Regarding effects of heave; "Krav Tunnelbyggande" (for bridges) states *"Loads caused by swelling material shall be analysed and taken into account"* and "TK Geo 13" *"Heave shall be accounted for, for example when volume increase occurs due to reduction of vertical stresses"*. Thus none of the codes explicitly specify how to estimate or calculate the effects on structures resulting from the drained case of long-term heave following excavation in clay. The pre-study (Tornborg 2017) investigated the effect of the remaining heave after excavation at the time the slab was cast, i.e. "locked-in" heave. An upper bound was presented as 0.5 times the vertical effective stress at the level of the excavation bottom before excavation. Also Simpson (2018) pointed out such an empirical approach could be useful, i.e. estimating effective heave pressure based on a proportion of σ'_{v0}. Effective heave pressures are described in more detail in Section 2.2.9.1.

2.2 Soil behaviour

2.2.1 Introduction

Based on the review in the previous section, it is clear that the classical approach for design of earth retaining structures has been to separate the response into idealised short-term undrained and/or long-term drained cases. The drained case is in Sweden (supposedly on engineering judgement) often being neglected in conditions of clay with low permeability. It is, however, also clear that the choice of the construction methods and restraints in the short-term, such as for example limiting the allowable deformations during the construction phase, may impact the long-term response and the permanent structure (for example locked-in heave). The transient response hence needs to be studied. This section covers some of the characteristics of soil behaviour relevant to the rate-dependent response of excavations and soil-structure interaction in soft clays. The focus will be on:

- Behaviour of clay during unloading situations, including the effects of dissipation of negative excess pore pressures.
- Viscous behaviour of clay including the strain-rate effect on the strength and stiffness response, as this in combination with consolidation influences the long-term response.
- Lateral earth pressure against structures in soft clay, focusing on description of K_0 as a measure of 2D stress states in soft soils.
- Vertical upward earth pressure as result of heave following excavation, i.e. the effective heave pressure.

2.2.2 Stress paths during excavations in urban environments

The soil elements adjacent and within an excavation will experience stress changes in various directions as a result of unloading and soil-structure interaction. The imposed stress change (possibly reversal) during excavation is more pronounced than during loading, and the typical settings in urban environments make excavation problems even more complex. Four idealised stress paths are summarised in Figure 2.11. In the figure it can here be noted that the model value of K_0^{nc} is rather low (review in section 2.2.7) resulting from Jaky's formula and a friction angle consistent with that of M_c.

As total stress change is imposed due to the various loading conditions in the field (or under controlled forms in the laboratory) the effective stresses will depend on the response of the soil (Wood 1990). If the soil behaves completely drained the effective stress path (ESP) will correspond to the total stress path (TSP). If partially drained conditions apply, the ESP will deviate from the TSP as excess pore water pressures are generated. Tests on Swedish soft clay, e.g. Larsson (1977) and (Züblin 2015b), have shown that the ESPs for undrained compression and extension tests were independent of the imposed TSPs, i.e. TSPs A and D in Figure 2.11 resulted in the same ESPs and the same applied for paths B and C.
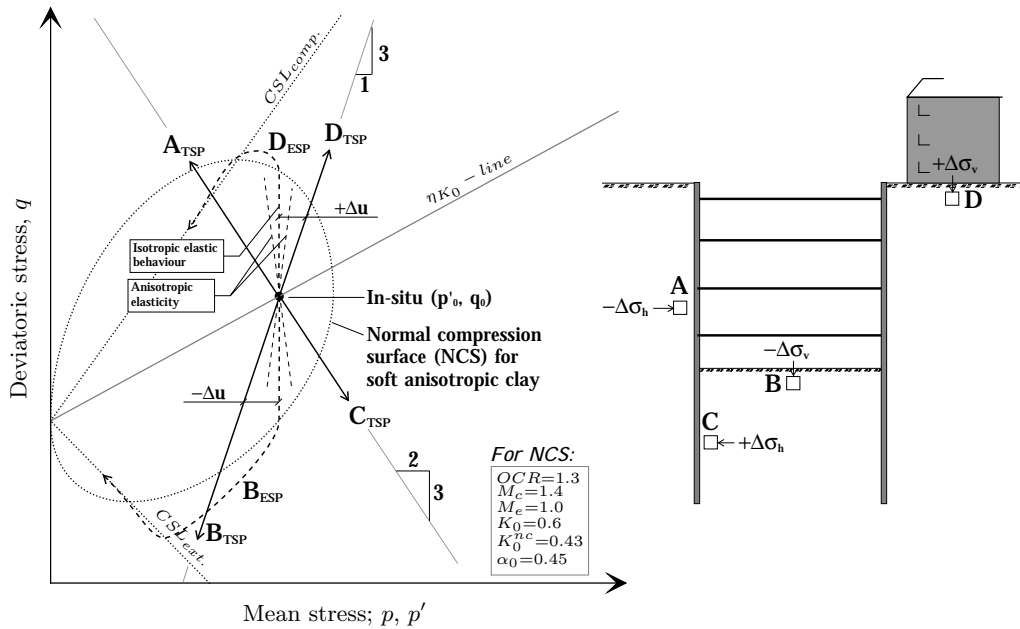
Figure 2.11: *Idealised modes of loading and total stress paths (TSPs) for excavations. Effective stress paths (ESPs) for undrained conditions are sketched, but depend on soil response to the imposed total stress change.*

2.2.3 General unloading and consolidation

As seen in Figure 2.11 the emerging shear strength will depend on; the in-situ effective stress level in the soil, the effective stress path and the size and shape of the normal compression surface (NCS), or yield surface, if the surface is considered as a static bounding surface. The size and shape of the NCS depends on the soil structure and stress history (reviewed in detail in section 2.4.2). Most notably, the preconsolidation pressure, K_0 and soil structure [1] have significant impact on the size and shape of the NCS and yield surfaces. The emerging shear strength is thus significantly dependent on the overconsolidation ratio (OCR) and the imposed loading direction (i.e. effective stress path to failure). The influence of OCR on undrained shear strength was expressed by Ladd et al. (1977) as:

$$\frac{(c_u/\sigma'_{vc})^{OC}}{(c_u/\sigma'_{vc})^{NC}} = OCR^m \qquad (2.9)$$

with m suggested as 0.8 on average (0.85 for normally consolidated clay decreasing with OCR to a minimum 0.75). It should be noted that the relationship was obtained by pre-loading, and subsequently unloading of clay samples to different OCRs followed by shearing in DSS tests. Thus, effects of various degree of destructuration are incorporated in the results. This relationship has been further elaborated (e.g. Karlsrud and Hernandez-Martinez 2013) and incorporated into the Swedish guidelines (e.g. Larsson, Sällfors, et al. 2007) for the cases of triaxial compression, extension and direct simple shear.

2.2.3.1 Combined effect of consolidation and creep

For soils with low-permeability, such as soft homogenous clays, the undrained and drained soil behaviour represent the extreme cases of the transient behaviour that the soil will experience in the field. As exemplified by Leroueil and Tavenas (1981) a high rate of excavation in a low-permeable soil may initially show a undrained response, if the generation of negative excess pore pressures corresponds to the total stress change, i.e. unaltered effective stresses. Note that the sign convention in this report is that a decrease in pore pressure during e.g. rapid excavation corresponds to negative excess pore pressures. However, due to the dissipation of the negative excess pore pressures, the effective stress state will move towards the failure line. Depending on the magnitude and direction of the imposed initial (total) stress change and the resulting soil response the dissipation may result in reaching the failure line. This is illustrated in Figure 2.12. If consolidation is allowed after a time, t_{exv}, following an undrained excavation process, the effective stress path will move towards the failure line. Included in Figure 2.12 are also results from undrained triaxial tests with varying imposed total stress change (the four TSPs as illustrated in Figure 2.11) as well as 41 undrained creep tests reported by Larsson (1977) (on Lilla Mellösa clay) including, for comparison, M_c and M_e values based on evaluation of triaxial tests performed for characterisation of the instrumented site presented in section 4.3.

---

[1]Involves fabric, which can be anisotropic, and bonding.
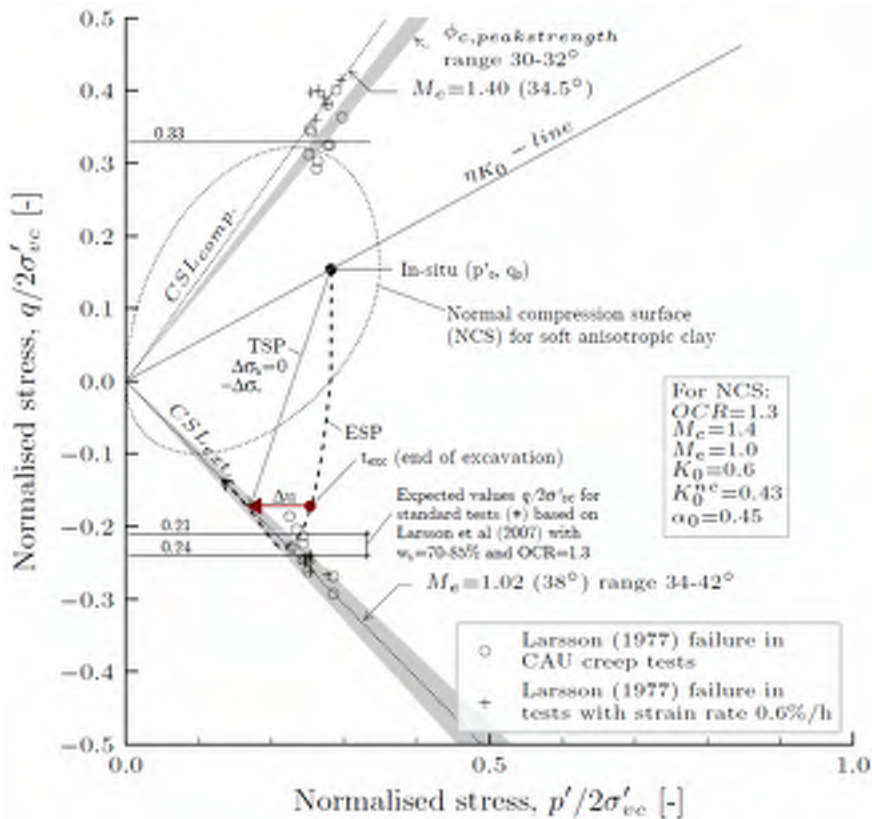
Figure 2.12: *Effect of consolidation (red arrow) after total stress change (rapid excavation) resulting in ESP from in-situ to point t_{exv}. Inspired by Leroueil and Tavenas (1981). Data from undrained triaxial standard and creep tests from Larsson (1977) compared to M_c and M_e from laboratory tests presented in Section 4.3. Note: an initial NCS is illustrated, upon loading this may evolve due to deviatoric and/or volumetric viscoplastic strains as described in section 2.4.2.*

In so called undrained creep tests, no dissipation of pore water pressure is allowed under a condition of constant total stress. Depending on the imposed shear stress level, the effective stress paths may move towards the failure line due to additional generation or dissipation of the excess pore water pressures as a result of creep deformations. However, as clarified by Augustesen et al. (2004) the term "undrained creep test" is somewhat misleading, since the deformations occur for a transient effective stress, and not for a constant effective stress as typically associated with creep. The deformations that generate pore pressure can thus, depending on the effective stress level, be a combination of primary and secondary consolidation (creep). Under field conditions, to avoid undrained creep failure, the dissipation of pore water pressure will have to overcome any generation of pore water pressure arising due to continued deformations. The response with time (e.g. heave, OCR and shear strength) is thus influenced by the rate of dissipation of negative pore water pressures i.e. consolidation, that is typically described by permeability k and confined modulus M, and the viscous behaviour of clay. These features are discussed in the following sections.

2.2.4 Consolidation and unloading

As soil is unloaded by a reduction of the total stress, there is a decrease in pore pressure. In a soil that behaves elastic and isotropic, Δu will correspond to the change in total mean stress, p (Leroueil 2001). Skempton's pore pressure parameters, A and B, were discussed in section 2.1.6.2. These parameters can be estimated based on laboratory tests (e.g. Larsson 1977), or field measurements, and link the change in pore pressure to changes in total stress.

The time required to dissipate the negative excess pore water pressures is essential, since it governs the response and factor of safety following excavation. As an example, L'Heureux et al. (2009) reported that 50 % of the difference between short- and long-term factors of safety for excavations was lost in only 8% of the time to reach complete equalisation of excess pore pressures.

The theory of consolidation was introduced by Terzaghi in 1923 for 1D conditions according to:

$$\frac{\partial u}{\partial t} = c_v \frac{\partial^2 u}{\partial z^2} \tag{2.10}$$

where u excess pore pressure, t time, z distance downwards from top of clay layer and c_v coefficient of vertical consolidation defined as:

$$c_v = \frac{kM}{\gamma_w} \tag{2.11}$$

where k is permeability (m/s), M is modulus (kPa) and γ_w (kN/m^3) unit weight of water. The assumptions associated with eq. 2.10 are e.g. homogeneous saturated and isotropic elastic soil. Taylor (1948) presented solutions to equation 2.10 for various boundary conditions as plots of average consolidation ratio, U, versus time factor T. Biot (1941) presented a theory for 3D consolidation assuming isotropic elastic soil behaviour. The theory was later extended to include anisotropy (Biot 1955).

There are extensive field measurements on pore pressure dissipation in slopes and excavations e.g. (Skempton 1984; Lafleur et al. 1988b; McRostie et al. 1996; Persson 2004; Kullingsjö 2007). Also, numerical studies of pore pressure dissipation have been carried out. For example Eigenbrod (1975), considered an idealised cut slope in isotropic elastic material on an impermeable base, and found out that full pore pressure equalisation (steady state pore pressures) were obtained when the dimensionless time factor, T:

$$T = c_{vs}t/H^2 = 0.33 \qquad (2.12)$$

where c_{vs} is the coefficient of consolidation for swelling (unloading), t the time after excavation and H the height of the slope. L'Heureux et al. (2009) studied the effect of the thickness of the soil stratum below an idealised cut slope in assumed isotropic elastic soil and derived safety factors at various times after excavation using the limit equilibrium method. For the studied cases T ranged from 0.33 to 2.15, however for $H_{tot}/H_{exc} \geq 1.8$ the time to reach equalisation increased only slightly (T=1.9 for H_{tot}/H_{exc}=1.8) due to the location of the long-term critical slip surface. An analogue to excavations within retaining structures, would mean that the geometry of the earth retaining system will influence the pore pressure equalisation process.

From the review so far, it is clear that pore pressure dissipation depends on factors such as the geometry of the excavation, permeability and stiffness of the soil (Leroueil 2001; Rowe 2001; Tan and Wang 2013; Callisto, Maltese, et al. 2014). The transient dissipation of pore pressure with time is of great interest, since it governs the amount of equalisation and affects the response during, as well as after, the construction phase (i.e. the performance of the permanent structure). Therefore soil permeability and unloading stiffness are reviewed in the following.

2.2.4.1 Permeability

The volume of water flowing through a unit cross-sectional area of soil can be estimated using Darcy's law (Bear and Verruijt 1987) which states that the volume of water flowing per unit time, q, due to a hydraulic gradient, i (dimensionless), is given by:

$$q = ki \qquad (2.13)$$

where k is the hydraulic conductivity. Hydraulic conductivity is in geotechnical engineering also commonly referred to as permeability or coefficient of permeability. From here onwards, k is referred to as permeability. The permeability of saturated soils depends on the flow channels through the soil and the characteristics of the liquid (Leroueil and Hight 2003):

$$k = K\gamma/\mu \qquad (2.14)$$

where K is the specific permeability (m^2) of the soil, γ the unit weight of the liquid and μ the viscosity of the liquid. For soft clays in Sweden the in-situ vertical permeability, k_0, based on laboratory test data is in general in the order of magnitude of 1×10^{-10} to 1×10^{-9} m/s and 0.6-1.1$\times10^{-9}$ m/s for Swedish west-coast clays (Berntson 1983). An international review of Leroueil and Hight (2003) reported values of 3×10^{-10} to 5×10^{-9} m/s for soft clays.

Regarding anisotropy in permeability, Larsson (1981) carried out CRS-tests on homogeneous clay samples trimmed in different directions. Although σ'_{vc} and M_L (modulus after yield) varied depending on loading direction, there was no indication that this was the case for k. However, due to the anisotropy of stiffness, the radial strains will not be uniform for the non-vertical samples, which will affect the interpretation. For homogeneous clay deposits Jamiolkowski et al. (1985) summarised a range of expected k_h/k_v ratios of 1 to 1.5 and Mesri, Feng, et al. (1994) stated the ratio for marine clays to near 1.0 and rarely above 1.5. It is however unclear what studies and test methods these general ratios were derived from. In addition to a summary of worldwide data Leroueil, Bouclin, et al. (1990) investigated anisotropy in permeability by means of using a radial-flow permeameter, triaxial cell and oedometer. Tests were conducted on four Canadian clays (three from Champlain Sea Basin) and clay from Bäckebol (4.3 m depth), Sweden, and reported a ratio generally smaller than 1.2 for soft marine homogeneous clays. Results are presented in Figure 2.13 where figure b) result in a ratio of k_h/k_v ca 1.2 for $e=1.2$ to k_h/k_v ca 1.3 for $e=1.4$.
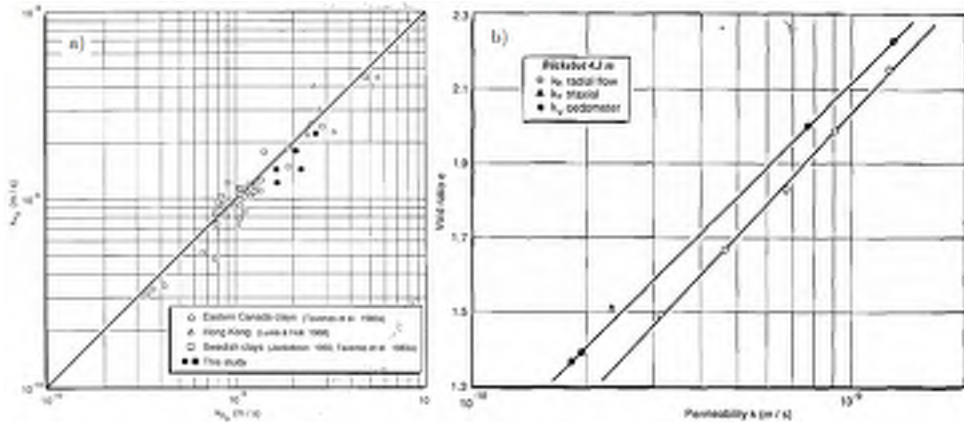
Figure 2.13: *a) Permeability anisotropy in soft homogeneous marine clays and b) Variation of vertical and horizontal permeability with void ratio for Bäckebol clay. From Leroueil, Bouclin, et al. (1990).*

As exemplified in Figure 2.13 b) plotting the permeability in log-scale versus void ratio typically, after initial irregularities, for soft clays results in a linear relationship (Larsson 1986; Larsson 2008). The relationship is defined by the permeability change index, C_k (Tavenas, Jean, et al. 1983):

$$C_k = \frac{\Delta e}{\Delta \log k} \tag{2.15}$$

where e is void ratio and k permeability. C_k has been found to be related to the initial void ratio, e_0, see e.g. Figure 2.14.

An analogue to C_k relating change in permeability to vertical strain, ε, is the permeability change index β_k (Larsson 1986):

$$\beta_k = \frac{\Delta \log k}{\Delta \varepsilon} \tag{2.16}$$

Since $\Delta\varepsilon=\Delta e/(1+e_0)$, C_k and β_k are related according to $\beta_k=(1+e_0)/C_k$. Using this relation and assuming $C_k=0.5e_0$ (from Figure 2.14) and $e_0=2.7\times w_n$ (saturated soil and specific gravity 2.7 t/m^3 based on Larsson (1981)) results in β_k values slightly below the trend line suggested by Karlsrud and Hernandez-Martinez (2013) from CRS tests on high-quality block samples of Norwegian clays.
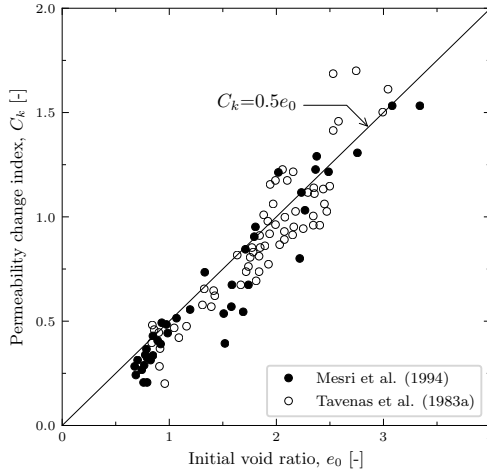
Figure 2.14: *Permeability change index, C_k, as a function of initial void ratio. After Mesri, Feng, et al. (1994).*

Methods for determining permeability in laboratory: A number of tests exist for determining the permeability of samples in laboratory. A comparison of different laboratory methods was presented e.g. by Tavenas, Leblond, et al. (1983) see Figure 2.15.

The results by Tavenas, Leblond, et al. (1983) also demonstrated the validity of Darcy's law on four different Canadian clays by means of falling head tests in triaxial cells (hydraulic gradients 1.4-26). They speculated that if any threshold gradient were to exist, it would be small (less than 0.1 based on the test data). Furthermore, falling head tests were performed by means of adapting a conventional oedometer. Also these test results conformed to Darcy's law. However, indirect evaluation of permeability from other types of tests were proven unreliable; incremental load (underestimate k), CRS (overestimate k in the range of σ'_{vc} and an interpreted void ratio-permeability relationship that differs from the true, see Figure 2.15) and CGT tests (underestimate k). The error in CRS-test is arising from the fact the deformation is measured in the top of the sample (low void ratio) and the excess pore water pressure in the bottom (higher void ratio).
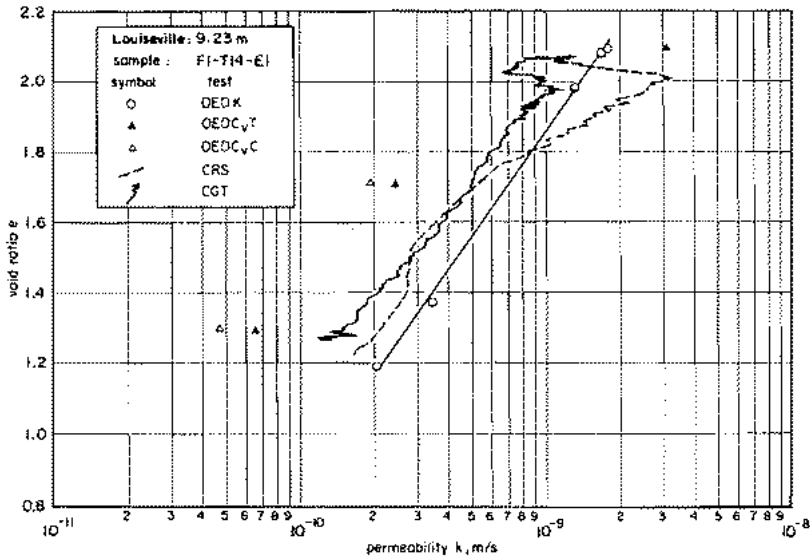
Figure 2.15: *Comparison of permeability from various oedometer tests on Canadian clay; falling head test (OEDK), interpretation of c_v in IL-test using Taylor's method (OEDc$_v$T) or Casagrande's method (OEDc$_v$C) as well as interpretation of CRS and CGT tests. From Tavenas, Leblond, et al. (1983).*

Tavenas, Leblond, et al. (1983) concluded that indirect methods of evaluating k should be disqualified as a means to determine the permeability of natural clays. Also, Muir Wood (2015) described the drawbacks of the CRS test and stressed that the observable test result is a system response and not a single soil element response. Errors in interpretation arise e.g. from the fact that the pore pressure and effective stresses varies within the sample. Thus, an assumption have to be made about the shape of the pore pressure variation within the sample. Furthermore, the accuracy of the registered excess pore pressure has a major impact on the evaluated permeability as opposed to a relative minor impact on the evaluated effective stress (since according to Swedish standard the pore pressure is to be kept below 10 % of the total stress).

Methods of determining permeability in the field: As pointed out by Berntson (1983) the variations in vertical to horizontal permeability may be great in varved or layered soil, as well as the permeability determined on small samples in the laboratory may underestimate the permeability compared to the field (macro) permeability of a soil mass. Values of c_v evaluated from test pumping were reported by Berntson (1983) to have been found to be ca 1000 times bigger than c_v determined in the laboratory (oedometer). It is not clear, however, if this was a result of a heterogeneous soil on macro scale, a result of poor sampling resulting in low oedometer modulus or error in testing (e.g. clogged porous stones).

In a recent infrastructure project in Sweden (Marieholm Tunnel in Gothenburg) c_h was

evaluated based on CPT-dissipation tests (Züblin 2015b) and a method referred originating from Mayne (2002) in which:

$$c_h = \frac{T^* a^2 \sqrt{I_R}}{t_{50}} \tag{2.17}$$

where T^* modified time factor, I_R rigidity index, a probe radius and t_{50} time to reach 50 % equalization of generated excess pore pressure. Setting T^*=0.245, I_R=200, a=0.0357/2 resulted in what was interpreted as c_h ranging from 8-12 m²/year (2.5-3.8x10⁻⁷ to m²/s) for dissipation tests at 17, 22 and 27 m below ground surface. Using a secant unloading modulus of 15 MPa (estimated average from IL tests) and k=10⁻⁹ m/s would result in 1.5x10⁻⁶ m/s. However, Jamiolkowski et al. (1985) reported difficulties and important aspects of interpreting CPTU dissipation test data for evaluation of permeability, of which some are given here:

- What coefficient of consolidation is measured? Vertical, horizontal or average?
- What degree of consolidation should be reached for estimation of c_h?
- What is the relevance of the measured coefficient of consolidation? That is, considering stress and strain levels during the test, which practical problem is the evaluated value applicable to? As the generated excess pore pressure around the CPTU probe dissipates, a re-load situation is occurring.
- Furthermore Leroueil and Hight (2003) points out that driving a piezometer or probe remoulds the soil (and in addition possibly result in clogging of the porous filter) therefore underestimating the evaluation of permeability. For this reason self-boring permeameters were recommended as opposed to push-in piezometers.

These aspects are not intended to be answered within the scope of this report, but rather included here in order to highlight some potential difficulties in the interpretation of dissipation tests for evaluation of consolidation coefficients and permeability.

2.2.4.2 Previous estimates of unloading modulus

Next to permeability, the stiffness of the soil governs the rate of dissipation of excess pore pressures according to classical (Terzaghi 1943) 1D consolidation theory. Some previous studies suggesting relationships for the unloading modulus of soft Scandinavian clays are reported in Figure 2.16.

The relationship presented by Persson (2004) was the basis for the relationship in the current Swedish guidelines (Trafikverket 2016c). Wood (2014) proposed the relationship suggested by Karlsrud (2012) to be used, due to highlighted potential drawbacks in the derivation of the relationship proposed by Persson. Two parameter sets for the relationship according to Karlsrud (2012) is given in Figure 2.16; a=250 and b=0.3 which was given by Karlsrud for Bjørvika clay, and a=175 and b=0.6 which appears to be a slightly better fit to the laboratory data presented in Section 4.3 (figure 4.15). It should finally be noted that the time for the dissipation of excess pore pressures decreases with; increasing soil stiffness, due to reduction of the ultimate volume change, or increasing permeability owing to e.g. increase in void ratio (Gaba, Simpson, et al. 2003).
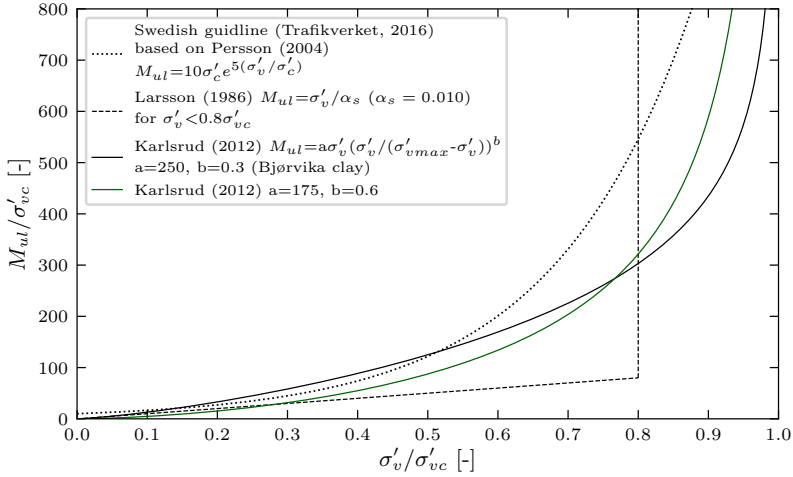
Figure 2.16: *Relationships for tangent unloading modulus, M_{ul}, of soft Scandinavian clays and vertical effective stress, σ'_v, normalised by preconsolidation pressure, σ'_{vc}.*

2.2.4.3 Field scale versus laboratory consolidation

There is a number of reasons which may cause discrepancies between the field response and predictions of pore pressure equalisation with analytical or numerical methods based on input data on c_v and c_h from laboratory tests. These are highlighted below based on Eigenbrod (1975) and Leroueil and Hight (2003).

- Two- or three-dimensional nature of field problems and anisotropy in permeability.
- Joints or fissures may form during excavation due to lateral stress reduction, resulting in an increased macro permeability in addition to the reduction in the shear strength.
- Permeability measured on small samples in the laboratory may underestimate the macro permeability of the soil mass, the effect being more severe in heterogeneous or stratified deposits.
- Heavy rainfall or underwater excavation resulting in the availability of water at the excavated surface will increase the rate of dissipation.

Berntson (1983) back-calculated k in the field, down to depths of approximately 5 m below ground surface, to be 10-50 times 10^{-9} m/s.

2.2.5   Strain rate / viscosity

2.2.5.1   Introduction:

When considering the strain rate effects and the effect of time on the performance of exca-
vations (and embankments for that matter), both the dissipation of excess pore pressures,
as well as the viscous response of clay need to be considered. The process of consolidation
was covered in the previous section, thus in this section the viscous behaviour of clay is
reviewed and discussed.

2.2.5.2   Combined effect of rate-dependency and consolidation

The combined rate-effect of consolidation and viscous material behaviour, discussed by
Leroueil and Tavenas (1981), has been illustrated in Figure 2.17. Idealised undrained
unloading resulting in ESPs O to 1,2,3 or 4 (depending on the magnitude of unloading)
and dissipation of excess (suction) pore pressures, Δu_e, will cause the stress paths to move
to the left. The strain rate dependency of the preconsolidation pressure has been reported
by e.g. Crawford (1964), Bjerrum (1967), Berre and Bjerrum (1973), Bjerrum (1973), and
Sällfors (1975) and a review is presented in section 2.2.5.3. The rate dependency reflect
that the size of the entire yield surface is rate dependent (Tavenas and Leroueil 1977;
Graham, Crooks, et al. 1983). In Figure 2.17 apparent yield surfaces with strain rates 0.1,
1.0 and 10 times a reference rate are included for illustration.

In the case of constitutive "creep-models" the effective stress state may lie outside what
is referred to as a normal consolidation surface. Such stress states results in viscoplastic
strains. If drainage is prohibited or partial, the viscoplastic strains result in excess pore
pressures, Δu_{vp}, causing the effective stress path to move further to the left. This is also
illustrated in Figure 2.17. The stress path either reach the failure line or stabilise at a
"long-term" yield surface. Such a long-term yield surface was proposed by Larsson (1977)
and is presented in Figure 2.25.

From the above it becomes clear that not taking rate-dependent effects into account, e.g.
if considering undrained conditions in combination with ignoring the viscous behaviour of
clay, could lead to unsafe design as the apparent yield surface determined at laboratory
strain rates, as well as the effective stress state, then are both fix.

As such it is important to realise the major difference in strain rate under field and
laboratory conditions, the strain rate in laboratory for practical purposes typically being
higher than in the field. Some reported strain rates in the field are presented in Figure 2.18.
It is however unclear if these represent field tangent or secant strain rates, but most likely
they are secant strain rates i.e. evaluated between timestamps of measurements/readings
(continuous logging of data with small time increments would provide tangent strain
rates). Strain rates in the field could thus be higher: the extreme case is when a soil
mass is moving as a consequence of quick clay landslide. In Section 5 (figures 5.3 and 5.4)
vertical secant strain rates during excavation and reloading have been evaluated and are
compared to the strain rates discussed.
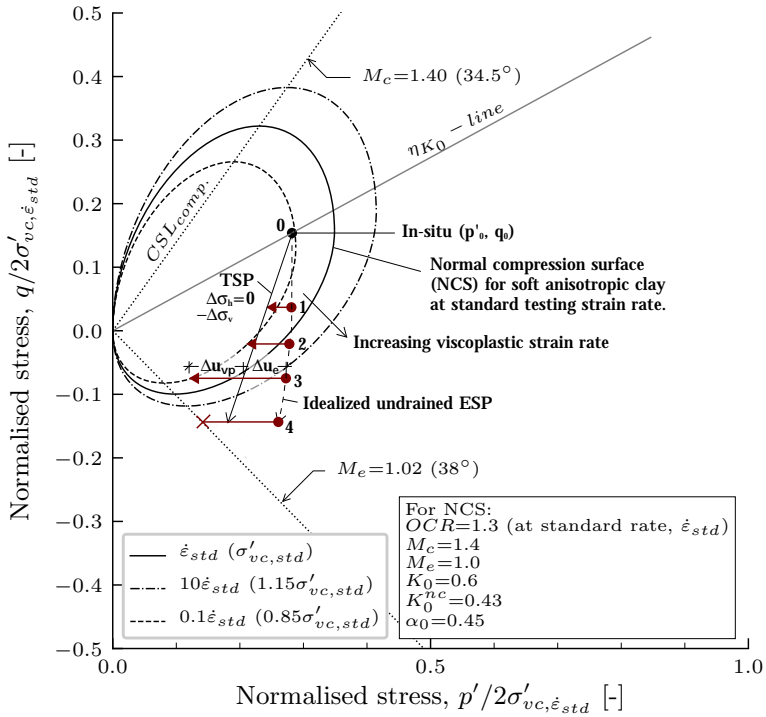
Figure 2.17: *Effect of time with respect to combined effect of the size of apparent yield surface and dissipation of excess pore pressure after undrained unloading. Inspired by Leroueil and Tavenas (1981) and results of undrained creep tests by Larsson (1977)*

.
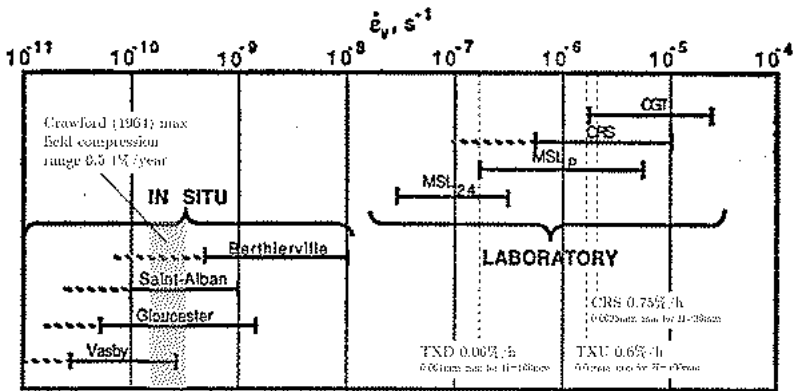
Figure 2.18: *Strain rates in the field compared to laboratory. After Leroueil, Kabbaj, and Tavenas (1988) including data from Crawford (1964). Annotated with strain rates used in standard Swedish laboratory tests.*

Bjerrum (1973) presented a hypotheses that failure occurs when a certain critical strain is reached within a material. It can be noted that the time, t, in Figure 2.17, to reach this critical strain is within only 2.5 hours in a undrained triaxial compression test consolidated to in-situ stresses and performed at a strain rate of 0.6 %/h (equivalent to $1.7 \times 10^{-6}\ s^{-1}$) assuming a peak strength at 1.5 %. Due to the rate-dependency of yielding and failure, Tavenas and Leroueil (1977) specified *apparent* yield surface.

The strain-rate dependency of yielding and irrecoverable strains affect thus both the emerging apparent (undrainend) shear strength and the preconsolidation pressure. This is illustrated in Figure 2.19. In the following paragraphs the influence of the rate-dependency of yielding is reviewed, considering the effects on the emerging preconsolidation pressure and the undrained shear strength separately.
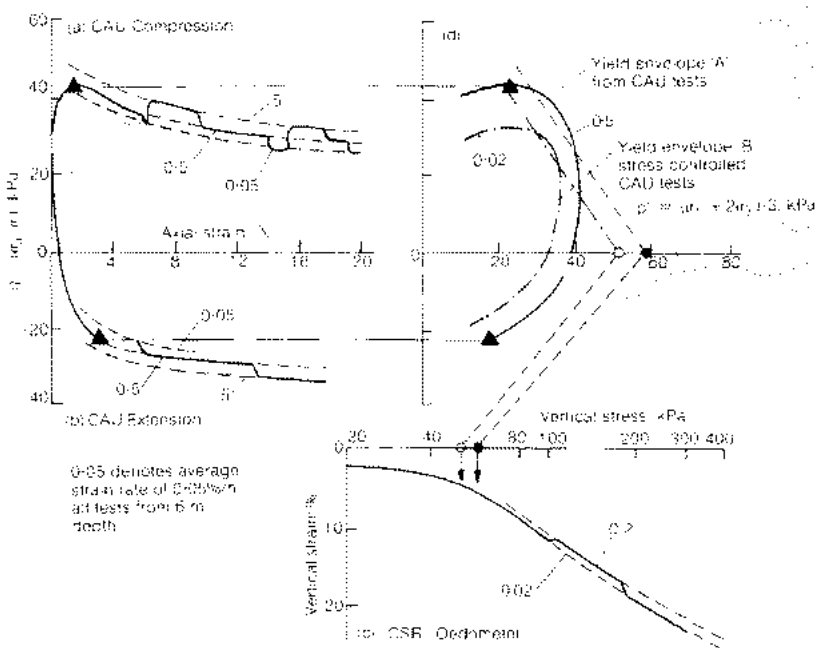
Figure 2.19: *Illustration of strain rate dependency of apparent yield surface and effect on emerging (rate-dependent) shear strength and preconsolidation pressure. From Graham, Crooks, et al. (1983).*

2.2.5.3   Strain-rate effects on preconsolidation pressure

A comprehensive collection of data summarising the strain-rate influence on preconsolidation pressure on clays from Eastern Canada (11 sites) was made by Leroueil, Tavenas, et al. (1983), see Figure 2.20. The study was expanded by Leroueil, Kabbaj, Tavenas, and Bouchard (1985) to include data from additional CRS and IL-oedometer tests on Canadian clays as well as data from Bäckebol, Sweden (Sällfors 1975; Larsson 1981). Further studies, also including triaxial testing, was reported by Graham, Crooks, et al.

(1983) including clays from Drammen (Norway), Belfast (Northern-Ireland) and Winnipeg (Canada).

The effect of varying strain rate can be related to preconsolidation pressures and effective stresses at a given strain according to (Länsivaara 1999):

$$\frac{\sigma'_{v1}}{\sigma'_{v2}} = \frac{\sigma'_{vc1}}{\sigma'_{vc2}} = \left(\frac{\dot{\varepsilon}_1}{\dot{\varepsilon}_2}\right)^B \tag{2.18}$$

where B was defined as "rate parameter" by Länsivaara (1999) and found to be approximately 0.07 for Finnish clays. Claesson (2003) reported values of B ranging from 0.06 to 0.08 in testing of soft Swedish clays. Equation 2.18 with B=0.06 has been included in Figure 2.20 since it provides a reasonable estimate given the compiled data. B=0.06 implies that when the strain rate is doubled, the preconsolidation pressure is increase by 4 %, and for a tenfold increase in strain rate the increase is 15 %.
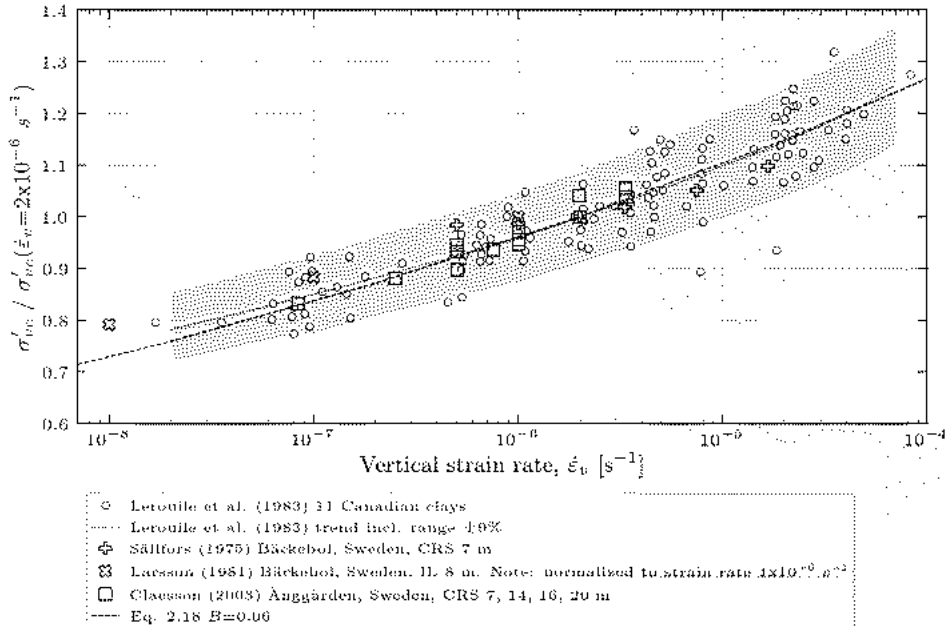
Figure 2.20: *Effect of strain rate on preconsolidation pressure. Data from Leroueil, Tavenas, et al. (1983) and Claesson (2003) in addition to evaluated data from Sällfors (1975) and Larsson (1981). The data from Leroueil, Tavenas, et al. (1983) have for comparison been adjusted to the normalised strain rate 2×10^{-6} s^{-1}.*

As seen in Figure 2.20, there is an almost linear relationship for normalised preconsolidation pressures over the logarithm of strain rate. The effect of the strain rate on apparent preconsolidation pressure, however, decreases somewhat with decreasing strain rate.

34

Plotting the results in a log-log diagram results in an essentially linear relationship (Graham, Crooks, et al. 1983) which can be expressed as (Claesson 2003):

$$C_p = \frac{\Delta \log \sigma'_{vc}}{\Delta \log \dot{\varepsilon}_v} \tag{2.19}$$

where preconsolidation index $C_p = C_\alpha / C_c$ (equal to B) and:

$$C_\alpha = \frac{\Delta e}{\Delta \log t} \text{ and } C_c = \frac{\Delta e}{\Delta \log \sigma'_v} \tag{2.20}$$

To derive a rational laboratory testing procedure for the determination of preconsolidation pressures for design purposes, Sällfors (1975) compared preconsolidation pressures evaluated from full scale field tests to that of IL tests and CRS-tests performed at various rates. A constant rate of deformation (0.0024 mm/min corresponding to 0.72 %/h) was suggested, as well as a graphical evaluation method for deriving preconsolidation pressures corresponding to the field cases. The tests were performed on samples from 2.5-10 m depth below ground surface. As samples have been extracted for greater depths for some recent major infrastructure projects, Sällfors and Larsson (2017) recommended to perform CRS-tests for which the expected preconsolidation pressure is >250 kPa at a rate of 0.0012 mm/min. This is due to that for a constant rate of deformation test, the rate of load application will be higher in tests performed on samples from greater depth, as the stiffness is higher.

2.2.5.4 Strain rate influence on shear strength

Similar to that of preconsolidation pressure, many authors have investigated the influence of time to failure, or the strain rate, on the undrained shear strength. An early report of triaxial testing to study the influence of strain rate is that of Lo and Morin (1972). For triaxial testing on block samples from Quebec (Canada), a decrease in peak deviatoric stress of 20 % was reported for isotropically consolidated drained triaxial compression (CIDC) tests with strain rates 0.1 and 0.0025 %/h (40 times slower). Bjerrum (1973) also reported on the influence of strain rate and noted that the influence was similar in undrained and drained compression tests. For St. Alban clay (also in Canada), Tavenas and Leroueil (1977) found a decrease in the peak deviatoric stress of 20 % in drained CIDC tests performed at 0.01 compared to 0.1 %/h. Further work was presented by Graham, Crooks, et al. (1983) who e.g. performed anisotropically consolidated undrained triaxial compression (CAUC) and extension (CAUE) tests at varying strain rates, as well as tests where the strain rate was varied including relaxation stops. Based on the data they indicated that the reduction in the size of the yield surface appeared to be approximately uniform for decreasing strain rates. Even though this is difficult to validate experimentally due to the effects of evolving anisotropy and different rates of destructuration in different loading directions. To summarise the previous findings (Bjerrum 1969; Berre and Bjerrum 1973; Graham, Crooks, et al. 1983; Lunne and Andersen 2007):

- Anisotropically consolidated samples indicated a general range of ca 10-20 % increase in peak deviator stress for a tenfold increase in strain rate.

- The strain-rate effect in undrained tests appears to be independent of test type (i.e.there is rate-dependency in triaxial compression, extension and direct simple shear). This was also confirmed in triaxial tests presented by Larsson (1980) and Zhou et al. (2005).

- Neither OCR or the plasticity index has major influence on the strain rate effect (based on CAUC, CAUE, DSS and pile load tests).

- Graham, Crooks, et al. (1983) did not identify a lower threshold strain rate where the shear stress-log strain rate relationship decreased. Such a threshold is, however, distinguishable and located in the range of ca 0.01-0.1 %/h in the data presented by Lunne and Andersen (2007), figure 2.21 b).

Bjerrum (1969) and Graham, Crooks, et al. (1983) reported decreasing strain rate effect with increasing strain, however Lunne and Andersen (2007) reported that the rate effect in remoulded Onsøy clay samples did not deviate significantly from the natural clay. In Figure 2.21 two previous compilations of shear stress-log strain rate relationships are presented.
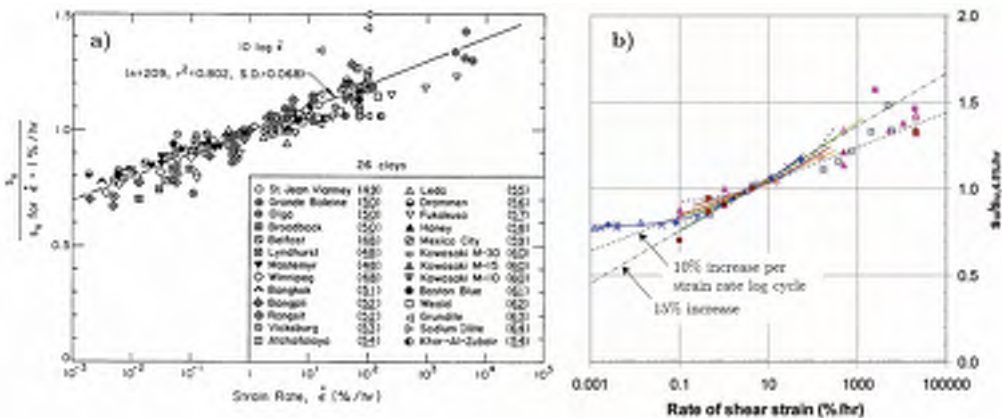
Figure 2.21: *Effect of strain rate on shear stress. Data from a) Kulhawy and Mayne (1990) (CAUC tests) and b) Lunne and Andersen (2007) (CAUC, CAUE, DSS tests) which also includes data from Berre and Bjerrum (1973) and annotations of change in shear stress per change in log-cycle. Note different reference rates for normalisation; 1 %/h in a) and 4.5 %/h in b).*

The time that a soil can withstand an imposed shear stress level is also of interest, and another way of considering (or visualising) the rate effect (Bjerrum 1973). The shear stress levels are then normalised to the value observed at a given rate of loading. Setting 140 minutes as the reference time to failure (approximate for CAUC triaxial tests) some of the data collected are presented in Figure 2.22. In this Figure is also included field vane tests performed with different rates of rotation, resulting in different times to failure.
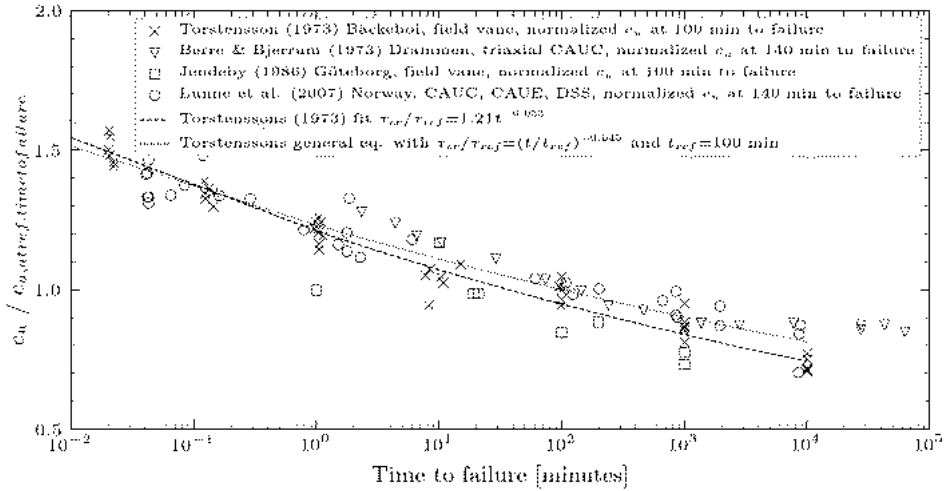
Figure 2.22: *Relationship between time to failure and shear stress. Data from Berre and Bjerrum (1973), Torstensson (1973), Jendeby (1986), and Lunne and Andersen (2007). Note the different reference times used for normalisation.*

Included in Figure 2.22 is also the formula proposed by Torstensson (1973):

$$\frac{\tau_{cr}}{\tau_{ref}} = (t/t_{ref})^{\beta} \tag{2.21}$$

where τ_{cr} is a shear stress for a time to failure t, and τ_{ref} is a reference value obtained at a time to failure t_{ref} and β is a soil parameter. Setting t_{ref}=100 min and β=-0.045 is included in the figure. It can be noted that β is equivalent C_p (eq. 2.19) and a value of -0.06 in eq. 2.21 result in a 15 % change in critical shear stress per time to failure log cycle and β=-0.045 (which seems to be a slightly better fit) result in 11 % change per log cycle.

Larsson (1980) reported tests on a number of Scandinavian clays, and normalised the undrained shear strength from triaxial CAUC, CAUE and DSS tests to vertical preconsolidation pressures. Relations were established between normalised undrained shear strengths and liquid limit. These relations of normalised undrained shear strengths were then checked against reported failures, i.e. a methodology similar to that of Bjerrum 1973. The results suggested that the undrained shear strength obtained from CAU tests at a standard rate (not specified but Author assumes 0.6 %/h based on Larsson, 1980) was applicable. It should be noted that this conclusion, however, depends on the strain rate in the field case records to which the triaxial test data were compared.

2.2.5.5 Creep and relaxation

In the review of literature relating to rate-dependence of soil behaviour, the paper by Augustesen et al. (2004) has been useful in clarifying definitions, regarding e.g. creep

and relaxation. For clarity in the later sections of this report, some of these definitions have been included in Figure 2.23. Creep is defined as deformation under constant effective stress, and relaxation as change in stress under constant deformation (Fig. 2.23 a and b). The soil response behaviour of relaxation is thus almost an intuitive inverse of creep (viscous response to constant deformation, respectively, constant stress) and triaxial relaxation tests have been reported by for example Graham, Crooks, et al. (1983), Silvestri et al. (1988), and Grimstad, Degago, et al. (2010).

A typical result of a single load increment of an oedometer creep test is given in Figure 2.23 c), including the coefficient of secondary compression, $C_{\alpha\varepsilon}$ (in this report referred to as C_α and in Sweden sometimes referred to as α_s). Creep occur during primary and secondary compression if following "hypotheses B" as defined by Ladd et al. (1977), however pure creep strains can only be determined after the excess pore water has dissipated at the end of primary consolidation (EOP).
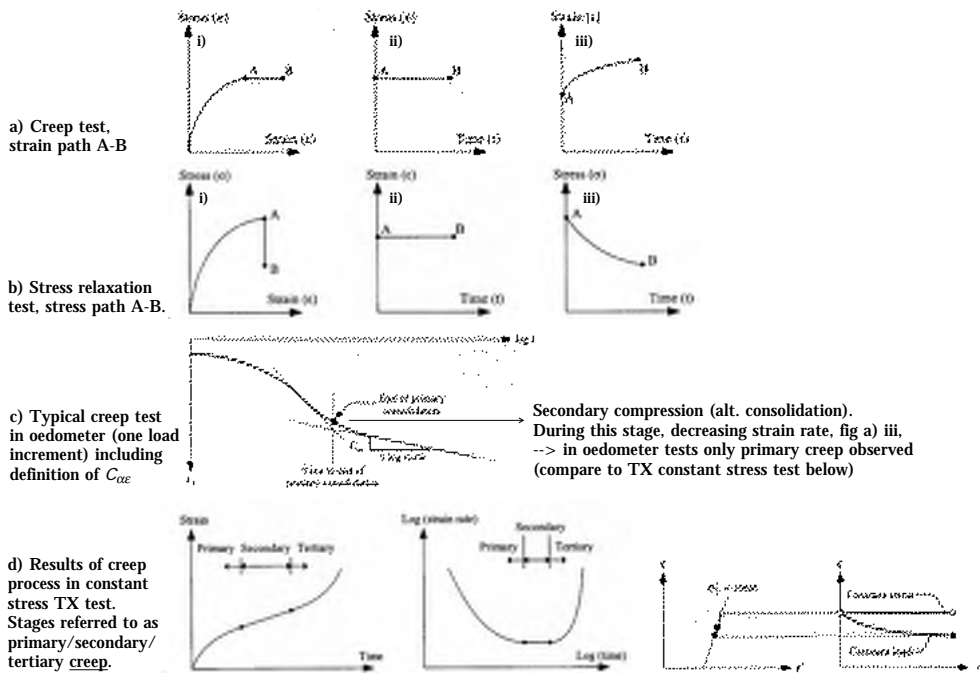
Figure 2.23: *Definitions relating to creep and relaxation. Compiled from Augustesen et al. (2004).*

The concept of delayed (secondary) compression and decreasing strain rate under oedometer conditions was illustrated by Bjerrum (1967), Figure 2.24. It can be noted that over the 5 log cycles of time in Figure 2.24, illustrating delayed compression during 3000 years, approximately 60 % is developed during the first 3 log-cycles i.e. within the first 30 years. The strain rate thus decreases for oedometric conditions as illustrated also in Fig. 2.23 c) iii.
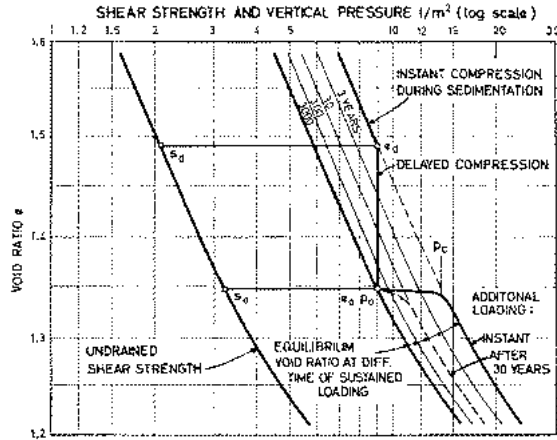
Figure 2.24: *Illustration of delayed compression. From Bjerrum (1967).*

Figure 2.23 d) illustrates the results of a constant stress triaxial creep test (the load is increased as the sample deforms). The stages are referred to as primary creep (decreasing strain rate), secondary creep (constant strain rate) and tertiary creep (increasing strain rate). Such behaviour can be observed also during e.g. static pile load tests and also in e.g. undrained creep tests as presented by Larsson (1977). From the undrained creep tests plotted in Figure 2.12, Larsson (1977) concluded that effective stresses under undrained conditions stabilised when the major effective stress corresponded to 80 % of the preconsolidation pressure (not specified at what strain rate this was determined) in that direction, see Figure 2.25. With respect to the undrained creep failure, a time correction factor of 0.8 was therefore suggested for long-term conditions. This is equivalent to creep loads (i.e. limiting load for creep failure not to occur) that in pile load tests are often found to be 0.7-0.8 of the ultimate load determined in short-term static load tests (Bergström 2017).
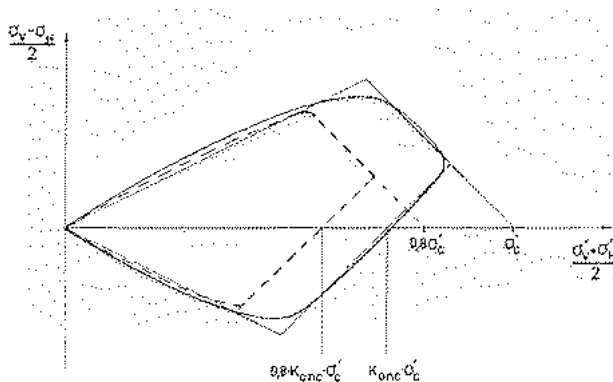
Figure 2.25: *Long-term apparent yield surface (dashed lines) deduced from undrained creep tests (Larsson 1977).*

The coefficient of secondary compression, defined in Fig. 2.23, is dependent on the stress level to which the soil is subjected during a load increment in the oedometer. Maximum values of C_α for soft Gothenburg clay were found by Claesson (2003) and Olsson (2013) at stress levels corresponding to 1.1 to 1.4 times the apparent preconsolidation pressure determined by CRS tests (at standard testing rate 0.0025 mm/min equal to 0.75 %/h). Tests on remoulded samples indicate that this is partly an effect of destructuration (as C_α for the intact and remoulded samples tends to converge at high stress levels). The creep number, r, is related to C_α according to:

$$r = \frac{2.3(1 + e_0)}{C_{\alpha\varepsilon}} \tag{2.22}$$

which in turn is the inverse of the modified creep index, μ^*. Values of r determined by Olsson (2013) are presented in Figure 2.26 for comparison in Section 6 with laboratory tests on remoulded samples for additional site characterisation.
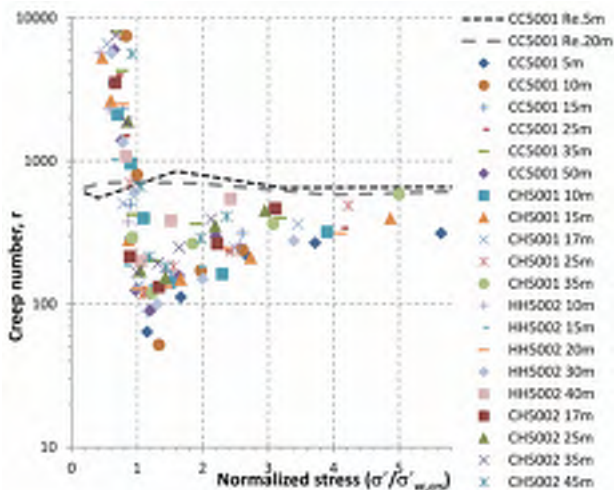
Figure 2.26: *Creep number, r, versus stress level. From Olsson (2013).*

2.2.6   Destructuration and bonding

Expanding on the model for delayed (secondary) compression by Bjerrum (1967), Leroueil and Vaughan (1990) included the effect of the development of soil structure with time. Leroueil and Vaughan (1990) described the effects of structure on the behaviour of clay soils and described the failure in triaxial shearing, compression and swelling. The relevance of considering structure (or rather destructuration) in excavation problems, with typically deviatoric stress paths, is that destructuration may occur as a result of plastic strains when effective stresses gradually decrease (as a result of consolidation) and ultimately may contribute to failure (Bertoldo and Callisto 2016).

Figure 2.27 illustrates how secondary compression due to reduction in void ratio result in an increased apparent preconsolidation pressure and shear strength (points B and yield surface B). Additional strength is however gained due to structure (apparent bonding) in the material, contributing to the increase from points and yield surface B to P. Structure was defined by Burland (1990) as increase in stiffness and strength due to combined effects of rearrangement of particles (thixotropy or 'fabric') and interparticle bonding (cementation due to chemical changes e.g. bonding by oxides or carbonates).
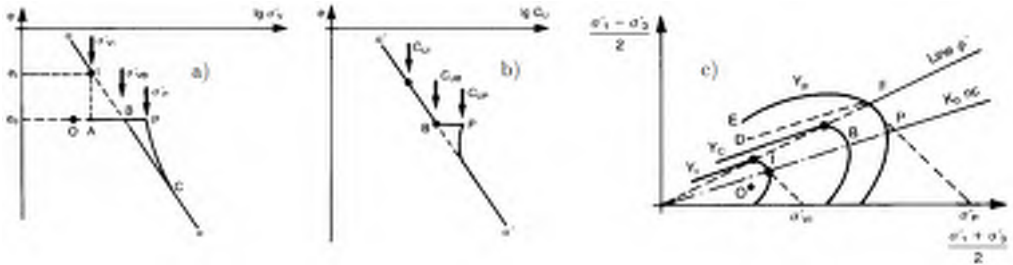
Figure 2.27: *Effect of secondary (delayed) compression and structure on a) apparent preconsolidation pressure b) shear strength and c) yield surface. From Leroueil and Vaughan (1990).*

Destructuration is also possible, and the state of a clay sample which has lost its structure is referred to as the intrinsic state. Intrinsic soil properties were reviewed for example by Burland (1990) and examples of the effect of destructuration is given in Figure 2.28 a) from Burland (1990) and b) from laboratory tests on Gothenburg clay presented in Chapter 6. Figure 2.28 a) has been annotated based on Leroueil and Vaughan (1990) to highlight that the stresses above the ICL-line are enabled due to structure. For additional laboratory tests related to intrinsic soil properties of soft Gothenburg clay, see Section 4.3.
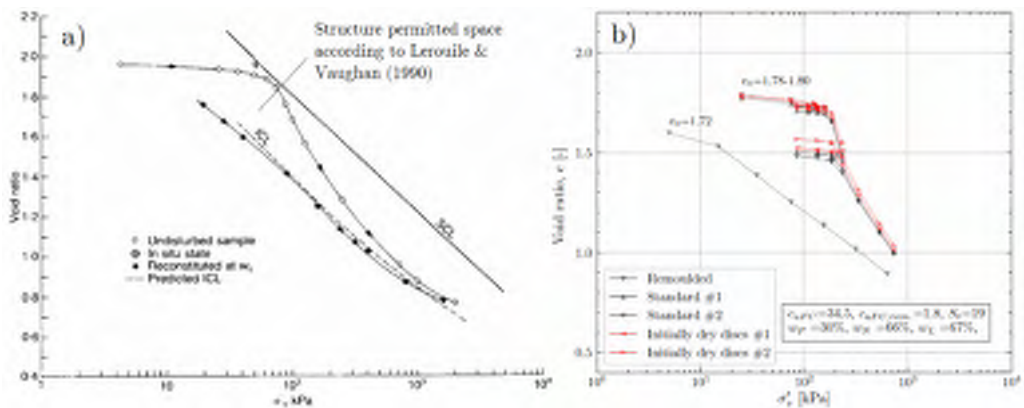
Figure 2.28: *Illustration of destructuration on compression curves for a) Bothkennar clay (SCL and ICL are sedimentaion and intrinsic compression lines) from Burland (1990) and b) Gothenburg clay as presented in Section 4.3.*

In his Rankine lecture Leroueil (2001) summarised the potential effects of destructuration and also noted that destructuration can be caused by compression, shearing or swelling. According to him the heave due to unloading consists of two mechanism: a) primary heave (denoted swelling by Leroueil) caused by change in effective stress and b) secondary heave caused by readjustment of particles and aggregates (destructuration) to new stress state. During unloading two outcomes/scenarios were described with respect to destructuration: 1) bonds are strong enough to withstand zero or negative effective stresses and soil remains intact 2) effective stresses are too small compared to bond forces and destructuration starts. What was denoted as secondary heave, will occur if 2) is fulfilled. In review of the work by Larsson (1977), it is possible that a threshold level for destructuration of soft Gothenburg clay in extension is located at a vertical effective stress level corresponding to approximately $0.4\sigma'_{vc}$, for which delayed swelling due to destructuration of bonds may occur.

2.2.7 Earth pressure coefficient at-rest, K_0

The ratio of horizontal and vertical effective stresses in soil is expressed by the earth pressure coefficient at-rest:

$$K_0 = \frac{\sigma'_h}{\sigma'_v} \tag{2.23}$$

K_0 is thus a representation of a 2D stress state in the soil. The subscript $_0$ is commonly included in literature even tough the stress state that K_0 represent does not necessarily reflect at-rest conditions. The ratio will be reviewed with respect to influence of the stress state and time as K_0 reflects the changes in the soil characteristics during the formation (consolidation history) to its present shear stress level. This highlights the importance of the ratio, as it contributes for example to shear stress induced anisotropy and also to the mobilised lateral earth pressures against permanent underground structures.

In 1944 Jaky derived an equation for the at-rest earth pressure coefficient, which was later simplified somewhat according to Jaky (1948):

$$K_0 = 1 - sin\phi' \tag{2.24}$$

where ϕ' is the friction angle. Brooker and Ireland (1965) suggested K_0=0.95-$sin\phi'$ for cohesive soils and further studied the influence of OCR on K_0. Hence they illustrated that eq. 2.24 holds for soft clays in the normally consolidated state (i.e. primary loading). The general validity of equation 2.24 was highlighted by Mayne (1982) by compilation of data from 81 cohesive soils. Due to eq. 2.24 being valid in the normally consolidated state, Mayne denoted it K_0^{nc}. In a more recent study including K_0 triaxial testing of clays worldwide (Japan, Scotland, Norway, Thailand, Indonesia and Canada); Watabe et al. (2003) found and differentiated:

$$K_0^{nc} = 0.95 - sin\phi'_{peak} \tag{2.25}$$

$$K_0^{nc} = 1.05 - sin\phi'_{CSL} \tag{2.26}$$

where ϕ'_{peak} and ϕ'_{CSL} correspond to the peak and critical state friction angle, respectively. This points to the importance of considering the definition and value of ϕ' in estimation of K_0^{nc}. Data from Watabe et al. (2003) is included in Figure 2.29.
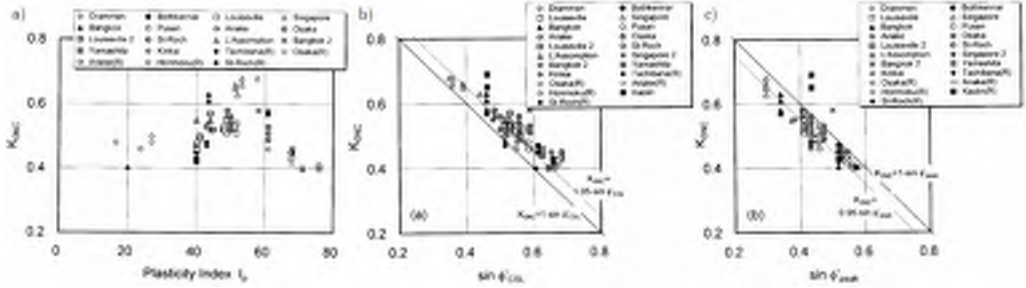
Figure 2.29: *Worldwide data on K_0^{nc} including definitions and refinement with respect to ϕ' in Jaky's formula. From Watabe et al. (2003).*

Triaxial so called K_0-tests[1] on Swedish clay (Kullingsjö 2007; Olsson 2013) and oedometer tests with measurement of radial stress (Sällfors 1975) indicate values of K_0^{nc} in the range of 0.50-0.55, respectively 0.53, for a truly normally consolidated state, $\sigma'_v/\sigma'_{vc}>1.5$ approximately, see Figure 2.30. The data agrees well with data from Watabe et al. (2003), Figure 2.29 a), for a typical homogenous Swedish clay with water content ranging from 60-90 % and plastic limit approximately 30 % (e.g. Wood 2014, on fresh clay samples from Gothenburg) and the laboratory site characterisation data presented in Section 4.3.

As seen in Figure 2.30, K_0 vary with stress level and load history with K_0^{nc} stabilising at high stress levels ($\sigma'_v/\sigma'_{vc}=1/OCR>1.5$). The lower values of K_0 at 1/OCR ca 1.0 was by Olsson (2013) attributed to destructuration. Similar findings, i.e. minimum values of K_0 before reaching constant K_0^{nc} values, were found in some of the clays tested by Watabe et al. (2003), in which the samples were isotropically consolidated. It was found that the drop in K_0 was more pronounced in tests were the stress path reached the CSL line initially after the isotropic consolidation. The results are included in Figure 2.31 and are in line in those by Kullingsjö (2007). The results illustrate that a specimen not consolidated to in-situ stress conditions may experience significant shear stresses during initial stages of testing, i.e. before reaching the asymptotic value of K_0^{nc}.

From review of Figures 2.30, 2.31 and Kullingsjö (2007) it is clear that for certain stress paths, K_0 during loading in the range of $\sigma'_v/\sigma'_{vc}<1.5$ may adopt values lower than K_0^{nc} and $K_0^{in-situ}$. This may be of importance for earth pressures against earth retaining and permanent underground structures, since excavation works may impose stress paths on the active (retained) side to move from the initial state towards upper left (as idealised by stress path A in Figure 2.11); subsequent reloading (for example back filling) may then result in K_0 values lower than $K_0^{in-situ}$ and possibly lower than K_0^{nc} as indicated in the results of Figures 2.30 and 2.31.

---

[1]Here referred to as tests where the vertical stress is varied under condition of constant radial strain ($\Delta\varepsilon_r=0$), i.e. not necessarily $\sigma'_h=\sigma'_{h0}$.
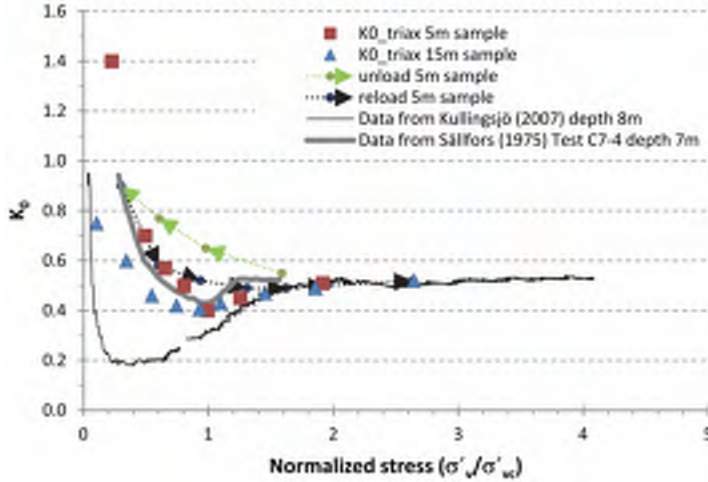
Figure 2.30: K_0 as a function of normalised vertical effective stress level in soft clay. From Olsson (2013) including data from Sällfors (1975) and Kullingsjö (2007). σ'_{vc} derived from CRS-tests.

In addition to structure, the in-situ K_0 is affected by secondary compression (e.g. Watabe et al. 2003; Schmertmann 2012). The special cases of increase in K_0 with time and influence of load history (unloading-reloading) are reviewed in the following paragraphs.

2.2.7.1 Increase in K_0 with time

Schmertmann (1983) raised a question whether the effective horizontal stresses "increase, remain the same or decrease" during the secondary compression of normally consolidated clay under oedometer conditions. Since then, experimental data (e.g. Bjerrum and Holmberg 1971; Bjerrum and Andersen 1972; Jamiolkowski et al. 1985) have shown that the lateral effective stress and thus K_0 will increase with time during secondary compression in soft normally consolidated clays. Schmertmann (2012) confirmed this and further described it being an effect of ϕ' being composed of a primary non-viscous friction component, ϕ'_β, and a secondary viscous/non-stable component, ϕ'_α. With time ϕ' reduce to ϕ'_β, the soil's ability to sustain shear stresses decreases and the horizontal stresses thus increase in order to main equilibrium. Results from Bjerrum and Holmberg (1971) on highly plastic Bangkok clay (w_P=62 %, w_n ca 140 % and w_L ca 155 % in the two samples) are re-plotted in Figure 2.32 (courtesy of communication with Toralv Berre, NGI, in 2019). The samples were loaded above just above $\sigma'_{vc,IL}$ in the oedometer and the trend included in Figure 2.32 indicates approximately $\Delta K_0/\Delta logt$=0.03, however the increase in K_0 with time decrease in less plastic clays (Bjerrum and Andersen 1972).
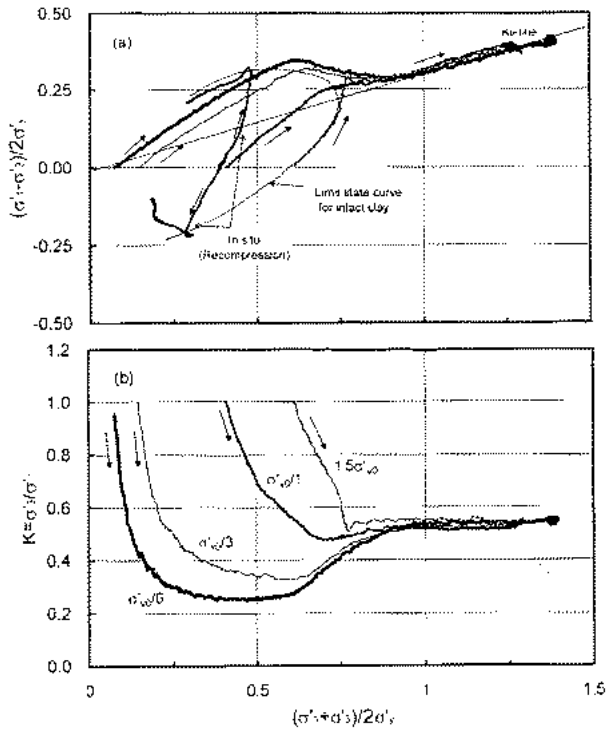
Figure 2.31: *Influence of consolidation stress levels on stress paths (a) and K_0 (b) obtained in triaxial K_0-tests ($\varepsilon_r = 0$). Note that two undrained tests, anisotropically consolidated to in-situ stress levels, are also included in the figure. From Watabe et al. (2003).*
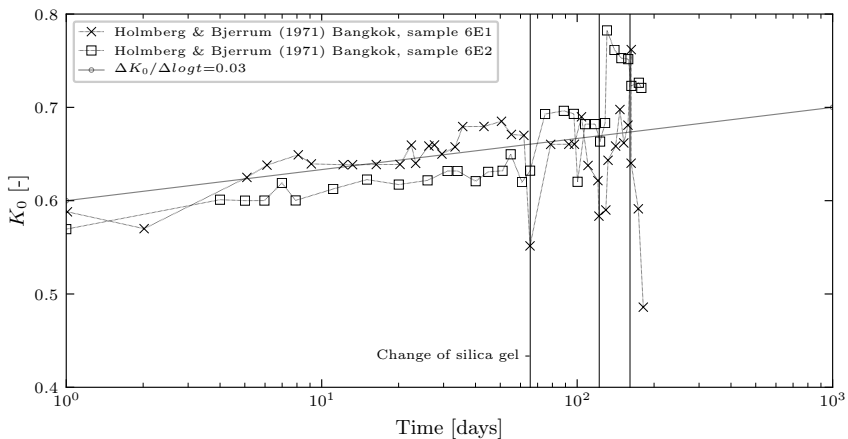
Figure 2.32: *Example of increase in K_0 with time during secondary compression, oedometer tests on highly plastic Bangkok clay. Data from Bjerrum and Holmberg (1971).*

By assuming OCR arising from secondary compression being similar to OCR resulting from unloading, Mesri and Castro (1987), expanded on the work by Schmidt (1966) and presented the following equation to estimate the increase of K_0 due to secondary compression:

$$K_0 = K_0^{nc} OCR^{sin\phi'} = K_0^{nc} \left(\frac{t}{t_p} \right)^{[(C_\alpha/C_c)/(1-C_r/C_c)]sin\phi'} \tag{2.27}$$

where t time, t_p time at end of primary consolidation, C_α creep index, C_c compression index, C_r recompression index and ϕ' friction angle. The 1.2 was dropped out of Schmidt's superscript 1.2sinϕ'. Computed ranges of $\Delta K_0/\Delta \log t$ varied from 0.014 to 0.031 for the four studied clays (C_α/C_c 0.022-0.05). For Gothenburg clay setting; C_r/C_c=0.05 (for example chosen same as Mesri and Castro), C_α/C_c=0.06 based on previously reviewed values for Gothenburg clay (data from Claesson (2003) eq. 2.19), ϕ'=32° (support of Kullingsjö (2007) and "slow" triaxial tests presented in Section 4.3), K_0^{nc}=0.53 (average of range of previous laboratory tests) and t_p=10 years result in Table 2.2 with an average ΔK_0=0.043 per log cycle.

Table 2.2: Increase in K_0 and OCR with time according to eq. 2.27, t_p=10 years.

t [years]	OCR [-]	K_0 [-]	ΔK_0 per log cycle
10	1.00	0.525=K_0^{nc}	-
100	1.15	0.566	0.041
1000	1.33	0.611	0.044
10000	1.53	0.658	0.048

The values of OCR and K_0 in Table 2.2 are likely upper bounds for the set of C_α/C_c and C_r/C_c since t_p was set to 10 years which deposition and primary consolidation of deep clay deposits naturally exceeds. In addition, t_p will vary with depth within a clay deposit depending on the drainage boundary conditions. Further, subsequent man made loading may also to some extent result in "reset" of previous increase in OCR and K_0 with time.

2.2.7.2 Development of K_0 during unloading

Schmidt (1966) re-examined oedometer tests on five remoulded clays presented by Brooker and Ireland (1965) and thereby proposed the following relationship for K_0 during unloading (denoted "rebound" and K_r by Schmidt):

$$K_0 = K_0^{nc} OCR^m \tag{2.28}$$

where m=sin(1.2ϕ') has been found to be approximately 0.60 for Gothenburg clay (Kullingsjö 2007) corresponding to ϕ'=30°. In section 5.3.7 equation 2.28 is compared to evaluated stress states from site measurements. Other empirical formulas have been proposed such as e.g. Kulhawy and Mayne (1990):

$$K_0^{un} = (1 - sin\phi'_{tc})OCR^{sin\phi'_{tc}} \tag{2.29}$$

with $sin\phi'_{tc}$=30° (subscript $_{tc}$ denotes triaxial compression) suggested as a best fit.

In the theoretical case of an isotropic elastic soil K_0 is given by:

$$K_0 = \frac{\nu}{1-\nu} \text{ which result in } \frac{\Delta q}{\Delta p'} = 3\frac{1-2\nu}{1+\nu} \qquad (2.30)$$

Stress paths during unloading for various constant values of ν' (eq. 2.30) as well as the formula by Schmidt (eq. 2.28) are illustrated in Figure 2.33 which is an extension of Figure 2.11. Based on unloading stress paths in K_0 triaxial tests a best fit, constant ν,
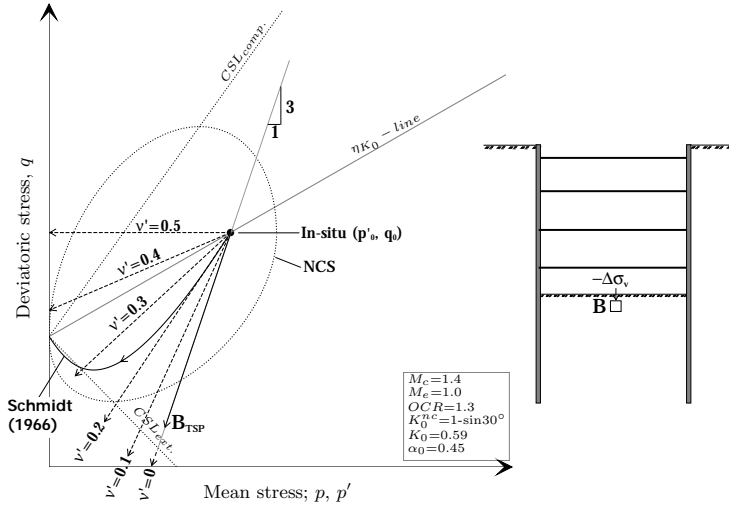
Figure 2.33: *Illustration of stress paths during unloading based on eq. 2.30 (isotropic elastic material, $\nu'=0$-0.5) and empirical formula proposed by Schmidt (1966) eq. 2.28. Stress path B is imposed in a drained (TSP=ESP) standard triaxial extension test.*

for small strains during drained stress reversal, denoted ν'_0, has been found by assigning $\nu'_0=0.15$ for soft Swedish clay (Persson 2004; Kullingsjö 2007). From Figure 2.33 it is clear that the stress path, B, imposed in a conventional drained triaxial extension tests does not follow a more probable stress path ($\nu'_0=0.15$ for small strains and then evolving according to Schmidts formula). In section 5.3.7 equations 2.28 and 2.30 are compared to field measurement data of K_0 during unloading-reloading.

2.2.7.3 Estimation of $K_0^{in-situ}$ from index properties and in-situ tests

In Swedish guidelines (Trafikverket 2016c) an empirical relation of K_0 to liquid limit, w_L, presented by Larsson (1977) is used for estimation of K_0:

$$K_0 = 0.31 + 0.71(w_L - 0.2) \qquad (2.31)$$

K_0 in equation 2.31 was denoted K_0^{nc} by Larsson, who defined K_0^{nc} as "the ratio of maximum 'preconsolidation' stresses". K_0 based on eq. 2.31 is therefore from here on denoted as K_0^{yield}. The basis for eq. 2.31 were comparisons of horizontal stresses calculated

using Schmidt's formula (eq. 2.28 with ϕ'=30°) with field and laboratory measurements of horizontal stresses in Scandinavia. However, Larsson (1977) did not specify which type of field and laboratory methods had been used. Sällfors (1975) specified Glötzl cells and pressometers in the field, and oedometer K_0-testing in the laboratory. Possible errors in estimation of K_0 (in-situ) based on the ratio of preconsolidation pressures (K_0^{yield}) may arise since determination of σ'_{hc} requires straining of the sample, whereas σ'_{h0} refer to effective stress under a zero strain condition. Furthermore, the sample disturbance likely result in increased values of K_0^{yield} (Mesri and Castro 1987).

Field measurements of in-situ K_0 values are scarce, owing to the fact that the installation of measurement equipment to some extent inevitably will change the stress state and/or disturb the soil around the measuring device (Chang et al. 1977; Mesri and Castro 1987; Tong et al. 2013). However, hydraulic fracturing was proposed as a method by Bjerrum and Andersen (1972), whom found good agreement between the measurement data and long-term oedometer K_0-tests on Norwegian clays. Massarsch (1975) highlighted uncertainties associated with the fracturing method (direction of crack, influence of fissures, pockets of permeable material, etc.) and contributed to field measurements of K_0 by use of push-in spade cells including a protection frame (measurements were made at Skå-Edeby during placement of a test fill).

Recent development have e.g. involved evaluation of K_0 from flat dilatometer tests (e.g. Watabe et al. 2003; Wood 2016). Tong et al. (2013) combined seismic (seismic CPT and cross-hole) and resistivity methods (measured in the laboratory) for prediction of in-situ K_0 and compared the results to laboratory tests as well as the formulas from Jaky (eq 2.24) and Kulhawy and Mayne (eq. 2.29). The methods were found to give good agreement to eq. 2.29 in normally consolidated soils whereas correction factors were suggested for evaluation of seismic and resistivity methods when $OCR>2$.

2.2.8 Anisotropy

Clays with one-dimensional loading history exhibit cross anisotropic behaviour arising from; 1) soil structure and particle orientation at microlevel and layering at macrolevel 2) in-situ at rest shear stresses and induced stress path upon loading (Ladd et al. 1977; Ladd 1991; Grimstad, Andresen, et al. 2012). Furthermore, soft natural clay exhibits elastic and plastic anisotropy. However, in this section only plastic anisotropy and the impact of boundary conditions (triaxial or plane strain) is reviewed. For elastic anisotropy see e.g. Graham and Houlsby (1983) for test data and e.g. Grammatikopoulou et al. (2015) for a study of impact when modelling an idealised excavation.

2.2.8.1 Plastic anisotropy

An example of an extensive investigation to determine the yield surface of soft Swedish clay was presented in Larsson 1981. Larsson performed drained triaxial and plane strain tests in various loading directions on clay samples from 5.5 m depth from Bäckebol north of Gothenburg. Based on the results, a simplified yield surface was proposed based on the vertical preconsolidation pressure and the assumed in-situ "at rest" K_0, see Figure 2.34. This simplified procedure for drawing the yield surface of soft Swedish clay was

presented in detail in Larsson and Sällfors 1981. As a result of the shape of the yield
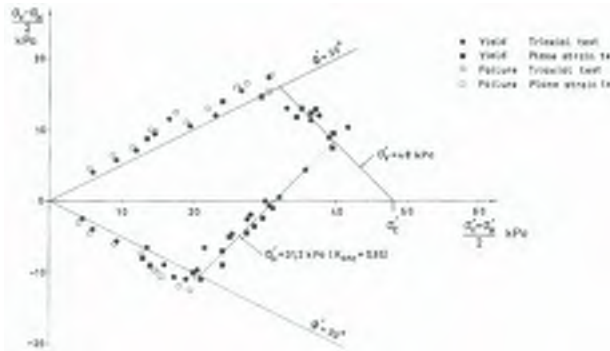
Figure 2.34: *Results of drained triaxial and plane strain tests on clay samples from 5.5 m depth from Bäckebol north of Gothenburg, Sweden. Results from Larsson (1981) including simplified yield surface.*

surface, the emerging ultimate shear strength upon loading of intact natural clays will exhibit plastic anisotropy. The undrained shear strength is thus not a constant but emerging, dependent on the soil deposition (K_0 history), stress history (implicit current void ratio), structure and the effective stress level and the stress path at which the soil is being sheared (the clearest example of anisotropy being that of shearing in compression or extension). Anisotropy in undrained shear strength have been compiled by for example Ladd 1991; Larsson, Sällfors, et al. 2007; Karlsrud and Hernandez-Martinez 2013; Sällfors and Larsson 2016.

For anisotropy expressed as friction angles corresponding to triaxial peak strength envelopes, Westerberg (1999) found $\phi'_{peak,ext}$=ca 1.2-1.3$\phi'_{peak,comp}$. This can be compared to critical state friction angles in Wood (2016) ranging from $\phi'_{CSL,ext}$=1.16-1.41$\phi'_{CSL,comp}$ (input values for soil model) with an average of 1.23 and a larger database (Kulhawy and Mayne 1990) with $\phi'_{TX,ext}$ ranging from ca 1.0-1.5$\phi'_{TX,comp}$ with an average of 1.22.

2.2.8.2 Influence of boundary conditions on anisotropy and strength

The magnitude of the intermediate principal stress, σ'_2, influence the result of testing in for example a plane strain compared to a triaxial test apparatus due to the varying imposed boundary conditions (Kulhawy and Mayne 1990; Grimstad, Andresen, et al. 2012). Ratios of undrained triaxial (TX) and plane strain (PS) compression as well as extension strengths were reported by Ladd et al. (1977):

$$c_{u,TXC}/c_{u,PSC} = 0.95 \pm 0.05 \qquad (2.32\text{a})$$

$$c_{u,TXE}/c_{u,PSE} = 0.82 \pm 0.02 \qquad (2.32\text{b})$$

Further studies on the impact of test boundary conditions were made e.g. by Callisto and Calabresi (1998) whom compared the results from triaxial and true triaxial apparatus

(TTA) tests on Pisa clay. They reported constant p' tests for comparison and reported 24 % lower shear strength in the triaxial test compared to the TTA. Possible differences were attributed to result from e.g. the non-uniform stress state in the triaxial test and the influence of geometry of TTA samples on the development of slip surfaces, i.e. different failure modes in the two types of tests.

Triaxial testing thus results in conservative strengths compared to plane strain testing and TTA tests. Possibly this is why the values for undrained shear strength obtained at a standard strain rate of triaxial testing in Sweden (0.6 %/h) was found by Larsson (1980) to correlate to back-calculated failures. That is, the effect of strain rate on the emerging undrained shear strength in laboratory (most likely results in overestimation compared to field) is cancelled out by the imposed boundary conditions in the triaxial apparatus (conservative results compared to potential plane strain conditions in field).

2.2.9 Heave pressures

2.2.9.1 Introduction and general principle

Vertical contact pressure against underground structures arising from equalisation of negative excess pore pressures (suction) after excavation are here referred to as effective heave pressure, $\sigma'_{v,ehp}$, and abbreviated EHP. EHP can be considered as an effect of restrained or "locked-in" heave (Jendeby 1986) that is remaining after casting of e.g. basement or tunnel slabs and can be illustrated as in Figure 2.35.
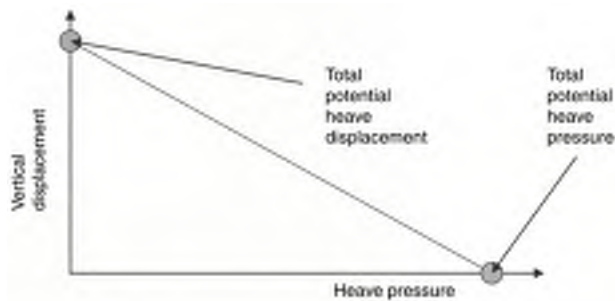
Figure 2.35: *General principle of dissipation of heave pressure with vertical displacement. From Ingram (2012). Notes: 1) vertical displacements can be displacements before and after the structure is in place. 2) assumes simplified linear elastic behaviour and e.g. disregards viscous effects such as stress relaxation.*

In order to establish a further introduction and provide a general picture of the behaviour of effective heave pressures, measurements of an extensively monitored 14 m deep excavation and pile-enhanced raft foundation in London clay is reviewed in the following. Burland and Karla (1986) were involved in the design and considered long-term drained conditions. They estimated EHPs after casting of the raft by imposing upward stresses corresponding to give rise to 70 % of the estimated long-term heave. Piles of ⌀1.8 m and 16 m length

(calculated ultimate shaft resistance 6.4 MN) were located under heavily loaded columns (O'Brien et al. 2012). The results of the monitoring with load cells in the raft foundation (2 m thick slab) and one pile was presented by Price and Wardle (1986), see Figure 2.36.
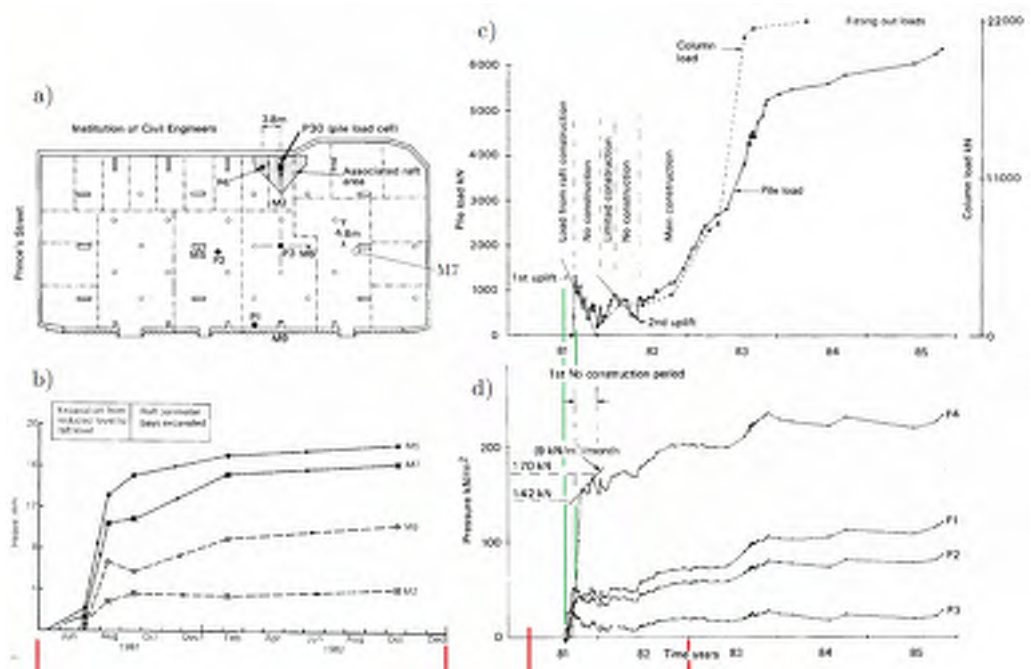
Figure 2.36: *Layout and monitoring of heave and loads at the Queen Elizabeth II conference centre in London. a) Layout b) Heave measurements c) Pile P30 recorded load d) Raft pressures. Figs. a), c), d) from Price and Wardle (1986) and b) from Burland and Karla (1986).*

Uplift loads were recorded in the raft load cells. Reviewing figures c) and d) it can be noted that the pile load reduced during the first time period of no construction, as a result of raft uplift load increasing in the nearby load cell due to heave. The results, furthermore, showed that the pressure cells located near the heavily loaded columns recorded higher pressures. Similarly, cells P1 and P4 near the raft edge developed higher pressures, as expected (stress concentrations for raft performing as an elastic foundation) (Price and Wardle 1986).

In a study on pile-raft foundations, Jendeby (1986) similarly measured initial uplift loads, prescribed as heave pressure (10 kPa) in early stages of the construction. Assuming a excavation depth of 3 m below ground surface the 10 kPa roughly corresponds to a factor $0.3\sigma'_{v0}$ at the excavation level. An example of design considerations of EHPs is that of the Göta Tunnel in Gothenburg, case study in section 3, where the tender documents stated an EHP corresponding to $0.8\sigma'_{v0}$ at the level of the excavation bottom (before excavation

works). This was prescribed as an extreme upper bound and the 0.8-factor was later, after an expert investigation (Alén and Sällfors 2001), revised to 0.25-0.40 depending on the depth of the clay layer beneath the excavation bottom. The analyses comprised analytical calculations of consolidation and effect of deflection of structural elements (i.e. dissipation of heave to reduce EHPs). A complete description of the expert investigation is given in the pre-study to this report (Tornborg 2017). No field measurements were made in order to monitor and compare the design and actual EHPs in the Göta Tunnel project.

As measurement results from field cases are valuable in revealing the full-scale soil-structure response. They are also inherently specific to their context e.g. site geology, loading and stiffness of structure (Simpson 2018). Therefore, parametric studies of heave pressures are reviewed in the following.

2.2.9.2   Parametric studies

Causes of upward/vertical pressures acting against underground structures and factors that may influence the magnitude of such pressures were summarised in Tornborg (2017), see Figure 2.37, and are in line with factors pointed out in a parametric study of EHP by Simpson (2018).
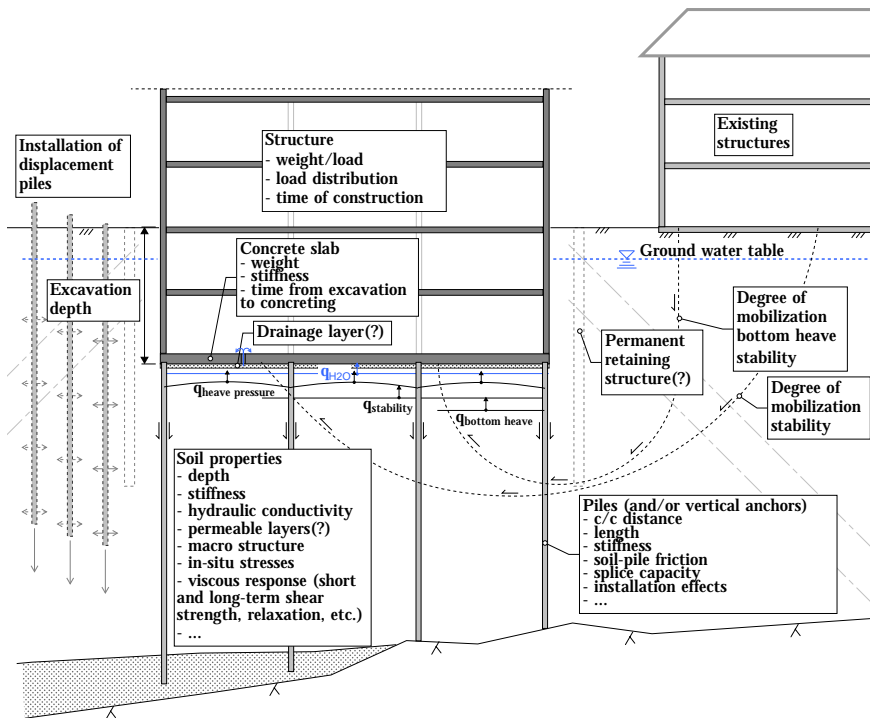
Figure 2.37: *Example of causes that may result in upward/vertical pressures against underground structures and potential influencing factors. Adopted from Tornborg (2017).*

Within the framework of Tornborg (2017), Björk-Tocaj and Toller (2017) carried out a numerical study to investigate the influence of excavation depth, clay depth, time (from final excavation to casting of slab) and pile shaft friction on effective heave pressures. The structural elements (piles and slab) were considered as rigid (i.e. upper bound EHP with respect to structural response) and the piles anchored to bedrock. Soil model parameters (Soft soil creep model) were calibrated against the field case presented by Alén and Jendeby (1996). In Tornborg (2017), these simulations were expanded to include the stiffness of slab and piles. The results are shown in Figure 2.38 for a total clay depth of 35 m and clearly illustrate the effect of time and structural stiffness (both allowing for vertical deformations) on EHP.
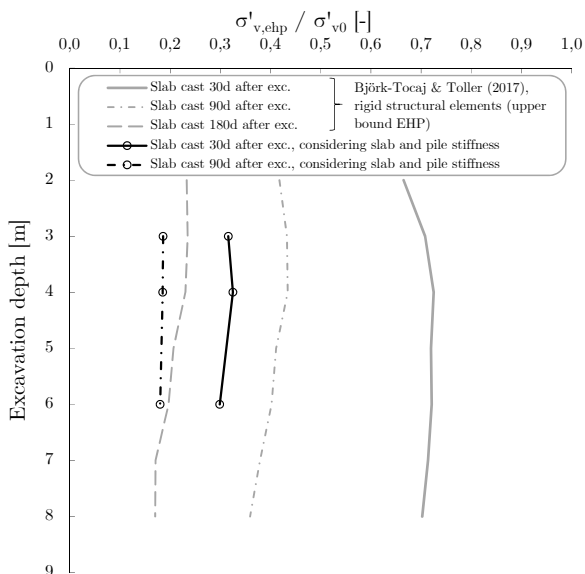
Figure 2.38: *Effective heave pressures, $\sigma'_{v,ehp}$, normalised to in-situ vertical effective stress at excavation level (before excavation), σ'_{v0}. Adopted from Tornborg (2017).*

Based on the results a factor of $\sigma'_{v,ehp}/\sigma'_{v0}$=0.5 was suggested as upper bound for initial estimates of EHPs. Simpson (2018) mentioned such an approach: taking EHP as a proportion of σ'_{v0} for estimation of $\sigma'_{v,ehp}$ could be a useful empirical approach. The study by Simpson (2018) compared the general British industry design principle for heave pressure to parametric FE-analyses. He concluded that the current industry design principle (described by Simpson 2018 and also in e.g. Chan and Madabhushi 2017) was flawed and recommended FEA as the general approach to incorporate realistic soil behaviour including for example strength, anisotropy, slab-soil interface roughness, suction limits and Poisson's ratio. Furthermore, he stated that *"Probably the most important driver for final EHPs is the water pressure (suction) in the ground at the time a slab becomes restrained. This is difficult to predict in real clay materials, which are non-linear in behaviour and often fissured. Field measurements of long-term heave pressures would therefore be very valuable"*.

2.2.9.3 Measures to reduce heave pressure

Since heave pressure reduces with vertical deformation, the most obvious method to reduce heave pressures is to allow deformation by one or a combination of modes; heave before casting the structure, deformation of the structure and/or deformation in the soil beneath the structure (by introducing a heave void). For example, Karlsrud and Andresen (2008) described placement of a 0.2 m compressible layer of glass foam mattresses on top of a 0.3 m gravel drainage layer before casting of an underwater concrete slab (which was followed by dewatering the excavation) for the Oslo opera house. As in the case of the Göta Tunnel, no field measurements were made in order to monitor EHPs in the Opera house project, or in any other project in Norway as known by Kjell Karlsrud (e-mail correspondence in 2020). However, the dissipation of heave pressure (i.e. negative excess pore pressures) can be associated with the reduction of effective stresses in the soil, resulting in loss of the undrained shear strength, reduction of e.g. pile capacity and potential increase in deformations (serviceability) within the structure as well as the surroundings (Ingram 2012).

2.3 Field measurements of earth pressures

This section presents a review of some previous measurements of soil-structure interaction in soft clay, the focus being on previous case studies involving measurements of earth pressures.

2.3.1 Horizontal earth pressures

The apparent earth pressure diagrams reviewed in Section 2.1.4 were at the time derived (back-calculated) from measurements of strut and anchor loads. This section reviews some previous direct measurement of earth pressures, focusing on (long-term) measurements against permanent structures.

2.3.1.1 Earth pressure measurements against permanent structures

The review has identified two studies of recorded long-term monitoring of lateral earth pressures against underground structures. In particular, the study of Carder and Darley (1998) contain data from several sites with instrumentation specifically intended for measurement of long-term earth pressures. Some of the walls, all in stiff overconsolidated clay, were instrumented during construction and measurements were continued, others were instrumented after construction. Some important notes from the findings are given below as it provides understanding on factors influencing long-term performance of underground structures:

- Wall installation needs to be taken into account and modelled in order to produce reliable model predictions of earth pressures.

- Long-term K_0 values of 1 to 1.5 were recorded in earth pressure cells located between 1.1-1.5 m from the instrumented walls. This should be compared to in-situ K_0-values of 1.5-2 in the overconsolidated clays that were studied.

- No significant change in total lateral earth pressures were recorded in long-term measurements (5-24 years after construction). Loads recorded in permanent props increased somewhat during the first years in service and then stabilised. Lateral wall movements continued to develop for about 5 years for walls propped at carriageway level.

- Measured bending moments (specification of how these were derived was only made for one of the case studies, then as being derived from strain gauge measurements on the walls) were less than calculated based on measured lateral total stresses. This was attributed stress relief close to the walls.

Richards et al. (2007) reported measurement of lateral earth pressures and pore pressures covering 6 years after construction of a retained cut with a propped bored pile wall (20 m long $\varnothing$1.05 m) in South-East England (Ashford, very stiff clay, OCR=4-10). It was stated that, according to British standards long-term lateral stresses against the retained side of propped retaining walls in overconsolidated deposits should be estimated based on K_0=1.5. It was, however, pointed out that this may lead to over-design if stresses are reduced and do not recover due to effects of e.g. wall installation or excavation. Measurements showed that the construction activities (wall installation and excavation) resulted in reduction in horizontal stresses. After construction K_0 evaluated on the retained side of the wall corresponded to lower than active limiting earth pressures (friction angles in soil layers varying 22°-27°) in a zone where the deflection of the wall was largest. Measured effective stresses are presented in Figure 2.39.
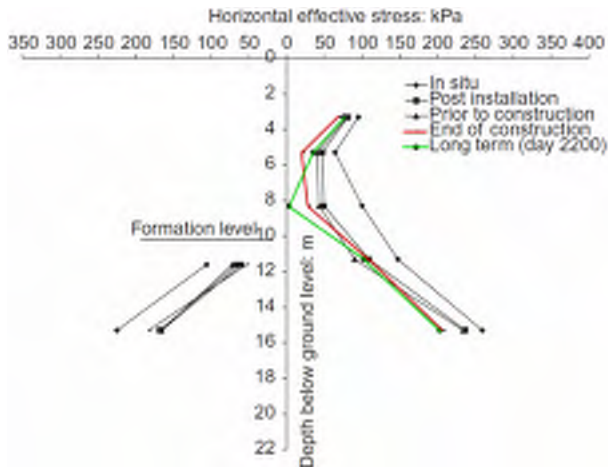
Figure 2.39: *Example of long-term measurements of horizontal stresses (excavation completed day 595 and last measurement day 2200). From Richards et al. (2007) with end of construction and long term highlighted on retained side.*

Gaba, Hardy, et al. (2017) also points to the two studies reviewed above (Carder & Darley and Richards et al.) when looking into long-term measurements of earth pressures. They further state that for walls in stiff overconsolidated clays the long-term effective horizontal earth pressures remain unchanged or reduce after construction. This should however be seen in the light of overconsolidated stiff clays with $OCR>>2$. The trend is also in-line with Jamiolkowski et al. (1985) who reported unchanged or slightly decreasing K_0 for overconsolidated clays with $K_0>1$.

2.3.1.2   Earth pressure measurements against retaining structures

Similar long-term measurements, as presented above by Carder and Darley (1998) and Richards et al. (2007), of horizontal earth pressures against permanent structures in *soft plastic clay* have not been found to this date during the review of literature. However, some of the reviewed measurements of earth pressures against retaining structures in such soils are presented in Table 2.3 (compilation of selected well documented and characterized sites).

2.3.2   Vertical upward earth pressures

The scope of this literature review deals with vertical upward earth pressures caused by restrained or "locked-in" heave, denoted effective heave pressure (EHP). In Section 2.2.9.1 the well documented case study of EHPs measured at the Queen Elizabeth II conference centre was reviewed as an introduction to the description of general behaviour of EHPs. The review has only identified one additional study set-out to monitor long-term vertical upward earth pressures. This was described in Carder and Darley (1998) were 5 pairs of pressure cells were installed in a sand and geocomposite drainage layer below a permanent concrete prop, located under carriageway level and hinged in centreline and in connection to diaphragm walls, at the Aldershot underpass. A reduction of stresses (largest reduction towards centreline) was recorded when the road opened, this was attributed to the sand and geocomposite layer and/or the hinged design of the slab. No data is available on pore pressures, therefore the data is not reviewed further.

From the reviewed data from previous measurements, as well as the reviewed parametric studies on earth pressures (horizontal as well as vertical), it becomes evident that although field measurements provide valuable input on field-scale response of (macro) soil-structure interaction, the data are inherently site specific (e.g. soil properties, construction sequence, geometry and stiffness of the structure). Part of future work, presented in Chapter 6, is therefore recommended to be composed of modelling and laboratory testing in order to study the governing factors for long-term earth pressures against underground structures. Such studies may aim to generalise the effect of e.g. excavation geometry and construction sequence on long-term earth pressures.

Table 2.3: Compilation of some well documented case histories with measurements of earth pressures against retaining structures in soft clay.

Reference and notes	Excerpt of measurement data
Tan and Wang (2013). Excavation in soft Shanghai clay. 18 m deep excavation within 34 m long diaphragm walls, top-down (4 floor levels) peripheral excavation preceded by a bottom-up excavation of a central-island cylindrical shaft. GWT assumed 1.0 m BGS.	
Kullingsjö (2007) excavation studied in Chapter 3. Soft Gothenburg clay. 11 m deep underwater excavation within 26 m long SPWs, one strut level. 0.7 m slab cast before dewatering.	
DiBiagio and Roti (1972). Oslo soft clay. 19 m deep excavation within 20 m long diaphragm wall (installed 1 m into bedrock), top-down (3 floor levels). Excavation was carried out from day 74 to 225 and bottom slab completed day 470. Note increase in total earth pressure partly a result of regain in pore pressures after casting of bottom slab (ground water lowering ceased).	
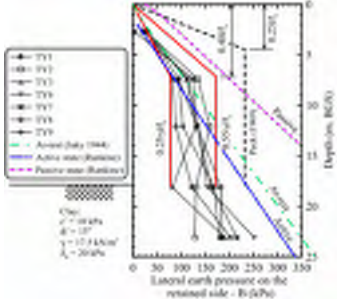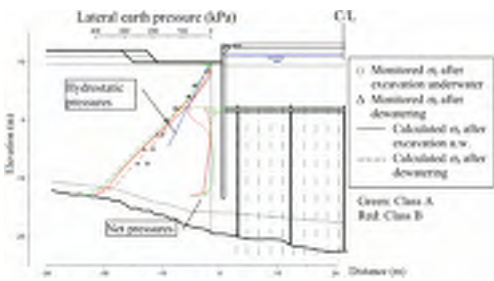
2.4 Numerical modelling

2.4.1 Comparison of constitutive soil models

Table 2.4 present a brief summary of some constitutive soil models encountered in the design and research of excavations in soft clay in Sweden. Key model features are highlighted including references. The next section presents a short description of the Creep-SCLAY1S soil model, including the model formulation, adopted for analyses of the case study (Göta Tunnel) and preliminary analyses of the instrumented site at Hisings Bridge.

Table 2.4: Constitutive soil models used for modelling of soft clays and design of excavations in Sweden.

Model features (✓) (-) = model limitation	NGI-ADP	NGI-ADP soft	SSC	HS-Small	C-SCLAY1S
Total stress	✓	✓	-	-	-
Effective stress	-	-	✓	✓	✓
Anisotropy	✓	✓	-	-	✓
Destructuration	-	✓	-	-	✓
Rate-dependency	-	-	✓	-	✓
Small-strain stiffness	-	-	-	✓	-
Features and major drawbacks	i)	i)	ii)	Constant ν'_{unl}	
References/examples	Grimstad, Andresen, et al. (2012)	Grimstad and Jostad (2012)	Vermeer and Neher (1999) Benz et al. (2013, small-strain extension)	Benz (2007)	Wheeler et al. (2003) Karstunen, Krenn, et al. (2005) Grimstad, Degago, et al. (2010) Karstunen and Amavasai (2017) Gras et al. (2017) and Gras et al. (2018) Petalas et al. (2019)

i) (-) Total stress based, does not include dissipation of negative excess pore pressures following excavation. (+) Anisotropic in strength and stiffness (stress path dependent non-linear hardening, allows for "pseudo" small-strain stiffness).

ii) Assumes contours of constant volumetric creep strain, result in overestimation of creep rate for stress states close to critical state (as η/M approach 1). See analogue for the Anisotropic Creep Model (ACM) in Sivasithamparam (2012).

2.4.2 A short description of the Creep-SCLAY1S model

The Creep-SCLAY1S model is based on critical state soil mechanics (Schofield and Wroth 1968) and is a rate-dependent extension of the Modified Cam Clay (MCC) model. The model also features anisotropy and destructuration and builds on the ACM (Leoni et al. 2008) and SCLAY1S models (Karstunen, Krenn, et al. 2005) with a plastic multiplier for creep strain rate (Grimstad, Degago, et al. 2010). The model formulation does not account for small-strain stiffness. Model features has been added gradually, so by switching these off the model falls back to a rate-dependent isotropic MCC model. The parameters of the Creep-SCLAY1S model are summarised in Table 2.5. Additionally the following parameters are used as model input values:

- Overconsolidation ratio, OCR, or pre-overburden pressure, POP.
- Initial void ratio, e_0.
- Poisson's ratio, ν' (constant, influence on elastic behaviour).
- Earth pressure coefficient at rest for normally consolidated state, K_0^{nc}.

Table 2.5: Creep-SCLAY1S model parameters.

Type of parameter	Parameter symbol	Definition
Conventional (MCC)	$\lambda_i^{*1)}$	Modified intrinsic compression index
	$\kappa^{*1)}$	Modified swelling index
	M_c	Stress ratio at critical state in triaxial compression
	M_e	Stress ratio at critical state in triaxial extension
Anisotropy	α_0	Initial amount of anisotropy
	ω	Rate of rotational hardening
	ω_d	Relative rate of rotational hardening due to deviator strain
Destructuration	χ_0	Initial amount of bonding
	a (alt. ξ)	Rate of destructuration
	b (alt. ξ_d)	Relative rate of destructuration due to deviator strain
Viscous	μ_i^*	Modified intrinsic creep index
	τ_{ref}	Reference time (days)

[1] Input of κ and λ for the MCC model. Subscript $_i$ refer to modified intrinsic compression index in the SCLAY1S model

2.4.2.1 Components of strain

The total strain is assumed to be composed of elastic and viscoplastic (creep) strains according to:

$$\dot{\varepsilon_v} = \dot{\varepsilon_v^e} + \dot{\varepsilon_v^c} \tag{2.33a}$$

$$\dot{\varepsilon_q} = \dot{\varepsilon_q^e} + \dot{\varepsilon_q^c} \tag{2.33b}$$

The subscripts v and q refers to volumetric and deviatoric strains respectively. Superscripts e and c refers to elastic and viscoplastic components and dot symbol has the meaning of strain rate (differentiation with respect to time) (Sivasithamparam et al. 2015). From eqs. 2.33 it follows that there is no purely elastic domain in the model. The elastic component of strain is (as in laboratory) observed during fast unloading-reloading, the viscoplastic (creep) component is irrecoverable and time-dependent (Leoni et al. 2008).

2.4.2.2 Elastic behaviour

The isotropic description of elasticity in the model results in the volumetric and deviatoric strains being related to the bulk and shear modulus, as in the MCC model (alternatively to Young's modulus and Poisson's ratio). In incremental form, the strains can be written as (Wood 1990):

$$d\varepsilon_v^e = \frac{dp'}{K'} \tag{2.34a}$$

$$d\varepsilon_q^e = \frac{dq}{3G} \tag{2.34b}$$

where bulk modulus, K', and shear modulus, G, govern the elastic change in volume (size) and shape respectively. Note that the undrained bulk modulus, $K_u = \infty$ ($\rightarrow \nu_u = 0.5$) whereas the shear modulus is unaffected by drainage conditions (given a change in deviator stress is independent of pore pressure) (Wood 1990). The bulk modulus, K', and shear modulus, G, can be determined e.g. from drained triaxial tests (from undrained test only G). The bulk modulus, K', is defined by the expression:

$$K' = \frac{vp'}{\kappa} \text{ where } \kappa = \kappa^*(1+e) \text{ and } \kappa^* = -\frac{\varepsilon_v - \varepsilon_{v0}}{ln(p'/p_0')} \tag{2.35}$$

and as a result $K' = p'/\kappa^*$. v is specific volume and κ compression index. E' is the drained Young's modulus. Note $d\varepsilon_v = (-dv/v)$ i.e. an increment in specific volume corresponds to an increment in volumetric strain. The shear modulus, G, can be related to the bulk modulus according to:

$$G = K' \frac{3(1-2\nu')}{2(1+\nu')} \tag{2.36}$$

which implies that the shear modulus (via the bulk modulus) is related to mean effective stress level. Note E' and E_u are the drained and undrained values of Young's modulus, and as seen above they are not independent. The relationship of oedometer modulus (one

dimensional compression) to Young's modulus and Poisson's ratio is given according to (Wood 2018):

$$E'_{oed} = E' \frac{(1 - \nu)}{(1 + \nu)(1 - 2\nu)} = K' + \frac{4}{3}G \qquad (2.37)$$

2.4.2.3 Intrinsic, current and normal compression surfaces

The Creep-SCLAY1S model (extending on the SCLAY1 and SCLAY1S models) does not incorporate a static yield surface, but a normal compression surface (NCS) which in triaxial stress space is defined by a sheared ellipse according to:

$$f_{NCS} = (q - \alpha p')^2 - (M(\theta)^2 - \alpha^2)(p'_m - p')p' = 0 \qquad (2.38)$$

where p'_m is the isotropic preconsolidation pressure. $M(\theta)$ is the modified, Lode angle dependent, value of M (stress ratio at critical state) incorporating that in-between the extreme values of M_c in triaxial compression (θ=-30°) and M_e in extension (θ=30°), M is a function of the (full 3D) stress state.

The current stress state is described by a current state surface (CSS) and the intrinsic state with an intrinsic compression surface (ICS). The ICS is an imaginary surface that would exist if the effect of soil structure (fabric and bonding) was to be completely removed yet keeping the void ratio the same. These surfaces all have the same shape and inclination but differ in size as illustrated in Figure 2.40.
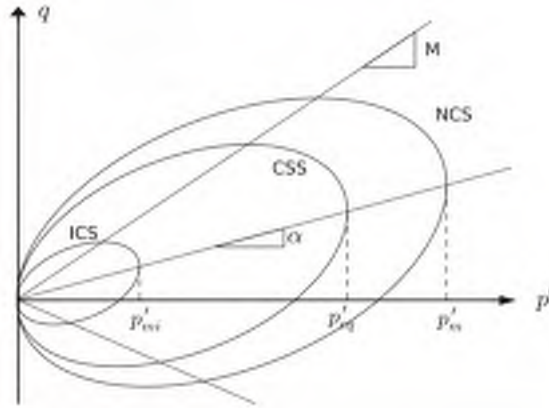
Figure 2.40: *Intrinsic compression surface (ICS), current state surface (CSS) and normal compression surface (NCS) of the Creep-SCLAY1S model. From Amavasai, Sivasithamparam, et al. (2018).*

The initial value of α, i.e. α_0, can be estimated based on (Wheeler et al. 2003) for normally consolidated or lightly overconsolidated clays as:

$$\alpha_0 = \frac{\eta_0^2 + 3\eta_0 - M_c^2}{3} \tag{2.39}$$

where $\eta_0 = 3(1 - K_0^{nc})/(1 + 2K_0^{nc})$ (Sivasithamparam 2012). The inclination of the sheared ellipses thus corresponds to that of one-dimensional consolidation.

Rewriting eq. 2.38, the equivalent mean effective stress, p'_{eq}, can be calculated according to:

$$p'_{eq} = p' + \frac{(q - \alpha p')^2}{(M(\theta)^2 - \alpha^2)p'} \tag{2.40}$$

The initial value of the isotropic preconsolidation pressure, p'_m, is calculated according to eq. 2.40 by inserting:

$$\alpha = \alpha_0 \ , \ p' = (\sigma'_{vc} + 2\sigma'_{vc}K_0^{nc})/3 \text{ and } q = \sigma'_{vc} - \sigma'_{vc}K_0^{nc} \tag{2.41}$$

The overconsolidation ratio at the hydrostatic axis, OCR^*, is defined as:

$$OCR^* = \frac{p'_m}{p'_{eq}} \tag{2.42}$$

The size of the intrinsic and normal compression surfaces are related according to:

$$p'_m = (1 + \chi)p'_i \tag{2.43}$$

where χ describes the current amount of structure in the soil (evolves with hardening law as described in the nex paragraph).

2.4.2.4 Hardening laws

The model incorporates three hardening laws which are related to; isotropic hardening, rotational hardening (feature of SCLAY1 model) and destructuration (added in SCLAY1S model) In the following paragraphs the hardening laws are outlined for the case of triaxial stress space for simplicity (not full 3D-formulations).

Volumetric hardening law: The hardening law that describes expansion of the intrinsic yield surface (to which the size of the NCS is related via eq. 2.43) due to viscoplastic volumetric strains, $d\varepsilon_v^c$, is defined as (Sivasithamparam 2012):

$$dp'_{mi} = \frac{p'_{mi}}{\lambda_i^* - \kappa^*}d\varepsilon_v^c \tag{2.44}$$

Note: setting χ=0 reduce Creep-SCLAY1S to Creep-SCLAY1 and the intrinsic modified compression index in eq. 2.44 should then be replaced by λ^*.

Rotational hardening law: Evolution of anisotropy is related to viscoplastic volumetric, $d\varepsilon_v^c$, and deviatoric strains, $d\varepsilon_q^c$ according to (Sivasithamparam et al. 2015):

$$d\alpha = \omega \left[\left(\frac{3\eta}{4} - \omega_d \right) \langle d\varepsilon_v^c \rangle + \omega_d \left(\frac{\eta}{3} - \alpha_d \right) |d\varepsilon_q^c| \right] \tag{2.45}$$

The parameter ω thus controls the rate at which the compression surfaces rotate (change of α) and ω_d controls the effectiveness of deviatoric viscoplastic strains in this rotation to the target value of α for a given stress path. Experimental evidence of target values for α for various stress paths (imposed viscoplastic strains) in soft clay is presented e.g. in Wheeler et al. (2003). Macaulay brackets, $\langle \rangle$, are included for $\langle d\varepsilon_v^c \rangle = d\varepsilon_v^c$ for $d\varepsilon_v^c > 0$ and $\langle d\varepsilon_v^c \rangle = 0$ for $d\varepsilon_v^c < 0$.

Hardening law related to destructuration: Similar to the rotational hardening law, the degradation of structure is related to volumetric and deviatoric viscoplastic strains:

$$d\chi = -a\chi \left[|d\varepsilon_v^c| + b|d\varepsilon_q^c| \right] \tag{2.46}$$

where a and b controls the rate of destructuration. Note: a and b are in some papers referred to as ξ and ξ_d respectively. a and b are parameters that have to be determined by model calibration against triaxial and oedometer test data. The value of χ_0 can be assumed to be related to sensitivity, S_t, according $\chi_0 = S_t - 1$ (Sivasithamparam 2012) but also need to be calibrated against laboratory data.

2.4.2.5 Viscoplastic formulation

Elastic and viscoplastic strains make up the total strains. Equations for elastic strains were outlined in eq. 2.34. The Creep-SCLAY1S model assumes an associated flow rule (vector of viscoplastic strain increment normal to the NCS) and the viscoplastic strain rates are thus calculated according to (Sivasithamparam et al. 2015):

$$\dot{\varepsilon}_v^c = \dot{\Lambda} \frac{\partial p_{eq}'}{\partial p'} \text{ and } \dot{\varepsilon}_q^c = \dot{\Lambda} \frac{\partial p_{eq}'}{\partial q} \tag{2.47}$$

where $\dot{\Lambda}$ is the rate of the viscoplastic multiplier introduced by Grimstad, Degago, et al. (2008):

$$\dot{\Lambda} = \underbrace{\frac{\mu_i^*}{\tau_{ref}} \left(\frac{p_{eq}'}{p_m'} \right)^\beta}_{\text{i)}} \underbrace{\left(\frac{M^2(\theta) - \alpha_{K_0^{nc}}^2}{M^2(\theta) - \eta_{K_0^{nc}}^2} \right)}_{\text{ii)}} \tag{2.48}$$

where the ii) term is added to ensure that the predicted creep strain rate reduce to i) for oedometer conditions (Sivasithamparam et al. 2015). β is defined as:

$$\beta = \frac{\lambda_i^* - \kappa^*}{\mu_i^*} \tag{2.49}$$

Due to β being a power of $p'_{eq}/p'_m=1/OCR^*$ in equation 2.48, β and the overconsolidation ratio have major impact on the predicted creep strain rates. This is illustrated in Figure 2.41 for a case where $\beta=27$ ($C_c=0.15$, $C_s=0.015$ and $C_\alpha=0.005$). It can be noted that this illustration of decreasing creep strain rate for increasing OCR is analogous to Bjerrum's illustration of delayed compression in figure 2.24.
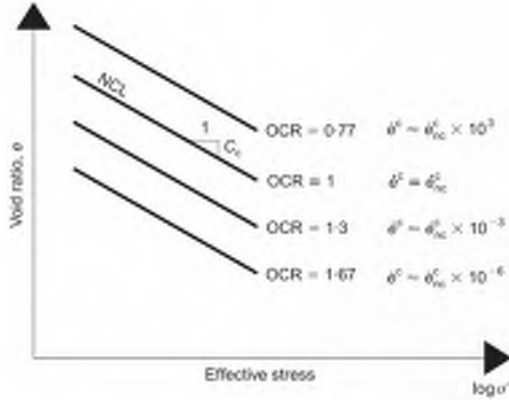
Figure 2.41: *Illustration of impact of OCR on creep strain rate. From Leoni et al. (2008).*

Finally, in incremental form the volumetric creep strain over time can be written as (Sivasithamparam 2012):

$$d\varepsilon_v^c = dt\dot{\Lambda}\frac{\partial p'_{eq}}{\partial p'} \text{ where } t \text{ is time.} \tag{2.50}$$

For further details on the Creep-SCLAY1S model, see references in Table 2.5.

In order to benchmark the viscous response of the Creep-SCLAY1S model with a given parameter set, comparison of model response to empirical strain rate dependency have been made at element level. Comparisons are presented in Appendix A with respect to rate-dependency of apparent preconsolidation pressure and undrained shear strength.

2.5 Review of research questions and proposed research

During the literature review, some light was cast upon some of the research questions posed during the initiation of this project. The initial research questions are therefore, based on the literature review, commented briefly on below and proposed research is suggested.

2.5.1 Review of research questions

The following questions were posed as examples of research questions during the initiation of this project:

- How do the effective stresses in the soil develop during the construction and design lifetime?

    - The effective stress state is initially depending on the undrained response immediately after excavation. This immediate response is in turn depending on factors such as: excavation geometry, stability number, soil behaviour, retaining wall system and stiffness.
    - The effective stresses thereafter depend on imposed loading and the equalization of excess pore pressure (consolidation) and viscous behaviour of clay (possibly resulting creep induced deformations and excess pressures).

- How do the horizontal earth pressures develop with time against the underground structure?

    - As the review shows the horizontal earth pressure and thus K_0 increase during secondary compression in normally or lightly overconsolidated clays. However, the increase under oedometer conditions is modest for a design lifetime of ca 100 years ($\Delta K_0 / \Delta \log t$ ca 0.04 per log cycle in time). Furthermore, as K_0 reflect a (2D) stress state the K_0 around underground structures will be influenced by construction works such as e.g. pile installation and excavation (lab.tests and long-term field measurements Carder and Darley 1998; Watabe et al. 2003; Richards et al. 2007). Neither the influence of time or the effect of construction processes on the long-term design earth pressures are rarely taken into account in design. The Swedish guidelines typically focuses on design K_0 corresponding to $K_0^{in-situ}$. Such an approach represent the interaction of structure and soil being by means of independent springs (Muir Wood 2004) and does not include e.g. soil-structure interaction or stiffness, excavation geometry, etc.

- What is the effect of rate-dependency on the emerging soil strength? Normally design is carried out for the (theoretical) extreme cases of undrained and/or drained analysis. Rate-dependent analysis, taking the transient progress into account, can possibly result in optimisation.

- The emerging shear strength is dependent on the stress state (OCR), imposed loading (direction and rate), consolidation and viscous behaviour of clay. Because of this, consolidation (equalisation of excess pore pressures and suction) and viscous behaviour (increasing viscoplastic strains for loading close to or outside the normal compression surface) must both be included when considering the rate-dependent response of excavations in soft clay.

- Will upwards effective heave pressures ("locked-in" heave) develop in the short- or long-term due to the rate-dependent response of heave?

  - The literature review highlights that this aspect is highly recognised and accounted for in the design of underground structures in overconsolidated low-permeable clays, such as e.g. London clay. Measurement data are, however, scarce and no measurements specifically targeting heave pressure in plastic normally consolidated clay have been found in the review of literature.

- How do the excavation and/or underground structure effect the settlements in adjacent ground and structures in the long-term?

  - Large databases of deformations during the construction phase have been reviewed. Long-term monitoring seems to be scarce, although satellite techniques provides a possibility to assess the long-term performance and impact of underground structures on the surroundings.

- How do on-going background creep settlements influence the questions raised above?

  - From the literature review it is evident that the viscous behaviour of clay influences the short- and long-term performance of excavations and underground structures in soft clay. Many "rheological" models have developed in order to account for viscous behaviour separately (creep settlements, strain-rate dependent preconsolidation pressure and undrained shear strength). Numerical modelling with constitutive models taking a more "unified approach" to incorporate viscous behaviour provides possibility to study the effects that background creep settlements have on underground structures. For example, in the case of upwards effective heave pressures, creep settlements in adjacent ground impose a "boundary condition" which may limit and/or counteract the upward movement with time.

From the above it is clear that a constitutive soil model that can incorporate viscous behaviour in a more "holistic" approach, has potential of aiding in the understanding of all the questions above.

2.5.2 Proposed additional current and future research based on literature review

In addition to the main objectives of this report (presented in Section 1.2) the following research proposals were raised during the literature review. This is further discussed in section 6 *Conclusions and recommendations for future work*.

- Benchmark (on element level) a soil model that accounts for viscous behaviour against collected datasets in the literature review presented in Figures 2.20 and 2.21. The benchmarking is presented in Appendix A.

- Long-term measurements of vertical and lateral earth pressures against underground structures are scarce. Although field measurements inherently are site specific (geology, construction sequence, structural stiffness), the full scale (macro) response of soil behaviour can only be assessed by measurements in the field. Field measurements are considered needed in order to provide valuable input on field-scale response of (macro) soil-structure interaction.

- As the field measurements provide insights from a site specific setting, parametric studies should be done in order to generalise the results of the field measurements. Multi-objective parameter optimisation can be done in order to study the governing factors for long-term earth pressures against underground structures. Further, the literature review gave examples on normalised results of generation of excess pore pressure due to excavation. Thus it should be possible to expand on such studies and generalise/normalise the effect of e.g. excavation geometry and time on e.g. factor of safety level, wall deflection and effective heave pressures.

3 Case study analyses of a deep excavation, Göta Tunnel J2

For the scope of this mid-term report, the Göta Tunnel case study is presented as a journal paper draft. The case study is included in Appendix B. The case study was carried out in order to benchmark the constitutive soil model Creep-SCLAY1S in order to evaluate it for use in design of excavations and future research.

4 Instrumented site: conditions, soil properties and sensor installation

This chapter describes the site and soil conditions, conducted laboratory tests as well as the sensors installed in the clay at the Hisings Bridge site. Chapter 5 presents and discusses the results of the monitoring so far.

4.1 Introduction

Field monitoring has been carried out in Central Gothenburg in order to study the short- and long-term response of an excavation and permanent underground structure in soft clay, see Figure 4.1. The monitoring data includes e.g. vertical and horizontal earth pressures under the structure, as well as pore pressures. The measurements are intended to be continued in the long-term. The instrumentation was carried out within an on-going construction project in order to include the stages of a normal construction sequence, scale-effects in field (compared to laboratory) and study for example the soil response including temperature effects arising during casting of the concrete structure. The instrumentation is an expansion on the monitoring program at the Göta Tunnel site, section 3. Although the Göta Tunnel site comprise unique field monitoring data of an excavation in soft clay, the scope of those measurements was limited to the construction phase and did not contain measurements of earth pressures acting against the permanent structure.

4.2 The excavation and structures

The studied excavation is located in Central Gothenburg, ca 400 m south-southeast of the Göta River and 150 m northwest of the Central Station, see Figure 4.1. The excavation is located within the construction site for the new Hisings bridge, that is under construction by joint-venture conctractors Skanska and MT Højgaard.

The position of the centre of the excavation in reference system SWEREF 991200 is (6398995, 148243) and in WGS84 (57°42'36"N, 11°58'14"E). The excavation is located East of an existing embankment/ramp for the Göta River bridge, built in the 1930s. In general the ground surface level in the area varies between ca +2 to +3 . At the perimeter of the excavation the level of the ground surface varies between ca +3 to +4 and northwest of the excavation, the maximum level of the existing ramp is +6.

4.2.1 Geological setting and historical structures

The geological setting of the Göta River valley is characterised by deep deposits of soft sensitive plastic clays. The clay layers are quaternary deposits formed either during the melting of the last glacial inland ice, i.e. glacial deposits, or through erosion processes following after the deglaciation, i.e. post glacial deposits formed during the accompanying land uplift. The ice front retreated from the Gothenburg area some 13'000 years ago (Fredén et al. 1981) and the current land uplift in the Gothenburg area is about 2 mm/year.

Figure 4.1: *Location of the instrumented excavation in Central Gothenburg.*

The boundary level between the glacial and post-glacial deposits varies within the city due to the sedimentation as well as man-made loading history. Previous studies (Wood 2016) set the boundary between the glacial and post-glacial clay deposits in the studied area to approximately level -20. During sampling at the site, a change from a grey coloured clay to a distinctive dark grey or black coloured clay, an indication on increased sulphide content, was found at and below 16 m depth (corresponding to level -19). This is considered to be the approximate boundary of glacial and postglacial deposits at the site.

The city of Gothenburg was founded in 1621 (*Gothenburg's history and heritage* 2020). The area of the excavation is located close to the old original shore line of the city and one of the old defence trenches/canals. The stress history at the site and the area around Gothenburg Central Station has been significantly effected by land reclamation works carried out during the 19th century. Historic city maps are included in Appendix C see Figure C.5. The only known previous building at the site is that of a locomotive workshop located just east of the studied excavation. The workshop was built sometime between 1820 and 1860 based on city maps from these years, although the exact time of construction is not known). The workshop was torn down no later than 1923 (based on city map of 1923). The outline of the old shoreline, defence lines, canals and the locomotive workshop can be seen in Figure C.5 in relation to the location of the studied site.

The existing bridge across the Göta River, Göta Älv Bridge, was built from 1935 to 1939. The embankment/ramp east of the studied excavation runs from ground surface level +3 in the south part of the excavation to +6 at the bridge abutment, west of the north part of the excavation. The embankment is partially founded on 5" wooden piles 15-17 m long, see details and approximate location in Appendix C Figure C.6.

Before start of the construction works the on-going settlement rate in the area varied from approximately 2 mm/year in general to a local maximum of 7 mm/year in the location of the road that connected up to the existing embankment. The settlement rates are based on InSAR satellite measurements and the data is included in Appendix C Figure C.4.

4.2.2 Permanent structure

The permanent structure is constructed as part of the project to build a new bridge across the Göta River. This new bridge, the Hisings bridge, will replace the existing Göta River bridge. The excavation is carried out in order to build a tunnel, on top of which trams and buses will connect to the new Hisings Bridge. The tunnel will connect to the building block (that houses a shopping centre) west of the excavation in order to facilitate future transport of goods to the stores. The part of the tunnel that is under construction at this stage is 15 m wide and ca 60 m long. A cross section of the tunnel structure is presented in Figure 4.2. The tunnel is ca 15 m wide at the base and 13 m at the top. The foundation as seen in Figure 4.2 contains rows of friction piles made out of a combination of a 11.5 m long top element of steel pipe $\varnothing$323.9-12.5 mm connected to 45.5 m of precast concrete pile elements 0.27x0.27 m^2. These combi-piles were hammered down with varying out-of-plane centre to centre (cc) distance, in general 3.6 m along the tunnel walls and 5.0 m within the slab. The concrete piles (concrete quality C60/75) were reinforced with 8 longitudinal $\varnothing$16 mm rebars (steel K500B) and the steel pipe elements were filled with concrete after installation.
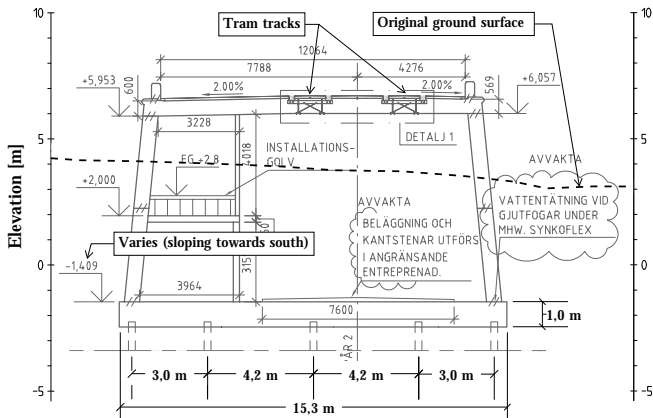
Figure 4.2: *Approximately west (left in the picture) to east cross section of the permanent structure.*

4.2.3 Earth retaining system

The design of the earth retaining system was made by the contractor's independent analyses. The excavation was carried out within steel sheet pile walls (SPWs) as illustrated in the overview, Figure 4.3, and the cross section, Figure 4.4. The SPWs consisted of PU12 and AU23 profiles of steel grade S355 and with lengths varying between 14 m (North and East walls), 16 m (South wall), 18 m (north 2/3 of the West wall including the studied and instrumented cross section) to 20 m (south 1/3 of the West wall). The top level of wailer beams (profile HEB300) and steel struts ($\varnothing$406-10.0 mm) were installed at level +3.0. The level of the lower wailer beam (HEB450 and HEB500 profiles) and steel struts ($\varnothing$559-12.5 mm) followed the slope of the excavation bottom (towards the south) and was located at level ±0 in the instrumented section.
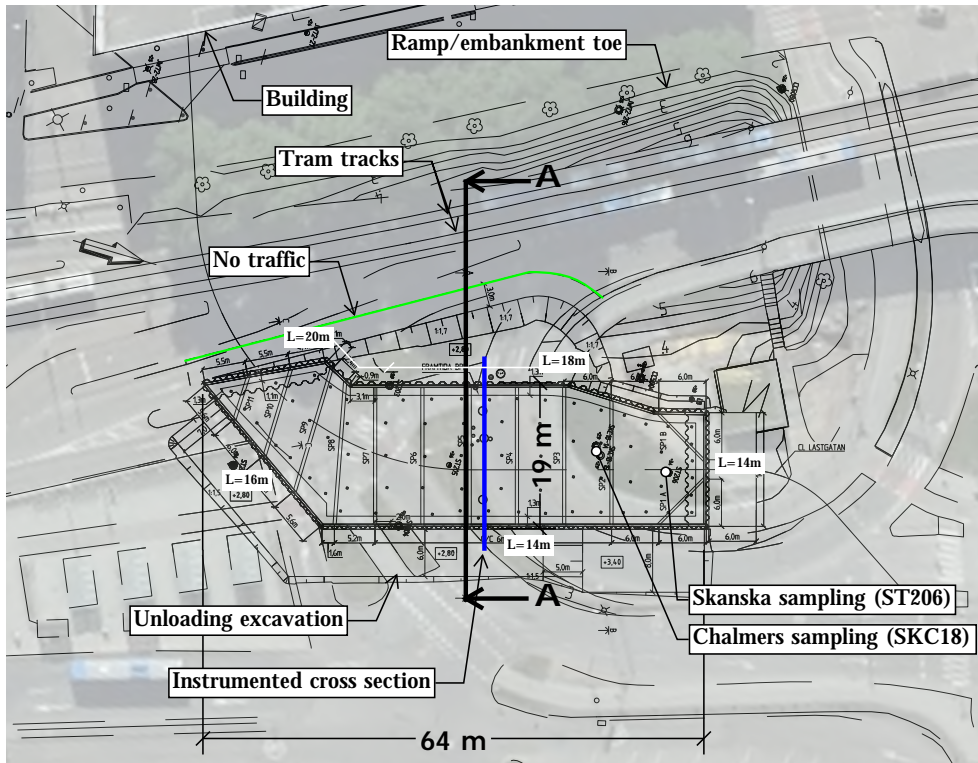
Figure 4.3: *Plan of the earth retaining and permanent structures. Cross section A-A is presented in Figure 4.4.*
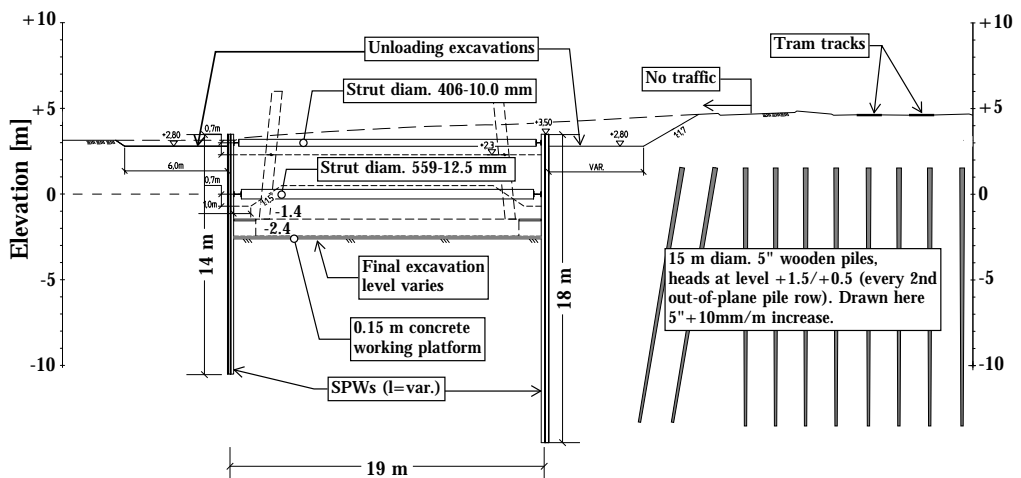
Figure 4.4: *Cross section A-A with location according to Figure 4.3.*

73

The working platform was made out of a 0.15 m thick layer of steel-fibre reinforced concrete. The working platform was designed as a support level for the SPWs. The excavation for the platform was carried out sequentially with immediate casting of the working platform along with the progress of excavation.

4.2.4   Construction sequence

A summary of the main construction stages and time intervals is given in Appendix C Table C.4. In this section the construction sequence and methods are described in more detail. The construction works in the area were initiated in September 2018 by pre-excavation in order to remove existing ground remnants, mainly from the historic locomotive workshop. This included removal of the foundation floor and the paving of the old courtyard (at level ca +1). Wooden piles ($\varnothing$0.15-0.25 m, L=8-9 m, pile heads at level ca +0.5) were located mostly under the old building walls. These pile were extracted in the southern most part of the sheet pile wall locations and excavation. In the section to be instrumented pre-excavation was carried out in mid October 2018. The ground surface was then levelled to ca +2.2 before pile installation.

Installation of the 71 piles of length 57 m was carried out from January 9th to February 1st in 2019 using a Junttan PM23 pile driving rig. The pile installation dates are given in Figure 4.5 with the location of the bellow-hose, piezometers and inclinometers which, in addition to conventional surveying, were used for the monitoring of the pile installation process. Pre-augering was carried out before installation of each pile in order to minimise the deformations in the surroundings. The main concern was the deformations in the nearby tram tracks to the west and main water pipes directly east of the excavation. The following observations of the augering process were made by the author after talks with the pile rig operator during the augering process. The auger was 20 m long but is in practice deployed down to ca 18 m depth. The flanges of the auger ($\varnothing$0.4 m) were mounted on a inner-rod ($\varnothing$0.14 m). The auger was deployed downwards by rotation and self-weight, when reaching final depth it was left to rotate until a volume of clay corresponding to the auger volume was obtained at the ground surface. The auger was then retracted with reversed rotation as long as possible for the pile rig machinery, i.e. until about 1/3 of the 18 m auger remain to be retracted, it was then pulled out by extension of the pile rig mast (rotation only possible during extraction of the first 12 m of the auger).

Installation of the steel sheet pile walls was carried out from February 7th to 27th 2019 using a vibrating hammer. The installation started with the West wall (installation order from south to north) and passed the studied section and location of the inclinometer on February 13th. Then the North wall was installed, followed by the East and South walls. Installation of the top wailer beam (level +3) was carried out from pre-excavation level +2.2 starting from the north in mid March, struts were installed successively with the progress of the wailer beam installation.

The excavations for the lower level wailer beams were done in dykes along the sheet pile walls, starting with the excavation for the wailer beam along the West wall, passing the
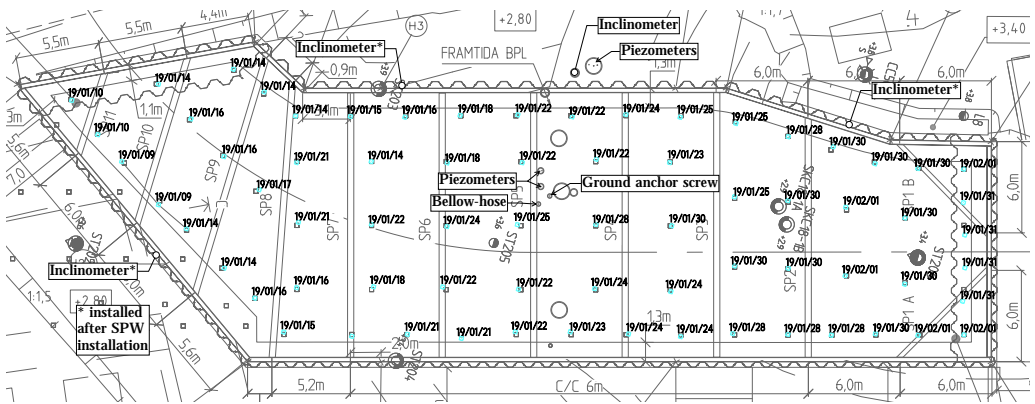
Figure 4.5: *Pile installation dates and location of measurement instruments installed at this stage. The general installation order was from south (left in plan) to north. The installed pile locations are given in blue, compared to the design locations in black.*

instrumented section in mid April from north to south. The excavation for the East wailer beam and the second level of struts were then carried out from south to north (the excavator retreating from the excavation). The struts were installed in excavated dykes in order to minimise heave within the excavation and the deformations in the surroundings. The installation and excavation for the East wailer beam and struts passed the instrumented section in the beginning of May and was completed on May 8th. The wailer beams, and thereafter struts, were installed from north to south (with installations of the struts reaching the instrumented section in the end of May).

Excavation to final depth started from north on May 29th in parallel with the strut installation. The final excavation was carried out sequentially in strips with successive casting of a concrete working platform across the excavation, see photo in Figure 4.6. Excavation in the instrumented section and around the piezometers and bellow-hose was carried out June 25th to 26th, see Figure 4.7. Before casting of the concrete working platform, on June 27th, concrete well-rings were placed on the excavation bottom to allow slots for installation of sensors in the clay. On June 28th and 30th earth pressure cells and piezometers for monitoring of horizontal earth and pore pressures were installed in the clay (inside the well-rings previously placed on the excavation bottom). On July 1st and 2nd earth pressure cells for monitoring of vertical earth pressures were installed. Concrete was cast over the instruments on July 2nd. Details and instrumentation methodology is described in Section 4.4.4. Once the concrete had hardened, the lower level struts located north and south of the instrumented section were cut on the 3rd and 4th of July.

Figure 4.6: *Excavation to final depth started from north (right in the photo) on May 29th. Studied section including instrumentation is highlighted. Photo from crane on June 5th 2019.*

Figure 4.7: *Excavation to final depth in studied section. Photo from drone on June 26th 2019.*

Rebar and form works for the 1.0 m thick permanent concrete slab began on August 13th. The slab was cast in two segments, the North part including the instrumented section was cast on September 10th and the South part on September 25th (concrete C35/45, $VCT_{ekv} \leq 0.45$). The gap between the East SPW and the slab was then filled with 1.0 m crushed rock (fraction 0-32) in level with the top of the slab in late September and the gap between the west SPW and the slab was filled with concrete on October 2nd. The 0.6 m thick walls of the tunnel were cast from October 24th to February 28th 2020 according to Figure 4.8. Included in this figure are also the times for casting of the 0.6 m thick tunnel roof.
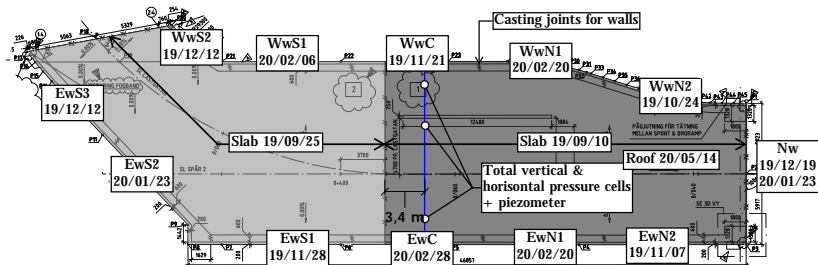
Figure 4.8: *Dates for casting of concrete slab and walls. The walls have been named for cross-references to results presented in Chapter 5.*

Back fill between the SPWs and walls started on February 26th 2020. The filling started along the West wall, from the south to north. Crushed rock (fraction 0-90 mm) was used as back fill material and compacted using a vibration plate compactor up to level +2. Filling of the West wall at the instrumented section was completed on February 28th.

Additional subsequent construction activities are presented in Appendix C Table C.4.

4.2.5 Construction activities at adjacent site

Construction works for the West Link tunnel started just north of the excavation in August 2019. The West Link tunnel is a railway tunnel running through Central Gothenburg. The excavation depth north of the studied excavation is ca 15 m. An overview and cross-section is presented in Appendix C including annotation of the times for some major parts of the construction works. In the following a general description of the construction works is presented.

The construction works started in August 2019 with excavation to approximately 2 m depth followed by form works for the guide walls for the diaphragm walls (D-walls). The guide walls including back-fill were completed in late August and followed by the installation of D-walls including cross walls. In December the wall installations were complete in the area and the guide walls were demolished. The clay within the D-walls were then reinforced by installation of lime-cement columns (dry mixing). Installation of the lime-cement columns started in the beginning of February 2020. In March installation

of piles began for the two bridge supports of the new Hisings Bridge that are located within the D-walls, and the future West Link excavation. Each support comprised 8 friction steel piles to 78 m depth (top 24 m ⌀610 mm on 54 m ⌀406 mm). Major future construction work involves excavation for the tunnel including successive truss installation along the bridge piles. Upon completion of the construction works, the bridge supports will rest upon the tunnel roof.

4.3 Site characterisation including additional laboratory testing

Due to numerous historic, planned and on-going construction projects, the clay deposit in the studied area is well characterised. Compilation of previous in-situ and laboratory tests indicate that the clay deposit is homogenous. Discrepancies, such as variations in the undrained shear strength or OCR are mainly found in the top part of the clay deposit and can be attributed to variations in man-made loading history. Due to such possibly local variations, complementary sampling and laboratory testing was initiated by the contractor for the design of the earth retaining structures.

Additional sampling and laboratory testing was carried out as part of this research project, in order to supplement previous testing with more advanced testing such as for example;

- IL oedometer tests on remoulded and intact samples. The intact samples were subjected to unload-reload cycles with unloading carried out to stress levels corresponding to those estimated upon final excavation depth.
- K_0 consolidated undrained triaxial tests performed with varying strain rates.
- K_0 consolidated drained triaxial tests with unload-reload cycle.
- K_0 consolidated drained triaxial tests were the radial stress was decreased and the axial load kept constant. Two such tests were carried out in order to simulate the imposed loading conditions on the retained side of excavations.

An overview plan with the location of collected in-situ tests and laboratory data is given in Appendix C.2.

4.3.1 In-situ tests and layering

At the studied site, fill materials (sand, gravel, clay, brick) extend down to level ca ±0 in the north part of the excavation and to ca -0.5 to -1 in the south part based on auger sampling. These levels correspond to ca 3 to 4 m depth from the ground surface. The fill material is situated on top of a deposit of homogeneous post-glacial and glacial clay. Based on e.g. Wood 2016 the transition from glacial to post-glacial clay is located at level ca -20. The extent of the clay layer at the site was determined to level -89 and -93 by means of two deep soundings. The soundings were cancelled after sounding in 5 m of frictional material under the clay layer (bedrock level not determined). Measurements of the undrained shear strength of the clay by means of field vane and cone penetration tests (CPTU) are presented in Figure 4.9 as uncorrected and corrected values. The uncorrected

field vane tests indicate an undrained shear strength of ca 20 kPa in the top part of the clay layer, increasing with ca 1.5 kPa/m towards depth. Field vane and CPTU tests are performed according to Swedish guidelines; (Swedish Geotechnical Society 1993) and Larsson 2015 respectively. Correction of vane test results with respect to liquid limit is made according to (Larsson, Sällfors, et al. 2007):

$$c_{u,vanecorr.} = c_{u,vane} \times \mu \times \left(\frac{OCR}{1.3} \right)^{-0.15} \quad \text{where } \mu = (0.43/w_L)^{0.45} \qquad (4.1)$$

where OCR is overconsolidation ratio, w_L is liquid limit (%/100) and μ correction factor with a lower limit of 0.5 and upper limit of 1.2, in cases with no support of additional testing. Evaluation of undrained shear strength from CPTU tests in cohesive soils is made according to (Larsson 2015) producing corrected values:

$$c_{u,CPTUcorr.} = \frac{q_t - \sigma_{v0}}{13.4 + 6.65w_L} \qquad (4.2)$$

where q_t is total tip resistance and σ_{v0} is total vertical overburden pressure.

Measurements of pore pressures in the clay layer are presented in Figure C.3, showing an pressure level corresponding to +1 with approximately hydrostatic increase towards depth.

4.3.2 Sampling for laboratory tests

In addition to the extensive previous data available at the site, additional sampling and laboratory tests were performed by the contractor (borehole ST206) as well as by Chalmers for this study (borehole SKC18). Sampling was made by field technicians Fredhy Hansen and Lennart Hedström (both from Skanska) using a 50 mm Swedish piston sampler, STI. The samples from borehole SKC18 were extracted and transported from the site to the climate controlled environment (8°C) of the Geotechnical Laboratory at Chalmers on September 27th. Before sealing the piston sampling tubes with conventional caps, they were wrapped with plastic film to further prevent oxidation during storage.

4.3.3 Laboratory test

Table 4.1 represent an overview of the additional laboratory tests carried out at Chalmers on samples from borehole SKC18 at the location of the studied excavation. Due to some of the testing being carried out in order to test different non-standard testing methodologies, such as e.g. CADC tests by means of decreasing the radial stress and examine effect of varying strain rates, some tests were carried out up to 2.5 months after sampling. In the light of e.g. Wood (2016), it can be discussed how representative some of these non-standard test results are due to the age of the samples. The test data is still presented, in order to exemplify the additional soil characterisation potential (rate dependence as well as response to stress paths adopted to the studied problem) that is available by means of simple non-standard testing.
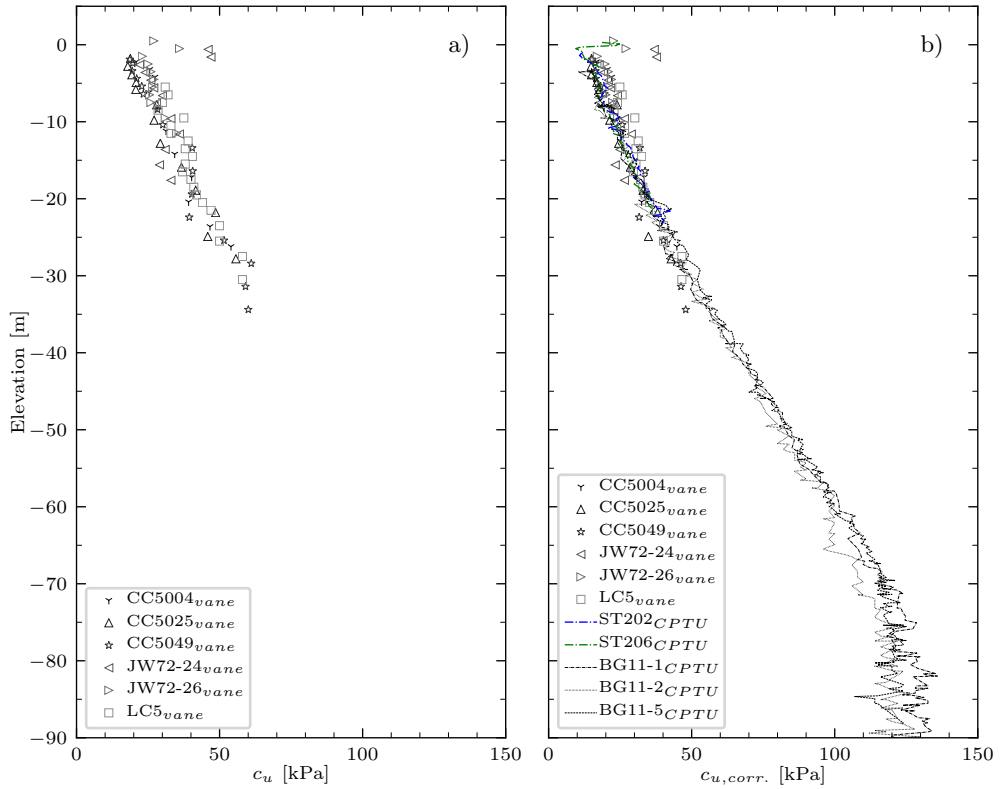
Figure 4.9: *Compilation of undrained shear strength by means of a) uncorrected and b) corrected in-situ tests according to equations 4.1 and 4.2. Borehole locations are presented in Appendix C Figure C.2.*

Index soil properties on the collected samples were determined for all sampling depths by means of standardized laboratory analyses. Index properties determined for borehole SKC18 are presented in Figure 4.10 including the results from collected previous investigations. Figure 4.11 presents the undrained shear strength determined by laboratory testing on SKC18 samples as well as previous investigation results. Correction of the undrained shear strength determined by the fall cone test is carried out similarly to correction of field vane tests but without correction for OCR, according to (Larsson, Sällfors, et al. 2007):

$$c_{u,fccorr.} = c_{u,fc} \times \mu \tag{4.3}$$

As for correction of field vane tests μ has a lower limit of 0.5 and upper limit of 1.2, in cases with no support of additional testing.
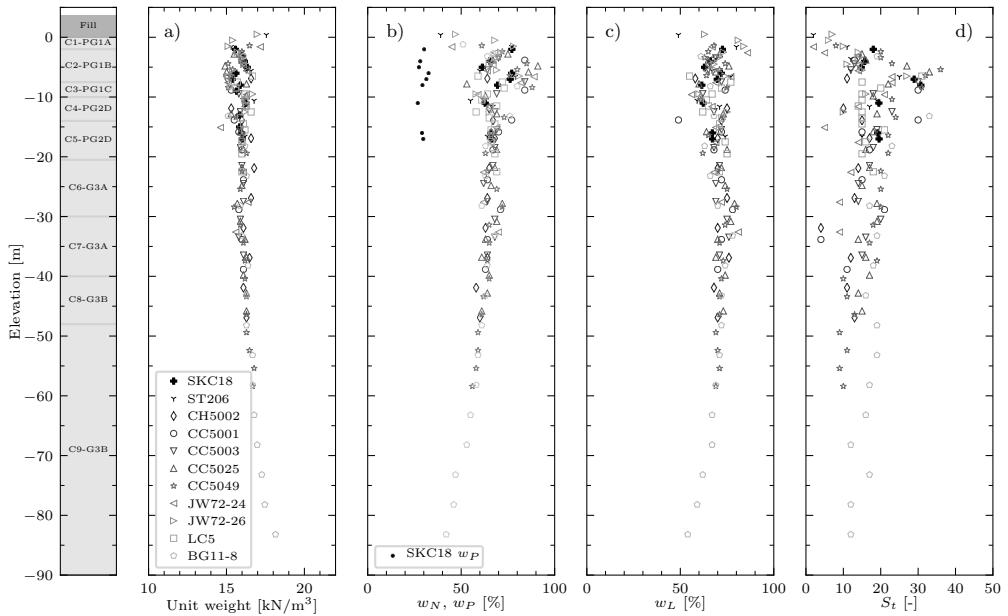
Figure 4.10: *Index properties of the clay layers. The clay layer stratigraphy according to Wood (2016) is outlined in the left column, indicating the transition from post-glacial to glacial clay at level ca -20.*

Table 4.1: Laboratory tests performed on samples from borehole SKC18.

Depth (m.b.g.s)	Elevation (m)	Test	Executed[1]	Note
6.09	-3.19	CAUC	18/10/12	
		CRS	18/10/11	
6.26	-3.36	CAUC	18/10/12	Strain rate 0.135 %/h
7.09	-4.19	IL (5 tests)	18/09/28	4 intact & 1 remoulded (18/10/04)
		CRS	18/10/25	
8.09	-5.19	CAUE	18/10/08	
8.26	-5.36	CAUC	18/10/08	
9.26	-6.36	CADC	18/12/14	Constant decrease of radial stress.
		CRS	18/12/14	
10.09	-7.19	CADE	18/10/30	
10.26	-7.36	IL (3 tests)	18/09/28	2 intact & 1 remoulded (18/10/04)
		CRS	18/10/17	
11.09	-8.19	CAUE	18/10/03	
11.26	-8.36	CAUC	18/09/28	
12.26	-9.36	CRS	18/10/23	
14.09	-11.19	CADC	18/12/10	[2]
		CRS	18/12/10	
14.26	-11.36	CADC	18/12/08	Constant decrease of radial stress.
		CRS	18/10/23	
16.26	-13.36	CAUC	18/11/16	Std strain rate with 1h relaxation stops.
		CRS	18/10/25	
18.09	-15.19	CAUC	18/10/16	Std strain rate until peak, after peak varied 5 then 10 times slower than std.
		CRS	18/10/16	Two CRS tests at std and half std rate.
18.26	-15.34	CAD	18/10/22	Unload-reload then to failure in extension.
19.09	-16.19	CAUC	18/10/03	
		CRS	18/10/04	
19.26	-16.36	CAUE	18/10/01	
20.09	-17.19	IL (5 tests)	18/09/28	4 intact & 1 remoulded (18/10/04)
		CRS	18/10/04	

[1]Samples extracted 18/09/27. [2]After consolidation stage, test unloaded to higher OCR (along K_0=0.6 line) in order to "hit" the same point of the CSL as the CADC test performed on the sample from level -11.36.
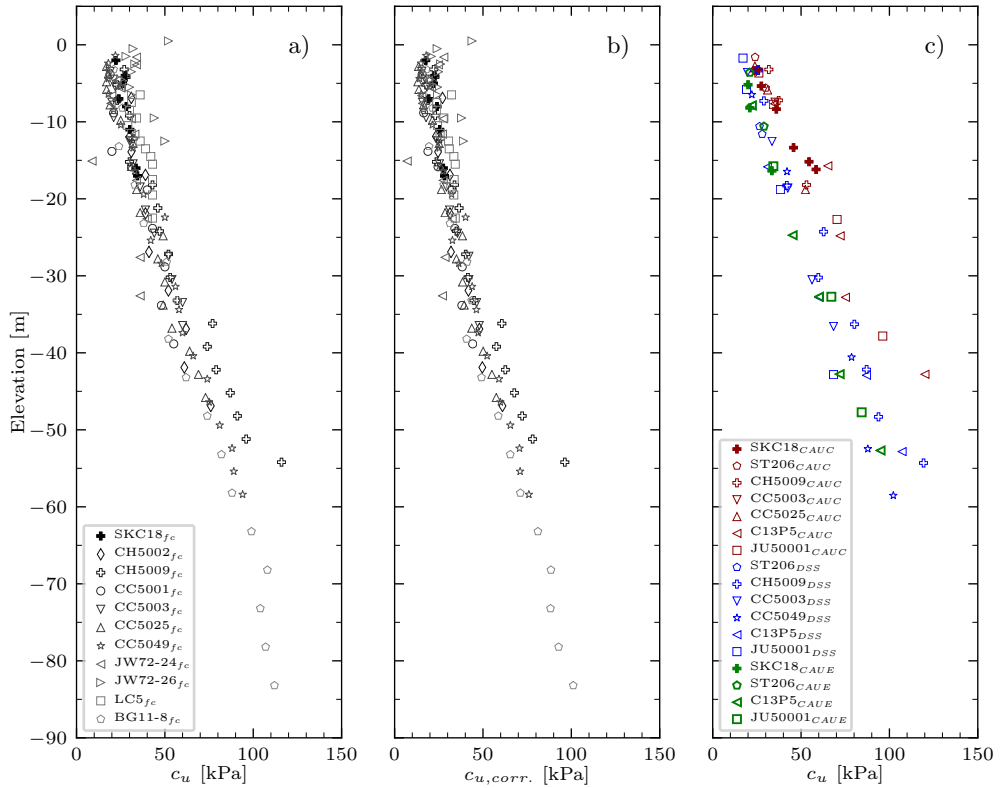
Figure 4.11: *Compilation of undrained shear strength determined by means of laboratory tests. Borehole locations are presented in Appendix C Figure C.2.*

4.3.3.1 Oedometer tests

Incremental loading oedometer tests (IL) were performed on intact as well as remoulded clay samples, see Figures 4.12 and 4.13. The tests on the remoulded samples were performed in order to determine the intrinsic properties of the natural clay. The natural clay was remoulded with a spatula and the undrained shear strength determined by means of fall cone testing, the clay was then remoulded again and the undrained shear strength determined. This procedure was carried out until the undrained shear strength did not decrease any further. The remoulded clay was then mounted in the IL oedometer rings, with the aim of minimising the amount of voids enclosed in the sample.

In addition, Constant Rate of Strain oedometer (CRS) tests were performed. The adopted standard rate of deformation in the CRS tests was 0.0024 mm/min corresponding to a strain rate of 0.72 % of the original sample height (20 mm). This constant rate of deformation is based on the work by Sällfors (1975) whom also proposed an associated graphical evaluation method which is still used in Sweden for deriving preconsolidation pressures from CRS-tests. In Sällfors and Larsson (2017) a strain rate of 0.75 %/h is suggested and furthermore that the standard rate of deformation should be reduced to 50 % for testing on samples where the apparent preconsolidation pressure is expected to exceed 250 kPa. Such correction has not been necessary for the tests conducted on the additional testing presented in this report.

The results from the CRS tests are presented as normalised stress-strain response in Figure 4.14. Before initiation of unloading stages, a relaxation stage was introduced after which a stress controlled unloading was executed. The adopted rate of constant unloading was 0.3 kPa/min. This rate was based on unpublished tests by Anders Kullingsjö (performed within the work of Kullingsjö 2007). The motivation being the resulting rate of deformation being sufficiently slow at this rate (in order to compare to results of IL tests). As an example, this type of operator control causes the rate of deformation to increase as the unloading modulus decrease with effective stress level. In the CRS test on the sample from 6 m depth (lowest unloading modulus according to Figure 4.14), the maximum rate of (reversed) deformation during unloading was 0.0020 mm/min (0.6 %/h). For comparison the maximum rate was 0.0006 mm/min for the sample from 18 m depth.

The unloading moduli derived from the IL and CRS tests from borehole SKC18 are presented in Figure 4.15 normalised with respect to the maximum value of; the trend value of in-situ preconsolidation pressure or applied load before start of unloading. The unloading moduli are secant values as in the case of IL tests they are derived over each unloading step. The moduli from the CRS tests have been derived by extracting values over 5 kPa stress increments. If negative or zero axial displacement occur during such a stress increment, the evaluated modulus has been plotted as an infinite value. In Figure 4.15 the values of σ'_v are plotted by taking the average stress for each load step/increment. The results can therefore not be directly compared to normalised results in e.g. Züblin (2015a), where σ'_v correspond to the stress from which each unloading step starts.
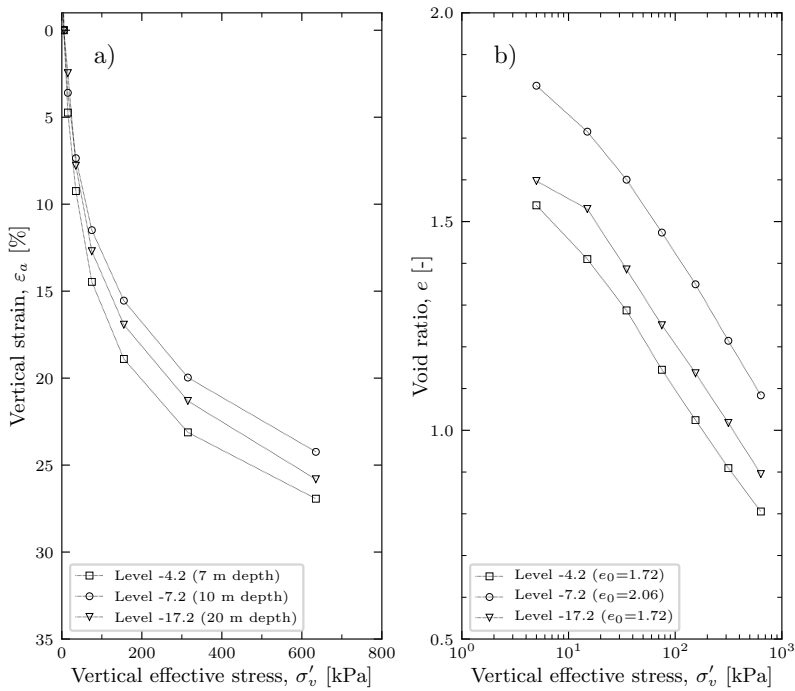
Figure 4.12: *Stress-strain response from IL oedometer tests on remoulded clay samples. The measured axial strains have been reset after the first load step in order to exclude effects of mounting the samples.*
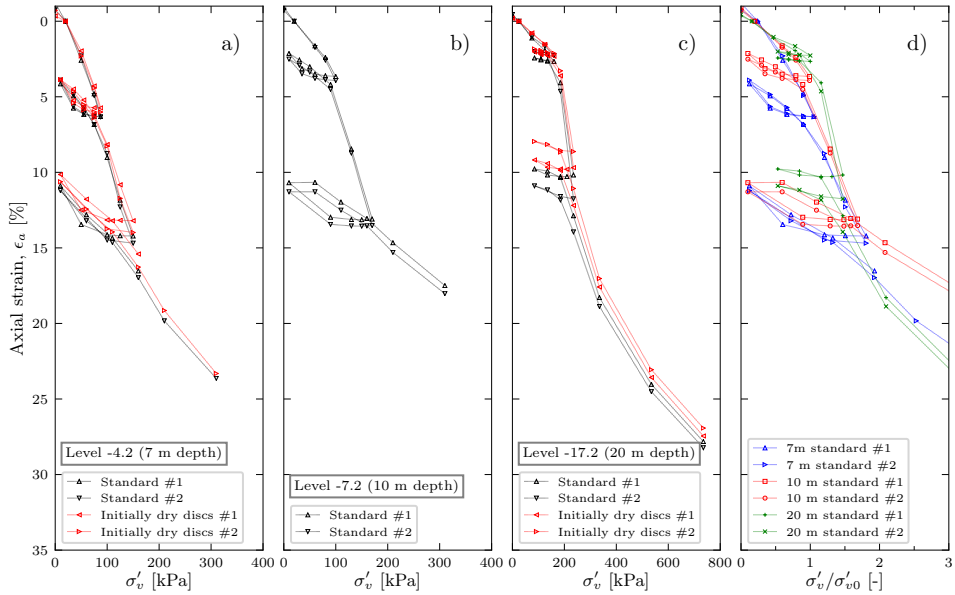
Figure 4.13: *Stress-strain (a-c) respectively normalised stress-strain (d) response from IL oedometer tests on intact clay samples. The measured axial strains have been reset after the first load step in order to exclude effects of mounting the samples.*

The CRS tests generally indicate lower unloading moduli than the IL tests. This can be attributed to for example; a higher ring friction developing in the IL tests owing to the longer duration before load reversal starts in these tests, or the fact that the CRS-tests have been normalised with *apparent* maximum stress, that is affected by the rate of deformation before start of unloading. The "true" maximum pre-stress before unloading is therefore lower and unknown. Therefore, the IL tests are considered more appropriate for this kind of testing and normalisation.

Values of previous semi-empirical relationships (Larsson 1986; Karlsrud 2012; Trafikverket 2014) for unloading modulus are included in Figure 4.15 as well as the results from a drained triaxial tests with a unload-reload cycle, for test details see Appendix C.1.2 Figure C.12. In general the normalised values are in line with previous relationships for unloading moduli. The relation given by Karlsrud (2012) seem to provide the most reasonable expression for estimation of a trend from the results. This finding is in line with Wood (2014). However, Karlsruds parameter values for Bjørvika clay (a=250 and b=0.3) appears as a upper bound for normalised stresses $\sigma'_v/\sigma'_{vc,max}$ lower than 0.6. For the presented data a=175 and b=0.6 provides a more reasonable approximation of a general trend.
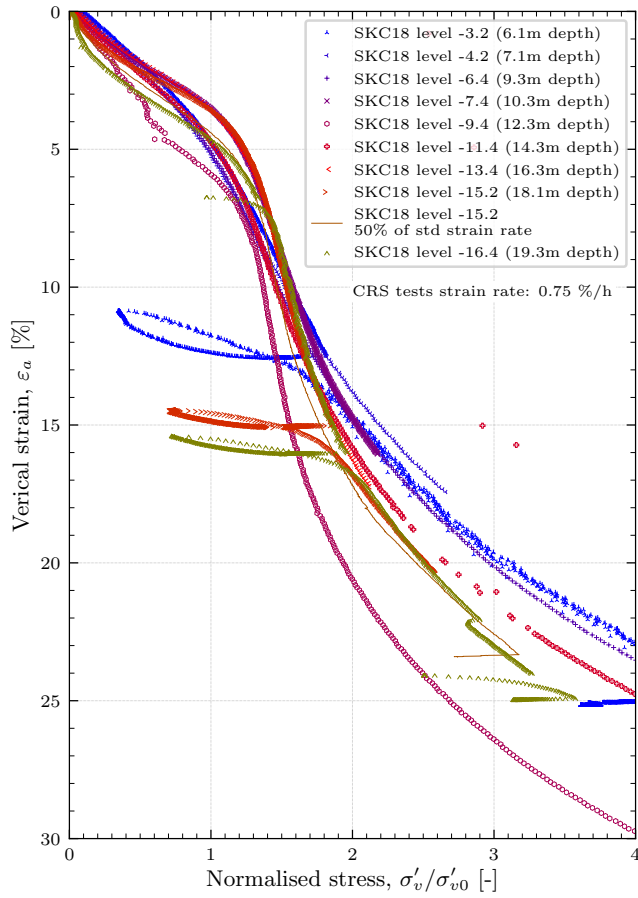
Figure 4.14: *Normalised stress-strain response from CRS oedometer tests.*
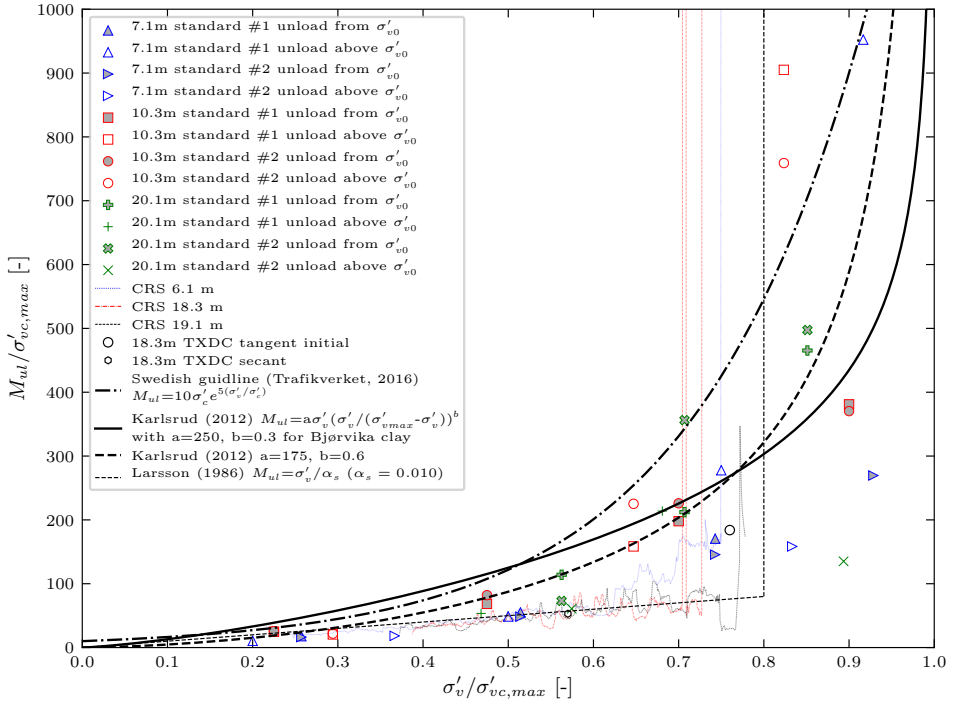
Figure 4.15: *Normalised unloading modulus derived from IL and CRS tests compared to previous empirical relations. Values normalised by maximum of; trend of preconsolidation pressures or maximum previous load in IL or CRS before start of unloading stage. Secant values from IL steps and semi-tangent modulus from CRS tests (average over registered values).*

4.3.3.2 Triaxial tests

Anisotropically (K_0) consolidated undrained triaxial compression and extension tests were performed for site characterisation and comparison with previous collected test data from the area. The undrained tests were preformed according to Swedish practice at a strain rate corresponding to 0.6 % of the sample height per hour (Larsson 1977; Larsson 1980). For a sample height of 100 mm the strain rate adopted for the standard undrained tests thus corresponded to a constant rate of deformation of 0.01 mm/min.

Specialised triaxial testing was performed on the remaining clay samples in order to study the strain-rate dependence of shear strength by means of tests performed with varying strain rates. Also, drained tests were carried out with one of the tests including an unload-reload loop with the unloading carried out to an effective vertical stress level corresponding to that after excavation (based on a rough 1D-estimation).

Furthermore, the drained compression behaviour was studied by tests in which the radial stress was decreased under a constant axial load. The motivation for these tests being that drained compression tests are typically, in Sweden, performed by constant rate of axial deformation under constant cell pressure. During this work it became obvious for the author that it would be more appropriate for excavation problems to study the soil response on the retained side of an excavation by decreasing the radial stress under a constant axial load. This mode of imposed idealised loading conditions is considered more logical and correct with respect to paths in stress space as well as in compression plane (volume change), see Figure 4.16 for illustration of difference of such type of test and conventional CADC test. Two such drained tests were carried out in order to simulate what is considered a more appropriate test for excavation problems (see detailed presentation of results in Appendix C.1.2). The adopted rate of constant decrease in radial stress was -0.03 kPa/min. This rate was estimate such that the time to failure would resemble that of standard drained compression tests (0.06 %/h to approximately 1.5 % axial strain at failure equals 25 h). The time to failure in the two tests was approximately 30 and 20 h for the samples from 9 and 14 m respectively. In Appendix C.1.2 also the measured axial strain rates are presented.

Compilation of the triaxial tests performed on samples from borehole SKC18 are presented in Figure 4.17. All samples were anisotropically consolidated to estimated in-situ stress levels and an estimated in-situ value of K_0=0.6. Estimated slopes of the evaluated critical state lines (CSL) in compression, M_c, and extension, M_e, are drawn. The CSL correspond to values of M_c=1.40 and M_e=1.02, which in turn corresponds to critical state friction angles of 34.5° in compression and 38° in extension (i.e. ratio $\phi'_{CSL,ext}/\phi'_{CSL,comp}$=1.1). For the critical state friction angle in extension, a range is included for 34° to 42° (0.9×38° to 1.1×38°). Furthermore, in Figure 4.17 is also included a range of stress ratios corresponding to peak strength friction angles in compression, ranging from ca 30° to 32° where the value of 30° seem to approach peak strengths in tests performed at a slower than standard strain rate. The stress-strain response of the triaxial tests are presented in Figure 4.18. The stress-strain response of drained triaxial tests are presented individually in Appendix section C.1.2.
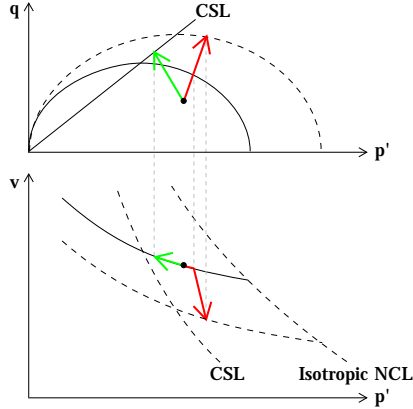
Figure 4.16: *Illustration of different imposed idealised modes of loading in drained triaxial compression "active" tests. Red: conventional CADC test ($\Delta\sigma_v=+$, $\Delta\sigma_h=0$) compared to Green: test where ($\Delta\sigma_v=0$, $\Delta\sigma_h=-$) considered more correct for study of soil behaviour on retained side of excavation problems.*

Results of p'-q stress invariants normalised with preconsolidation pressure (derived from trend line presented in Figure 4.21) are presented in Figure 4.19. The results are compared with Swedish empirical relations which assumes a correlation to liquid limit (Larsson, Sällfors, et al. 2007) in Figure 4.20. The range of the triaxial test data fall slightly below the empirical estimates, this is likely an effect of normalisation of the maximum shear stresses was done with the trend line of vertical preconsolidation pressure, σ'_{vc}, presented in Figure 4.21, which is an assumed average trend line and slightly overestimates σ'_{vc} obtained from triaxial tests. Furthermore it is not clear in Larsson, Sällfors, et al. (2007) what testing method (and strain rate) that has been used for obtaining σ'_{vc} for normalisation (IL, CRS or triaxial tests or trend line constructed from a combination of all methods).

Evaluated preconsolidation pressures from IL, CRS and undrained triaxial compression tests are summarised in Figure 4.21 together with the results from collected previous investigations. In general, the IL tests[1] on samples from SKC18 indicate lower values on the preconsolidation pressure compared to the corresponding CRS[2] and triaxial tests [3]. The lower preconsolidation pressures obtained in IL testing is an effect of, for example, the varying strain rates adopted for the different types of tests. Included in Figure 4.21 is also the in-situ vertical effective stress at the location of the studied excavation. The vertical effective stress was derived from a trend line of soil unit weight (derived from Figure 4.10 and pore pressure according to Figure C.3. The trend line of the preconsolidation pressure that was adopted for initial FE analyses is also indicated in Figure 4.21. The trend of the preconsolidation pressure is based on values of OCR presented in Table 4.3.

---

[1] σ'_{vc} from the IL tests were evaluated by plotting the stress-strain response in linear scales.

[2] Evaluated according to Swedish standard based on a methodology proposed by Sällfors (1975).

[3] Evaluated from triaxial CAUC tests at standard strain rate 0.6 %/h.
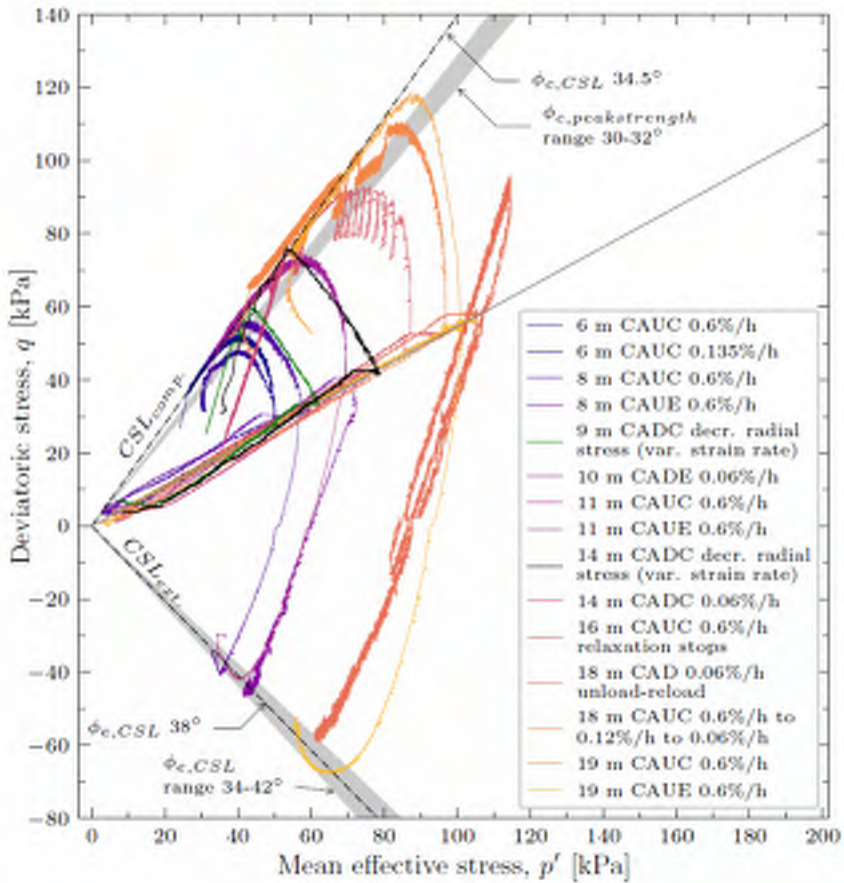
Figure 4.17: *Results from triaxial tests performed on samples from borehole SKC18. Plot of deviatoric stress versus mean effective stress.*
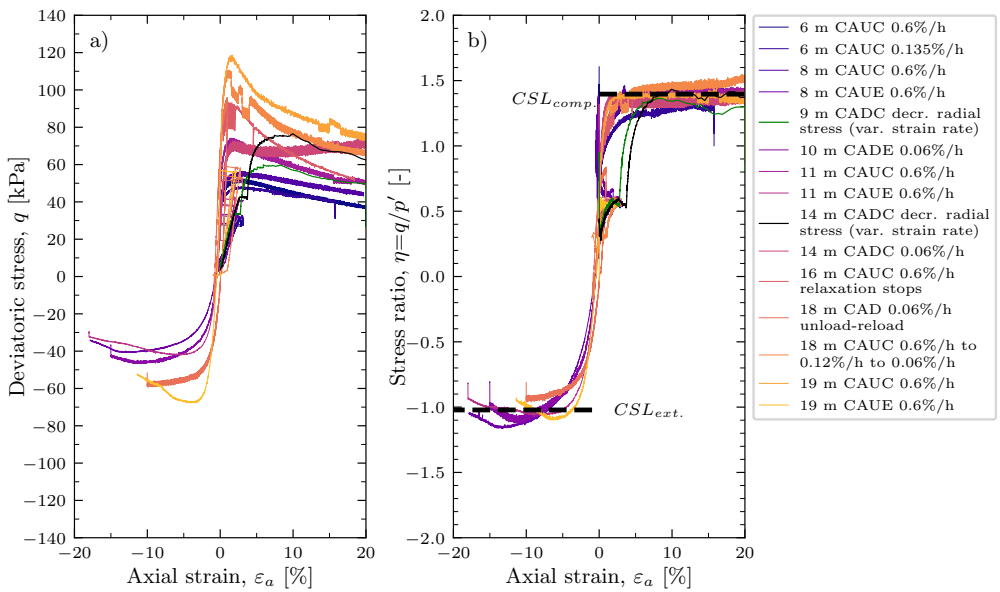
Figure 4.18: *Results from triaxial tests performed on samples from borehole SKC18. a) Plot of deviatoric stress versus axial strain and b) plot of stress ratio versus axial strain.*
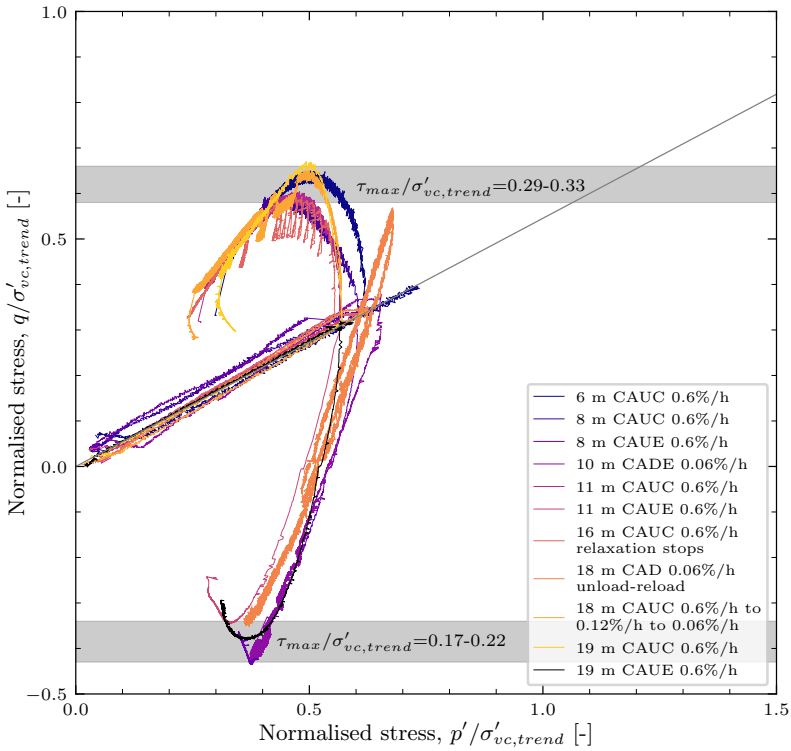
Figure 4.19: *Results from triaxial tests performed on samples from borehole SKC18. Plot of normalised deviatoric and mean effective stress.*
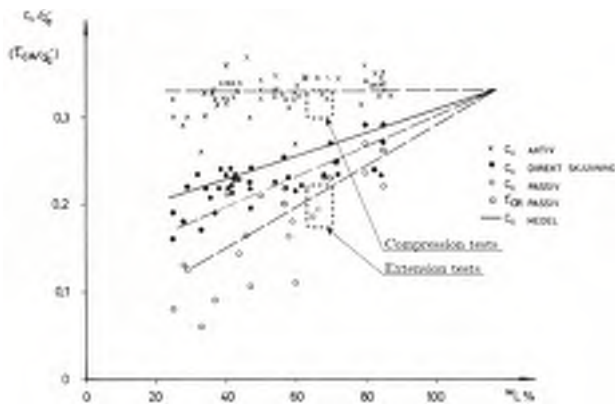
Figure 4.20: *Comparison of triaxial test results versus Swedish empiricism (Larsson, Sällfors, et al. 2007). Ranges of normalised maximum shear stress in compression and extension to liquid limit are annotated.*

93
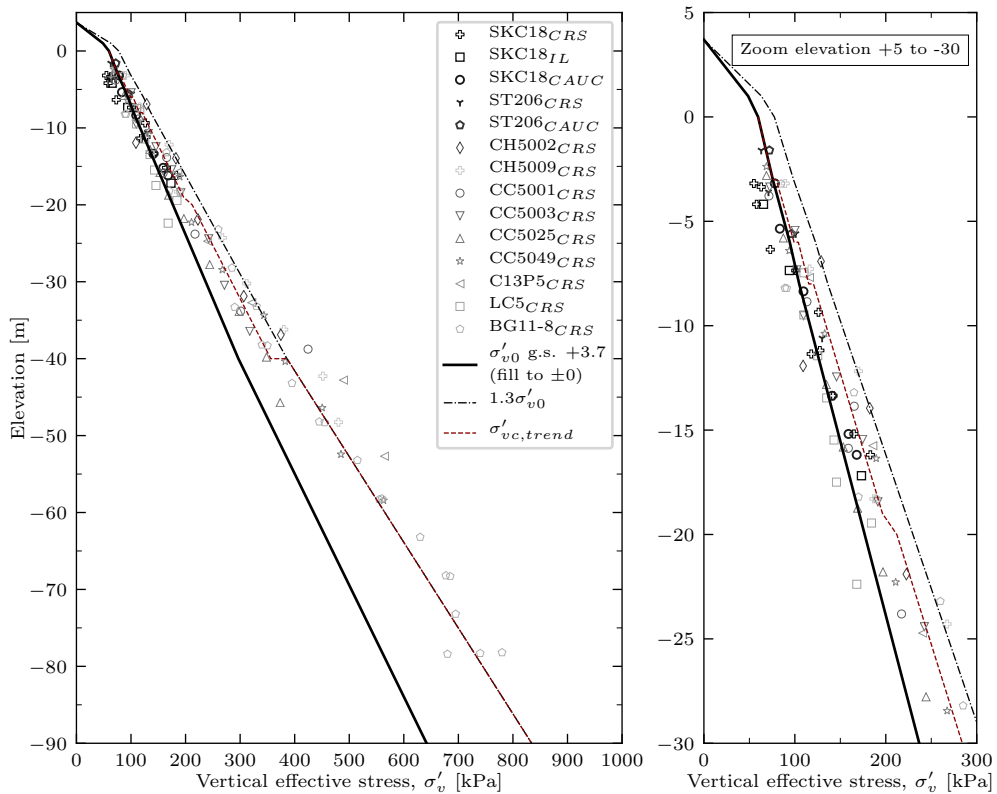
Figure 4.21: *Compilation of preconsolidation pressures from performed and collected previous laboratory tests in relation to effective vertical stress in the location of the studied excavation. $\sigma'_{vc,trend}$ plotted based on σ'_{v0} and OCR in Table 4.3.*

4.3.4 Numerical analyses based on the laboratory tests

Based on collected previous data and the previously presented additional laboratory testing (i.e. IL and CRS tests) - preliminary model parameter values for the Creep-SCLAY1S constitutive soil model were derived. Furthermore, the model parameter values were calibrated (Harlén and Poplasen 2019) against the additional triaxial tests that were carried out. The model parameters and values are presented in Tables 4.2 and 4.3.

Table 4.2: Creep-SCLAY1S model parameters and range of values for initial analyses of Gothenburg clay at the location of the studied excavation (Harlén and Poplasen 2019).

Parameter	Definition	Value
λ_i^*	Modified intrinsic compression index	0.046-0.062
κ^*	Modified swelling index	0.005-0.017
M_c	Stress ratio at critical state in triaxial compression	1.37-1.42
M_e	Stress ratio at critical state in triaxial extension	1.0-1.1
ω	Rate of rotational hardening	35-65
ω_d	Relative rate of rotat. hardening due to deviator strain	0.93-0.96
a	Rate of destructuration	8
b	Relative rate of destructuration due to deviator strain	0.5
α_0	Initial anisotropy	0.53-0.55
χ_0	Initial amount of bonding	9-24
μ_i^*	Modified intrinsic creep index	0.0015-0.0020

The range of derived parameter values (where specified) are based on initial analyses carried out within the framework of a Master thesis (Harlén and Poplasen 2019) which was supervised by the author.

Table 4.3: Additional parameters of clay layers used for initial analyses (Harlén and Poplasen 2019).

Layer	Level [m]	ρ [t/m^3]	OCR [-]	e_0 [-]	$k_x=k_y$ [m/s]
1	+0 to -3	1.57	1.00	2.08	1.2×10^{-9}
2	-3 to -6	1.65	1.05	1.81	0.7×10^{-9}
3	-6 to -8	1.55	1.10	2.16	2.1×10^{-9}
4	-8 to -19	1.63	1.15	1.76	1.2×10^{-10}
5	-19 to -40	1.63	1.20	1.76	0.8×10^{-10}
6	-40 to -90	1.72	1.30	1.51	0.5×10^{-10}

4.4 In-situ monitoring set-up

4.4.1 Introduction

The excavation and permanent structure is located in a setting of soft sensitive plastic clay. The aim of the monitoring program has primarily been to study the development of vertical and horizontal effective stresses in the short- and long-term (construction and design period). However, in order to study the response over time, the monitoring also covers the response of for example horizontal and vertical displacements as well as pore pressures during the construction period. This section describes the layout and details of the instrumentation.

4.4.2 Design considerations

The excavation is a part of the on-going construction of the Hisings Bridge in Gothenburg. The excavation and permanent structure are thus located in an area where the soft clay is well characterised. Furthermore, due to the restrictions on allowable deformations to the surroundings, the excavation was intended to be monitored and instrumented in the original design by the contractor (Skanska). Due to these settings, it was considered worthwhile for extra monitoring and instrumentation. Due to the authors affiliation with Skanska, the site was accessible for installation of additional instrumentation. This extra instrumentation included e.g. a bellow-hose and piezometers within the excavation, which demanded the attention of the personnel at site during excavation works, and special requirements such as for example excavation by hand. This was carried out by the author and the personnel at site, which were most helpful in assisting with constructing and placing special protections (e.g. well rings) and making sure the instruments were not damaged during excavation. The survival of the instruments would not have been possible without the attention and knowledge of the personnel at site.

The instrumentation for the monitoring of vertical and horizontal earth pressures and pore pressures under the permanent structure also required special considerations to be made. The instruments were placed in the clay below the concrete working platform. In order to protect the cables, plastic tubes were placed on the excavation bottom from the location of each sensor to the location of the logger. In total, this involved placing 13 tubes which were cast into the working platform. This enabled the sensor cables to be routed to the logger without being in harms way during the construction of the permanent structure (rebar and form works followed by pouring of concrete).

4.4.3 Layout of instrumentation

The layout of the monitoring program and the location of the instrumented section is presented in Figure 4.22 and summarised below. The location of the instruments within the excavation were chosen with respect to the layout of the piles.

- One extensometer (bellow-hose) within the excavation.
- Three piezometers (type BAT) within and three outside the excavation.
- Four inclinometers along the perimeter of the excavation.

- Monitoring points installed on of the ground surface, the sheet pile walls and concrete working platform.
- Monitoring of strut force (3 struts with 4 strain-gauges at each strut, one of the monitored struts located in the instrumented section).
- In one section, three stations with automated data collection of:
  - Vertical and horizontal earth pressure by means of vibrating wire (VW) total earth pressure cells
  - Pore pressure by means of VW piezometers including thermistors for measurement of temperature.
  - Vertical relative displacement of concrete slab and clay layer by means of a VW extensometer (installed in of the three locations).
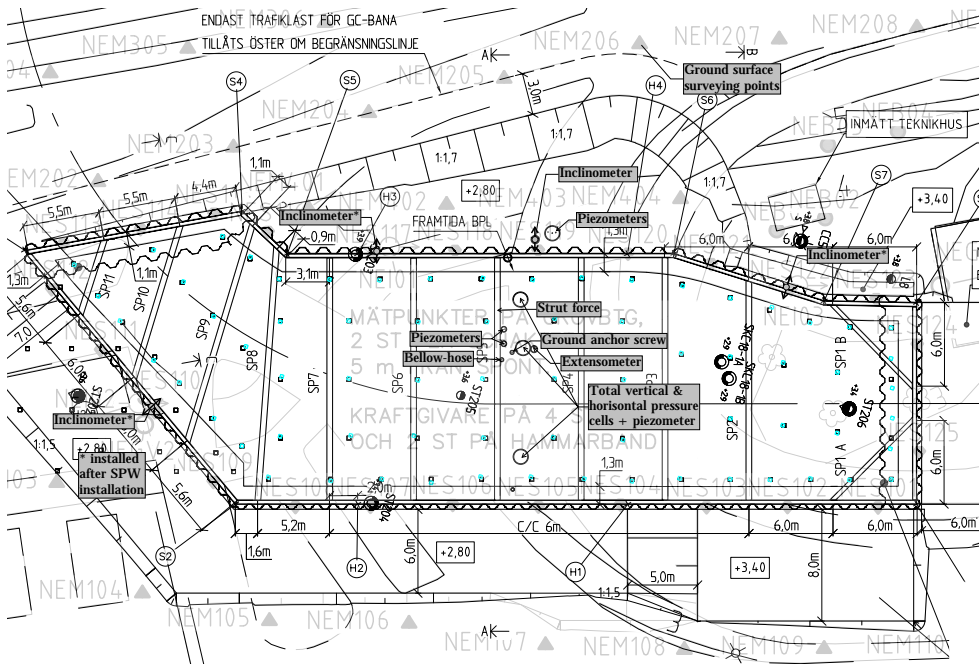
Figure 4.22: *Plan of the monitoring and instrumentation at the Hisings bridge site.*

4.4.4 Details of instruments and sensors installed in the clay

4.4.4.1 Vertical displacement

The vertical displacements have been measured using different methods, see Table 4.4. Details of the methods are described in the following (excluding surveying points).

Bellow-hose: The vertical displacement was measured manually throughout a bellow-hose installed within the excavation. The hose have an outside diameter of ∅30 mm with

Table 4.4: Instrumentation and monitoring for measurements of vertical displacement.

Instrument	Note
Extensometer (bellow-hose)	Bottom level -38.4 (installation depth 41 m)
Extensometer (vibrating wire)	Grouted spider legs anchor with centre at level -4.0 (1.6 m below bottom of concrete slab).
Earth anchor screw	Top at level -3.4 (centre screw at approximately -3.7).
Surveying points (levelling)	Ground surface and working platform.

metal rings placed on the inside continuously with a distance of 1.0 m. The bellow-hose was installed on November 8th 2018 to 41 m depth below installation level (bottom metal ring at level -38.4) through a casing. Before pulling the casing bellow-hoses intended for measuring settlements are normally pre-tensioned using an inner steel rod in order to facilitate for compression and measurements of settlements. However, for this monitoring program, concerning measurements of heave, the hose was pulled just enough to straighten out the slack before pulling the casing. That is, no pre-tensioning was applied in order to minimise the stiffness of the hose to effect the measurements. The zero-reading was established as the average of two readings performed on December 14th and 17th. All measurements have been performed by the author to reduce measurement error due to operator handling of e.g. the measurement tape. For every measurement set-up, readings were taken on the way down (lowering the electric probe attached to a measuring tape to the bottom of the bellow-hose) and on the way up (extracting the probe). The readings were in general the same or differentiated by maximum 1 mm. The accuracy of the bellow-hose readings is therefore estimated to ± 1 mm.

Since the clay layer extend down to ca 90 m depth, the bottom of the bellow-hose floats in the clay layer. Normally the bottom is installed into firm soil layers and used as a reference for levelling. This method could not be used in the current case. Therefore, a tripod was customised, see Figure 4.23, for which the reference level was established by surveying for each individual set-up, 24 in total. The surveying was carried out by Skanska's surveyor using a Leica TS16 total station. The accuracy of the instrument itself is high in controlled environments, 1 mm ± 1.5 ppm for distance and 1 arcsec for angular measurements (Leica 2020). However the accuracy of the levelling at site was estimated to ± 2 mm (empirically based on measurements of multiple reference objects in the geodetic system used for each measurement set-up and affected by e.g. weather conditions) which ads to an estimated total accuracy of ± 3 mm in the bellow-hose measurements (possible off-set ± 2 mm due to levelling and ± 1 mm per measurement level).

The bellow-hose was maintained throughout the pile installation and excavation process by means of protective measures (well rings) and excavation by hand. Once the excavation had reached final depth, the bellow-hose was then first cast into the working platform (within an outer $\varnothing 0.3$ m PVC pipe) and then into the 1.0 m thick concrete slab. The bellow-hose was protected from debris going into the hose by a rebar iron including a clamp. The rebar iron was damaged and broke during the construction activities that followed casting of the slab, it was not able to retrieve the debris and the final measurement

in the bellow-hose was therefore on December 3rd 2019, approximately 3 months after the slab was cast and 1 year after the first measurement in the bellow-hose. A total of 24 individual measurements were carried out.

Figure 4.23: *Customized tripod for measurements of vertical displacements in bellow-hose "floating" in the clay layer. The reference level of the tripod was established by surveying for each measurement setup, 24 in total.*

Earth anchor: An earth anchor was installed so that the top of the anchor rod was located at level -3.41 and the centre of the screw approximately at level -3.7. Levelling by means of surveying was carried out by inserting a smaller steel rod of known length into the casing rod and on top of the anchor. The anchor was installed using a casing rod with a clutch, i.e. when the anchor was screwed to the intended level, the rotation of the casing was reversed and then pulled up 0.1 m. This enabled the anchor screw to float in the clay unaffected by the casing.

Vibrating wire extensometer: For automated data collection of vertical displacements, a vibrating wire (VW) extensometer was installed after excavation to final depth. The purpose of the VW extensometer was to monitor the relative movement of the concrete slab and the clay just below it. The extensometer was manufactured by RST instruments. The sensor range is 100 mm and was set to allow for 75 mm compression and 25 mm extension. The specified accuracy from the manufacturer is $\pm 0.25\%$ FS i.e. ± 0.25 mm and the resolution 0.02% FS i.e. 0.02 mm. Figure 4.24 show a photo of the assembled extensometer before installation.

The automated extensometer measurements is done in conjunction with the measurements of vertical and horizontal earth pressures beneath the slab (described in the subsequent section 4.4.4.4). The bottom of the extensometer is located 1.6 m below the slab and a detailed cross section is included in Appendix C Figure C.21.

Figure 4.24: *Assembly of vibrating wire extensometer including spider anchor legs before installation 2019-07-02.*

4.4.4.2 Horizontal displacement

The horizontal displacements were monitored using inclinometers with automated logging. Three inclinometers were installed after installation of the sheet pile wall in steel casing tubes welded to the wall. These inclinometers were part of the contractors monitoring program and installed by subcontractor Geometrik. An extra inclinometer was installed at a distance ca 1.5 m behind the sheet pile wall (west wall) before the start of construction works. This inclinometer was installed in order to monitor the entire construction process (starting with pile installation). The inclinometer pipe was installed to 27.7 m depth below ground surface (i.e. bottom level -25.1 in the inclinometer location). This inclinometer was also instrumented by Geometrik with the sensors located at 2.0 m center to center distance throughout the pipe. The sensors were manufactured by Geometrik and referred to as "Multi-inclinometers" with a specified accuracy of 0.2% FS (corresponding to ±0.2mm/m).

4.4.4.3 Pore-pressure

BAT piezometers: Piezometers were installed in- and outside the excavation in order to monitor the pore pressures in the clay during construction. BAT-sensors (BAT 2020) were installed and connected to the data logging system of the inclinometers. The BAT system consist of a filter tip mounted to 1" galvanised steel rods and pushed into the clay. The filter tip is sealed by a water tight membrane which is penetrated by an injection needle when taking readings. Three piezometers were installed inside the excavation (for location refer to Figure 4.22) with filter tips at 11, 21, 31 m below installation level (corresponding to levels -9.4, -19.4 and -29.4). Three piezometers were installed outside the excavation, ca 1.5 m behind the west sheet pile wall, with filter tips at 5, 12, 22 m below installation level (corresponding to levels -2.2, -9.2 and -19.2). The piezometer outside the excavation at level -19.2 were damaged during SPW installations and have thus been excluded from the results. The other BAT piezometers were active from the start of construction (installation of piles) and throughout the excavation process, requiring excavation by hand and rerouting of the cables to be placed under the concrete working platform after the excavation had reached final depth.

Vibrating wire piezometers: In order to monitor the pore pressure under the slab, piezometers with vibrating wire (VW) transducers were installed at three locations (for location refer to Figure 4.22) in a section located central in the excavation. The piezometers were installed together with the total earth pressure cells described in the next paragraph. The VW piezometers were manufactured by RST instruments (item number VW2100) and have a diameter of 19 mm and length of 130 mm. The transducer pressure range is 350 kPa with a specified accuracy from the manufacturer of $\pm0.10\%$ FS i.e. ±0.35 kPa and a resolution 0.025% FS i.e. 0.09 kPa. The piezometer housing also includes a thermistor for measuring the temperature (specified resolution $0.1°C$), which in turn is used for correction of the measured pore pressure. Glycerine was selected as cell fluid in the piezometers and the filters were saturated by submersion in glycerine under vacuum in the geotechnical laboratory at Chalmers. Verification of the calibration factors supplied by the manufacturer, including verification of the thermistors, was also made at Chalmers for all sensors.

4.4.4.4 Total earth pressure cells

In order to measure the vertical and horizontal effective stresses under the slab, total earth pressure cells were installed at three locations (for location refer to Figure 4.22) in a section located central in the excavation. The total pressure cells were manufactured by RST instruments (item number LPTPC-09-V-LP). A photo of one of the cells is presented in Figure 4.25. The cells are constructed of stainless steel plates which are welded together. The space between them consist of deaired 50/50 water and ethylene glycol which via a steel tube is connected to a housing containing the vibrating wire transducer. The cell diameter is 241 mm (9.5") and the thickness is 10 mm. The low ratio of thickness to radius was one of the reasons for choosing this type of cell (as opposed to for example push-in spade cells). The thickness of the hydraulic fluid inside the cell is 1.52 mm (communication with RST Instruments, 2020). One side of the cell have a raised surface (sensitive side) and the housing for the vibrating wire transducer is located 46 cm from the cell in order to avoid influence on the pressure readings. The transducer housing also contains a thermistor enabling recording of temperature. The transducer pressure range was set to the lowest possible value of the model, 700 kPa, with a specified accuracy from the manufacturer of $\pm0.15\%$ FS i.e. ±1.05 kPa and the resolution 0.025% FS i.e. 0.18 kPa. Verification of the calibration factors supplied by the manufacturer was made in the Geotechnical Laboratory at Chalmers for all sensors.

4.4.5 Data acquisition

The vibrating wire sensors installed under the permanent structure (piezometers, total earth pressure cells and an extensometer including their associated thermistors) were connected to a remote data logger to enable automatic data acquisition. The monitoring is intended as long-term monitoring extending beyond the end of the construction period. The data logger was manufactured by RST instruments (model number DT2040) and allows for automatic readings of 40 sensors (e.g. 20 vibrating wire sensors and 20 associated thermistors). The adopted interval for data readings have varied between 0.5-6 hours, with the shorter intervals at times of significant construction activities such as for example

Figure 4.25: *Photo of total earth pressure cell.*

during the pouring including hardening process of the concrete for the concrete slab.

The vibrating wire piezometers and total earth pressure cells were manufactured with RST instruments EL380004 meter marked cables (which were cross referenced with the calibration protocols in the case of damage to the cables). In order to avoid cable splicing and to minimise potential signal distortion, the cables were ordered in full lengths of 20, 30 and 40 m depending on the location of respective instrument within the excavation. The inclinometers and BAT-piezometers were connected to data loggers with remote GSM transfer supplied by Geometrik as part of the contractors system for continuous monitoring during the progress of excavation.

4.4.6 Verification of sensor calibration factors

The frequency from a vibrating wire transducer is transformed from raw units ($Hz^2/1000$ for the sensors used in this study) to e.g. load, pressure or deformation using conversion equations and calibration factors. Before installation in the field, the sensors unique calibration factors specified by the manufacturer were verified in a controlled laboratory environment at the Geotechnical Laboratory at Chalmers. These VW sensors were to be installed in the clay under the permanent concrete structure and connected to the data logger for unattended long-term monitoring. The verification focused on the expected pressure ranges during operation in the field. During these verifications, it was made sure that the instruments were assigned to the logger channels that would later be used during the field installations. Thus verification of the instrument calibration factors as well as a test of the logger set-up was achieved in the laboratory.

The piezometers were set under pressure in a plexiglas cell which was filled with water. The applied pressure, as presented in detail in Appendix C.2.2, was increased in steps from 0 kPa to approximately 10, 40, 70, 140, 210, 280 kPa and then reversed back. The maximum value was selected well below the transducer pressure range of 350 kPa. A photo of the pressure cell as well as results of the calibration factor verifications is presented in Appendix C.2.2.

As for the piezometers, it was decided to pressurise the total earth pressure cells in water. A special chamber was set-up due to the sheer size of the earth pressure cells. The set-up comprised of a PVC-pipe which was filled with water and sealed in the ends by wooden plates with rubber membranes in between them. The cell was assembled using clamps, since it had to be disassembled and reassembled for all of the total pressure cells. A photo of the pressure cell as well as results of the calibration factor verification is presented in Appendix C.2.3. The cells were submerged resulting in the first reading resulting from water pressure only. Air pressure was then applied so that the total applied pressure was increased in steps to approximately 15, 20, 50, 70, 100, 150 kPa and then reversed back. As described further in Appendix C.2.3 the set-up worked satisfactory for verification of pressures in the expected working range, but not above approximately 70 kPa.

4.4.6.1 Potential errors in total pressure cell readings

The accuracy of hydraulic total earth pressure cells is depending on for example ratio thickness to diameter (large diameter to thickness preferable), uniformity of loading, temperature, installation procedures and ratio of soil and cell modulus. Some of the potential sources of errors associated with total pressure cell readings in this project are highlighted in the following paragraphs.

Arching: Initial tests to verify the calibration factors of the total earth pressure cells in the laboratory were made by placing the cells in gravely sand (particle size 0-4 mm). However, it proved very difficult to get consistent readings due to e.g. difficulties in reproducing the compaction of the sand (different readings were obtained based on the amount of compaction and wetting of the sand), applying a uniform large stress by use of dead weights, as well as the presence of arching effects in the sand-cell membrane interface. This and reviewing e.g. David Suits et al. 2005 highlighted the problem of arching around embedded earth pressure cells to the author and, as described later in section 4.4.7, it was decided to level the excavated clay surface with only a minimum layer of sand in order to minimise arching effects in the field. This potential cause of error was therefore recognised before the field installations, however the error described below was not.

Cell fluid temperature correction: Considering the influence of temperature variations, temperature correction factors were supplied from the manufacturer (communication with RST Instruments, 2020). However, this only accounts for temperature correction for the VW pressure transducer. That is, it does not consider the effect of temperature on the fluid within the cell. Unfortunately this was not recognised by the author during the verification of the calibration factors in the laboratory. This would have enabled for example measurements of pressure change due to temperature variation under a condition of zero load. Such studies are described in e.g. Daigle and Zhao (2004) and Huntley and Valsangkar (2016) whom also studied the influence of temperature change for various stress levels. Average thermal correction factors (approximately linear) for cells under zero load condition were -0.12 kPa/°C (Huntley and Valsangkar 2016) for ⌀230 mm t=12 mm cells and -0.30 kPa/°C (Daigle and Zhao 2004) for ⌀228 mm t=6 and t=12 mm cells. For cells under condition of loading the correction factors increased as well as non-linearity.

However, as pointed out by Huntley and Valsangkar (2016) even deriving temperature cell fluid correction factors in the laboratory will be associated with uncertainty as the cell boundary conditions (stress and stiffness) in the field would be difficult to recreate in laboratory conditions. Estimates of the magnitude of correction factors for cell fluid temperature change were described by Sellers in 2000 (Huntley and Valsangkar 2016):

$$CFT_{cell} = \frac{aEKD}{R} \tag{4.4}$$

where CFT_{cell} is correction factor due to change in temperature (kPa/°C). The subscript $_{cell}$ is added here to differentiate from the CFT_{vw} supplied by the manufacturer only accounting for effect of temperature change on the WV-transducer itself. a is a factor (1.5 for embedded earth pressure cells and 3.0 for contact pressure cells attached to structures), E is Young's modulus of the soil (in GPa), K is coefficient of thermal expansion of the cell fluid (10^{-6}/°C), D is thickness of fluid inside cell (in mm) and R is cell fluid radius (in mm). This leads to an estimate of CFT_{cell}=0.2 kPa/degr (see details in Appendix A section C.2.1). Another way of (more accurately) obtaining CFT_{cell} values is by evaluating the pressure change during temperature variations under expected periods of zero change in pressure. That may however be difficult in the case of a clay deposit with on-going construction activities as well as creep settlements in the surroundings.

The results presented in Chapter 5 does only include temperature correction for CFT_{vw} and have (at this stage) not been corrected with respect to CFT_{cell}. As presented in Chapter 5 Figure 5.11 the maximum temperature change, approx. 15°C, was recorded after pouring of the concrete for the 1.0 m slab. The temperature change in the long-term is modest (temperature stabilizing at 7-8°C) and temperature influence on long-term measurement data is therefore likely to be reduced substantially. It should also be noted that the thermistors for temperature readings is located in the VW transducer housings. The horizontal earth pressure cells (centre of hydraulic housing located at level -3.28) thus likely experienced temperature changes equal to or less than that recorded in the piezometers (level -3.05). The vertical stress cells (laid out flat at level -2.67), being most exposed to temperature increase during the concrete hardening process, as stated before exposed to approximate increase of 15°C. Taking a CFT_{cell} value to 0.2 kPa/°C this may have resulted in stress increase due to increase in temperature of maximum ca 15x0.2=3 kPa, that is only an effect of change in temperature and not in earth pressure. Results of adding CFT_{cell}=0.2 kPa/°C to CFT_{vw}s supplied by the manufacturer are presented in Appendix A section C.6 figure C.25-C.27.

4.4.7 Field installation of sensors for unattended monitoring

This section describes the details of installing the instruments which are located in the clay under the permanent concrete slab and intended for long-term unattended monitoring, i.e. the sensors equipped with vibrating wire transducers.

4.4.7.1 Total earth pressure cells

Total earth pressure cells were installed in order to measure the vertical and horizontal total stresses in the ground at three locations in the instrumented cross section (for locations see Figure 4.22). A detailed installation layout adopted for these locations is given in Appendix C.3 Figure C.20. Before the "final" installations described in the following, a number of trial installations were made in some of the first parts of the sequential excavation progress. These trials were carried out in order to make sure that the installations could be made; as planned, with a high level of detail and during a limited time due to the on-going construction activities and finally in order to minimise drying or wetting (if raining) of the clay.

As described in Section 4.2.4 the excavation reached final depth on June 26th in the instrumented section. Three well rings with inner diameter $\varnothing 1$ m and $\varnothing 50$ mm plastic tubes (one for each sensor cable) were then placed on the excavation bottom to the location of the logger. The well rings can be seen in Figure 4.26.
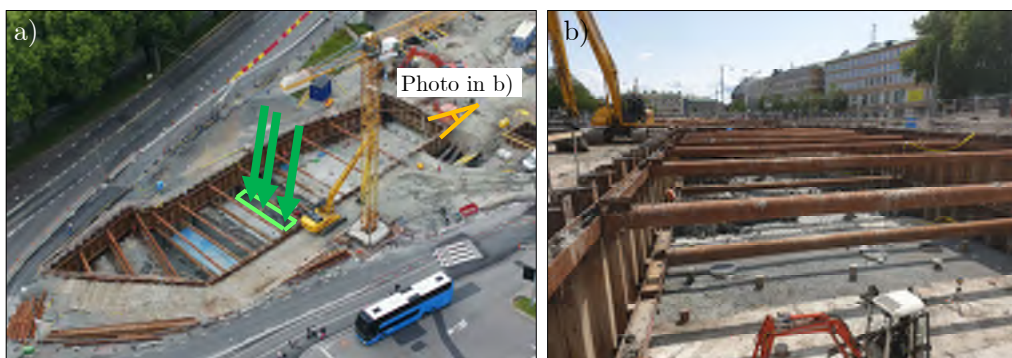
Figure 4.26: *Well rings placed on excavation bottom before pouring of concrete working platform. Green arrows in a) point approximately to well rings seen between piles in b).*

Before the well rings were set in place, plastic film and geotextile had been placed on top of the clay in order to prevent it from drying. The well rings were used in order to allow slots/holes for the installation of the total pressure cells and piezometers as the concrete working platform was cast on June 27th. Installation of the sensors and routing of cables to the logger through pre-drawn plastic tubes was carried out within the well rings on June 28th (location closest to west SPW) and June 30th (location closest to east SPW and approximate centerline). Site zero readings were taken immediately before installation of each cell. The total earth pressure cells for monitoring of the vertical total stresses were placed on the excavation bottom, levelling was made with gravely sand (particle size 0-4 mm). Measures were taken in order to prevent the concrete mortar to go into the sand during the subsequent pouring of concrete over the instruments. The sand was therefore carefully enclosed with double layers of plastic film. As the concrete for the working platform was reinforced with steel fibers, geotextile was placed as a last layer in order to prevent the steel fibers to punctuate the plastic film. Some photos from the installation is

presented in Figure 4.27. Full working order, details and photos of the installation process is given in Appendix C.4. On June 30th, concrete was carefully poured by means of shovel and wheelbarrow into the well rings and over the instruments. The concrete was supplied from the pouring of concrete in the next part of the sequential excavation progress.

Figure 4.27: *Installation of total earth pressure cells within one of the three well rings; a) and b) cell installed to measure horizontal earth pressure perpendicular to SPWs, c) cell to measure vertical earth pressure and d) careful pouring of concrete over instruments as final part of the installation.*

4.4.7.2 Piezometers

The vibrating wire piezometers were installed in conjunction with the earth pressure cells at three locations under the permanent concrete structure. For the piezometer installations, vertically hand-cut trenches were made in the clay as outlined in the detailed layout presented in Figure C.20. A 80 mm deep $\varnothing 16$ mm hole was then formed (using a drill bit) in the sidewall of the trench in order to ensure the fit when inserting the piezometer (L=130 mm, $\varnothing 19$ mm) into the hole. As for the total earth pressure cell, the size of the drill-bit and length of the hole was selected based on trial installations carried out in advance of the final installations. Site zero readings were taken immediately before installation of each cell. The piezometers were pushed slowly into place with simultaneous monitoring of the registered pressure in order to detect and avoid any over-range pressures to develop. The vertical trenches were then back-filled with remoulded clay (remoulding was carried out in a bucket with a hand-held mortar mixer and addition of small amounts of water).

4.4.7.3 Extensometer

The VW extensometer was installed in one location in the section that was instrumented with total earth pressure cells and piezometers. For location of the extensometer refer to Figure 4.22. The bottom anchor of the extensometer is located 1.6 m below the permanent concrete slab, a detailed cross section is presented in Appendix C.3 Figure C.21. For installation of the extensometer, a $\varnothing 90$ mm hole was extracted into the clay (the size of the spider legs in retracted position corresponded to ca $\varnothing 70$ mm). The extensometer was lowered into the hole and the release line for deploying the spider anchor legs was pulled.

The bottom anchor of the extensometer was thus fixated in the clay. After deploying the spider legs, the lower part of the installation hole was grouted followed by backfilling with sand and remoulded clay. The top of the extensometer was then cast into the working platform and bottom of the permanent concrete slab.

4.4.7.4 Temperature at ground surface

The temperature at the ground surface is registered in the datalogger and also by an additional thermistor placed outside the logger housing.

5 Instrumented site: results and discussion

5.1 Introduction

This section presents and discusses primary results from selected parts of the extensive set of measurement data. Extended analysis of the measurement data as well as final discussions and conclusions will be presented in forthcoming publications.

5.2 Soil response during excavation

The soil response during excavation was monitored by means of a bellow-hose (vertical displacements) and BAT-piezometers inside the excavation in addition to inclinometers outside the excavation. The results of these measurements are presented in this section. In addition, conventional monitoring of surveying points, strut forces (strain gauges) and groundwater in the upper aquifer/fill material were made within the contractors monitoring program. The results of remote measurements of total stresses, pore pressures and displacement under the permanent concrete structure using vibrating wire sensors are presented in Section 5.3.

5.2.1 Vertical displacements

Results of measurements of vertical displacements in the bellow-hose inside the excavation are presented in Figure 5.1 as displacements versus elevation and in Figure 5.2 as displacements versus time. Figure 5.2 also includes measurement results of the earth anchor screw, installed below the final excavation level.

As seen in Figure 5.1 the installation of the pile elements (combined steel and concrete elements) initially resulted in heave. However, pre-augering was carried out in order to reduce the deformations to the surroundings. When pre-augering was carried out in the pile locations in the proximity of the bellow-hose, this resulted in settlement in the soil layers above 18 m depth (the depth to which the augering was carried out). The measurement data from this stage of the construction process provides valuable information on the vertical deformations arising during augering and pile installation, as measurements in typical Swedish construction projects focus on minimising the deformations to the surroundings and therefore only monitor the horizontal deformations outside the pile installation area. The subsequent sheet pile walls installation resulted in heave above level -12. Mass displacement due to installation of SPWs in soft clay is normally neglected (current practice at Skanska) in relation to the large displacements typically resulting from hammered concrete piles. The registered maximum heave of 10 mm during installation of the SPWs was therefore larger than expected. These results show that installation of SPWs should not be considered as wished in placed neither during planning of construction works or when modelling excavation problems.
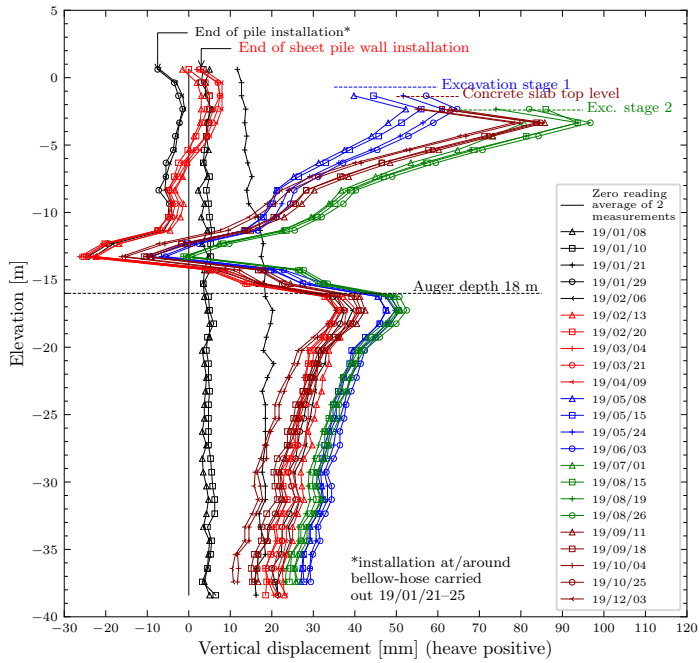
Figure 5.1: *Vertical displacements measured in the bellow-hose inside the excavation. Presented as displacement at respective measurement level throughout the bellow-hose.*
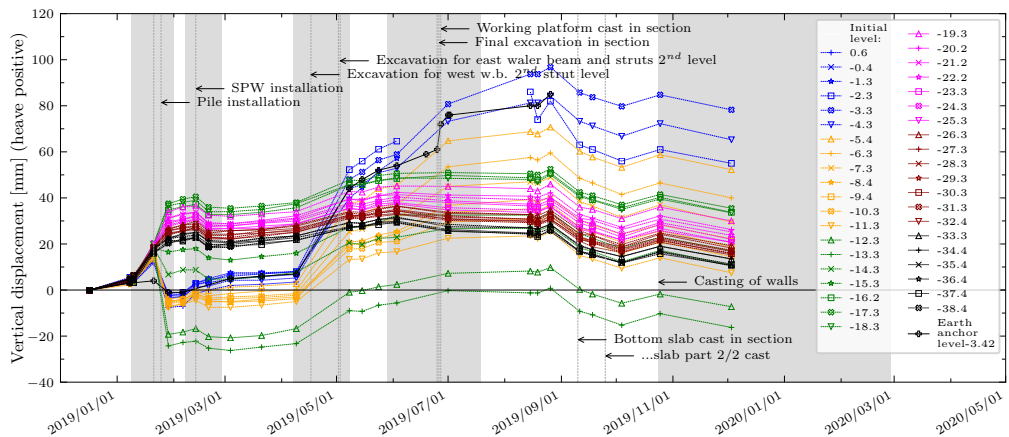
Figure 5.2: *Vertical displacements measured in the bellow-hose and earth anchor inside the excavation. Presented as displacement at respective measurement level versus time. The timestamps for occurrence of main construction stages in the studied section are annotated and the shaded areas indicate the total time span for these activities.*

Heave continued to develop during the subsequent sequential excavation and strut installation processes which extended over approximately two months (from April to end of June 2019). A maximum heave of 97 mm was registered at level -3.3 corresponding to ca 0.7 m below the final excavation level in the location of the bellow-hose. The maximum heave corresponds to 2.0 % of the excavation depth (4.8 m by comparing the level of the ground surface, +2.2 during pile installations, to the lower level of the concrete working platform, level -2.6). After casting of the concrete working platform on June 27th in the location of the bellow-hose, heave continued to develop above level ca -12 until the time of casting the permanent concrete slab. Below level -12 the measurements indicate no significant continued vertical displacements (possibly small settlements, but within the estimated accuracy of the measurements).

The casting of the 1.0 m thick concrete slab, on September 10th in the location of the bellow-hose, caused settlements throughout the entire bellow-hose based on measurements the day after casting. The settlements continued to develop the subsequent three months that the measurements were continued. This result disregards the measurement on October 25th, based on the general trend extracted from the 4 other measurements after casting. Based on the general trend no distinguishable settlement continued after the last measurement on December 3rd 2019. The bellow-hose was then clogged by a broken rebar iron and clamp that was intended to protect the bellow-hose from debris entering during the remaining construction works.

The vertical strain rate in field has been evaluated from the bellow-hose measurements and the vibrating wire extensometer located under the slab. The strain rates are evaluated as average strain rate in between two readings (secant values). For the bellow-hose, the displacements were reset so that only the relative displacements occurring over the measurement length of the bellow-hose is considered, i.e. displacement below lower metal ring is discarded. The strain was calculated over the length of the bellow-hose (maximum difference throughout bellow-hose between two readings divided by length of bellow-hose divided by time period). In the bellow-hose the maximum strain rates occurred during pile installation (1.7×10^{-9} s^{-1} eq. to 5.4 %/year) and during the two main excavation stages ($3\text{-}4 \times 10^{-10}$ s^{-1} eq. to 0.9-1.3 %/year). The results are included in Figure 5.3 relating to some other recorded field and laboratory strain rates from the literature review.

The strain rate as evaluated from the VW extensometer readings is presented in Figure 5.4. The maximum strain rate occurred 3 hours after the start of pouring of the wet concrete for the 1.0 m concrete slab. The maximum strain rate (secant value between readings every 30 minutes) was 1.0×10^{-7} s^{-1}.
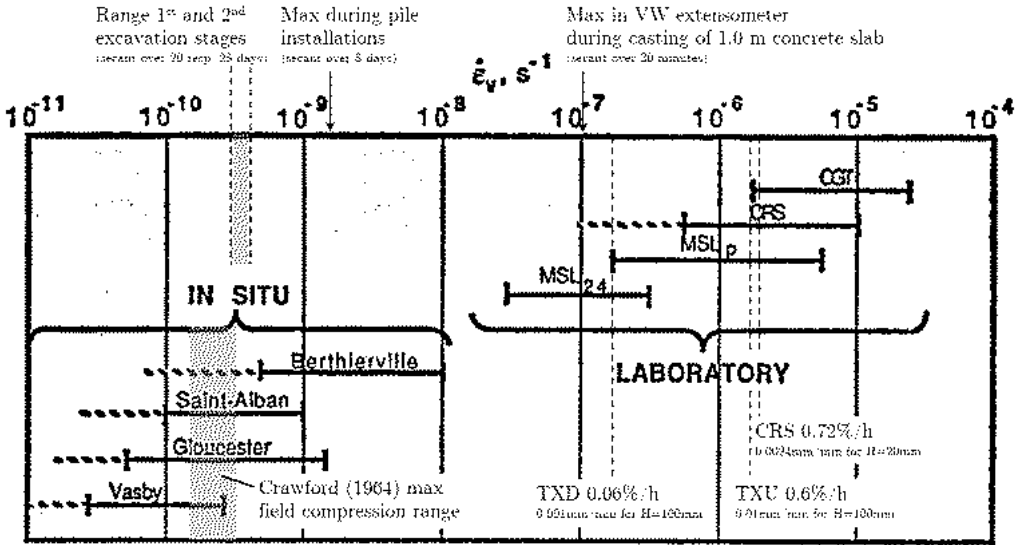
Figure 5.3: *Evaluated average vertical field strain rate over measurement depth of bellow-hose and VW extensometer (both secant values between timestamps of readings). Comparison to strain rates in laboratory tests and in the field from Leroueil, Kabbaj, and Tavenas (1988) as presented in literature review Section 2, Fig. 2.18.*
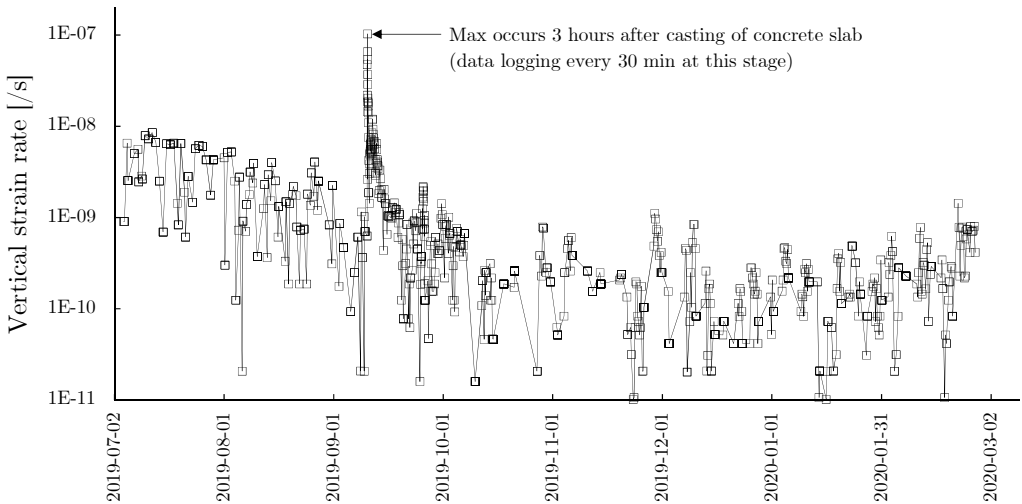
Figure 5.4: *Evaluated vertical field strain rate from VW extensometer readings plotted versus time.*

5.2.2 Horizontal displacements

Results of measurements of horizontal displacements in the inclinometer installed behind the SPW in the studied section are presented in Figure 5.5 as displacement versus elevation and in Figure 5.6 as displacement versus time. The inclinometer readings are corrected due to the bottom of the inclinometer not being a fix reference. The displacements are thus corrected with respect to the surveyed displacements in the top of the inclinometer.
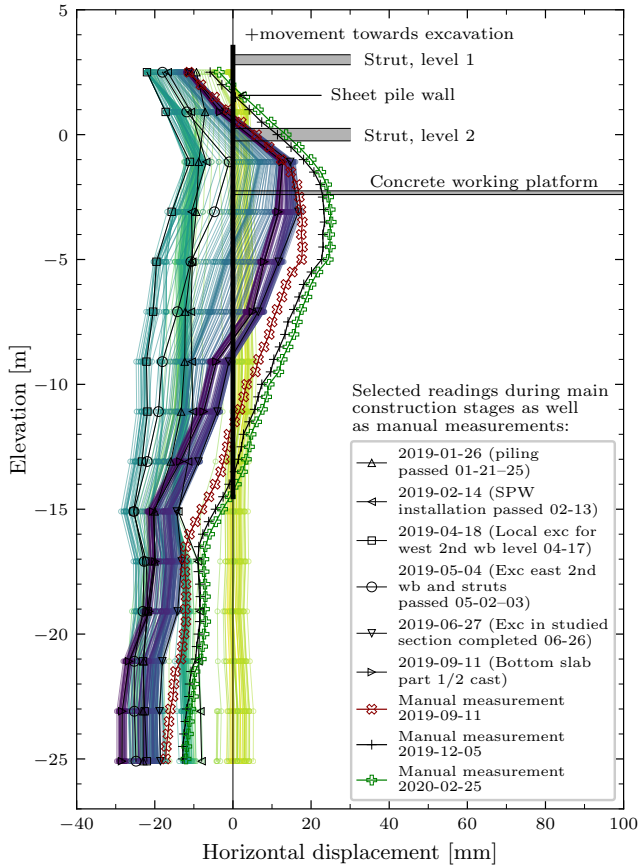
Figure 5.5: *Horizontal displacements measured in inclinometer behind the SPW in the studied section. Plot of daily average values. The color mapping include all of the automated measurements (2018-12-06 to 2019-09-11).*

Figure 5.6 indicate that the pre-augering down to level -16 during pile installation reduced the pile induced horizontal displacements in the top soil layers (approximately 10 mm compared to 20 mm below level -16). This is connected to the observed settlements down to level -16 in the bellow-hose during pre-augering. During the excavation process the maximum horizontal displacement occurred at level -3. The maximum excavation induced displacement was 32 mm 2019-06-27 (net displacement 17 mm).
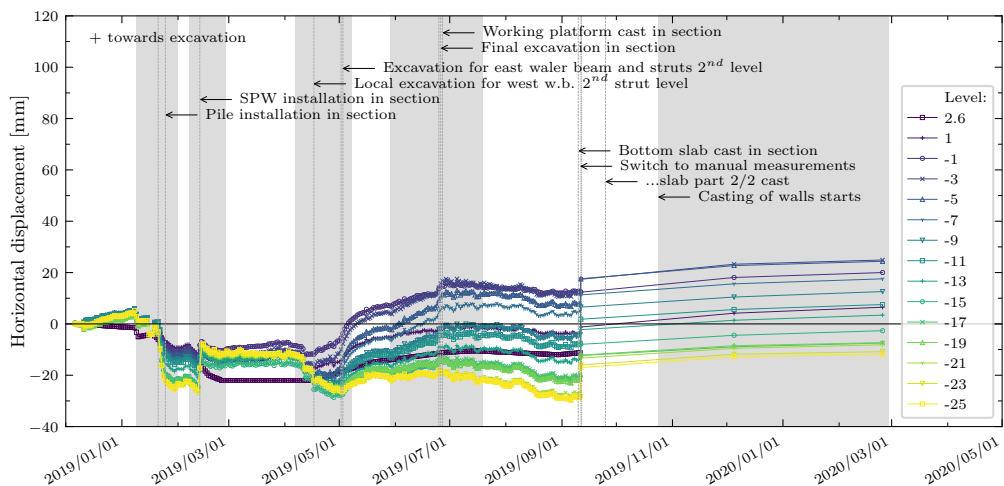
Figure 5.6: *Horizontal displacements measured in inclinometer behind the SPW in the studied section. Plot of daily average values. Presented as displacement at respective measurement level versus time. The timestamps for occurrence of main construction stages in the studied section are annotated and the shaded areas indicate the total time span for these activities.*

After casting of the slab 2019-09-10 the automated sensors were extracted and a manual measurement was made. The maximum displacement obtained from the manual measurement was 18 mm and agree closely with the automated measurements down to level -3. Below level -3 they differ by maximum 10 mm. The manual measurements in this case provide better accuracy compared to the automated sensors. This is due to the manual readings being carried out at 0.5 m intervals. Thus the potential error in accumulated horizontal displacement is minimised (the automated sensors were located with 2.0 m cc-distance towards depth, which increases the error due to the extrapolation of accumulated displacement).

After casting of the concrete slab the manual measurements 2019-12-05 and 2020-02-25 indicate continued displacements towards the excavation of maximum 6 mm (corresponding to 1 mm/month) at approximately level -3. The continued deformations towards the excavation may be a result of relaxation of the pile induced displacements.

5.2.3 Pore pressure

Pore pressures were measured using BAT-piezometers down to level -29 during the pile installation and excavation works. The results are presented in Appendix C Figure C.24.

5.3 Soil response after excavation - sensors under concrete slab

This section presents selected results from the measurements of earth pressures, pore pressures and displacements under the permanent concrete structure. The measurement data is evaluated and discussed in this chapter, although future additional analyses are to be carried out as these measurements are intended for long-term monitoring of the development of earth pressures.

5.3.1 Vertical and horizontal total stresses

The results of measurements of vertical and horizontal total stresses under the concrete working platform and permanent slab are presented in Figure 5.7. When studying these results it should be noted that the centre of the membrane of the cells measuring the horizontal stress are located 0.6 m below the level of the cells measuring the vertical stresses (for detailed layout see Figure C.3). The measurement data from the earth pressure cells have been corrected for change in temperature and barometric pressure. For details on these corrections refer to Appendix section C.2. Uncorrected measurement values are presented in Appendix Figure C.28.

Based on the data in Figure 5.7 the total vertical stress increased at the time of casting the concrete slab on September 10th (pouring of wet concrete started ca 07:00). The 1.0 m thick wet concrete corresponds to a vertical load of approximately 25 kPa. The registered increase in vertical total stress during the pouring of the wet concrete were 13, 26 and 15 kPa (recorded ca 13:00) in the locations corresponding to; west of centre line, approximate centre line and east of centre line. The reason for the smaller increase in vertical stress in the cells located closer to the SPWs are believed to be due to the fact that the working platform was "locked in" between the SPWs. Therefore, closer to the SPWs some of the weight of the wet concrete rested on the working platform. Closer to the centre of the excavation the working platform was not restrained to displace vertically and the load exerted on the clay layer corresponded to approximately the weight of the wet concrete. The pouring of the wet concrete of a known thickness provided an excellent opportunity for verification of the sensor installations and setup in the field. The results provided information on an overall satisfactory performance of the sensor installations and the preparatory work in the geotechnical laboratory at Chalmers.

5.3.2 Pore pressures

The results of measurements of pore pressures under the concrete working platform and permanent slab are presented in Figure 5.8 with change in barometric pressure obtained from Swedish Meteorological and Hydrological Institute 2020a. The measurement data from the piezometers have been corrected for change in temperature and barometric pressure. For details on these corrections refer to Appendix section C.2.
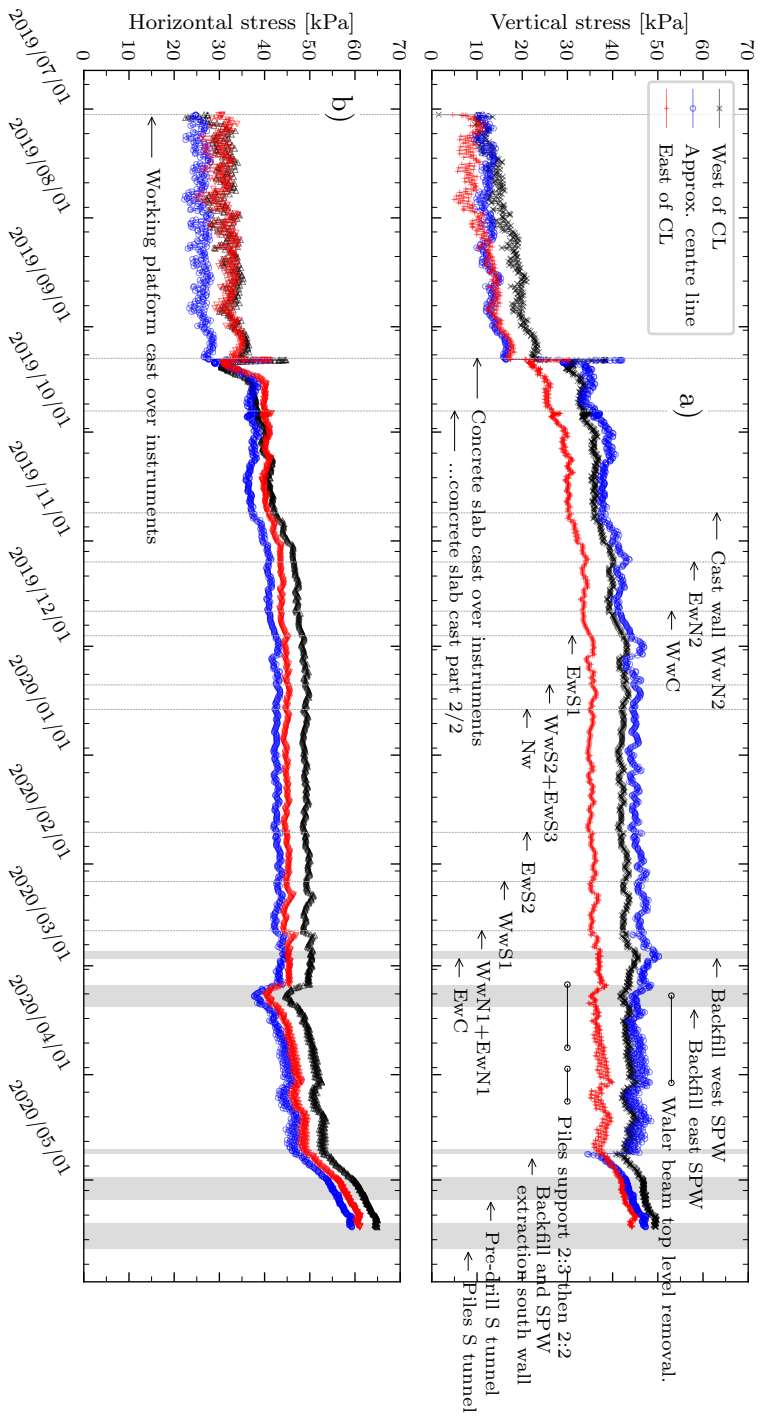
Figure 5.7: *Registered total stresses under concrete slab, a) vertical and b) horizontal stresses. The measurements have been corrected for changes in temperature and barometric pressure. The change in barometric pressure with reference to 2019-07-02 13:00 (101.2 kPa at the time when puring) is included based on data from Swedish Meteorological and Hydrological Institute 2020a. The occurrence of main construction stages including casting order for the walls of the structure are annotated. For layout of wall locations refer to Figure 4.8.*
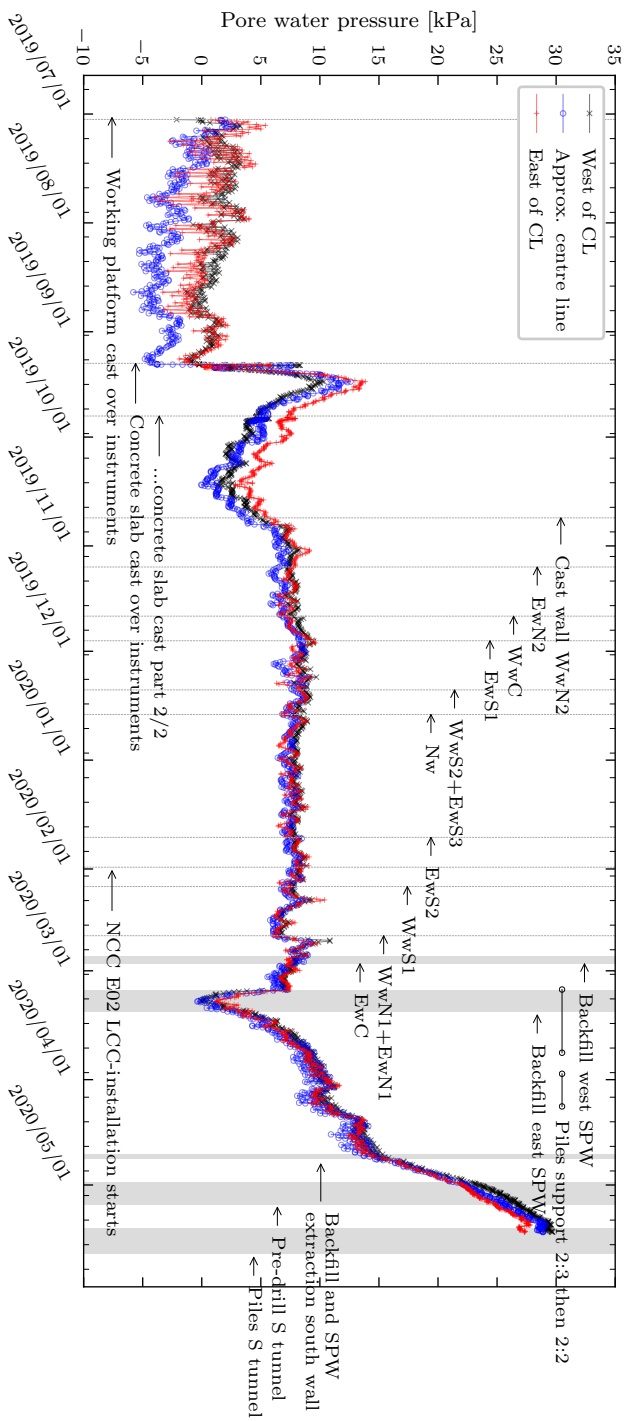
Figure 5.8: Registered pore pressures under concrete slab and change in barometric pressure. The measurements have been corrected for changes in barometric pressure and temperature. The occurrence of main construction stages including casting order for the walls of the structure are annotated. For layout of wall locations refer to Figure 4.8.

From the time of pouring the working platform in the location of the instruments (2019-07-02) up until casting of the concrete slab (2019-09-10) the pore pressures should be approximately 0 kPa based on pumping from excavation level within the pit. Close to 0 kPa values were recorded in the piezometers located in the west and east locations. However negative pore pressures (suction) was recorded in the centremost location. These values have been left unadjusted, since the recordings in the three stations have been in close agreement ever since casting of the slab.

During casting of the concrete slab 2019-09-10 (pouring of wet concrete started ca 07:00) the pore pressures increased to maximum values (at ca 13-14:00). The registered increase in pore pressures were 9, 11 and 6 kPa in the locations corresponding to; west of centre line, approximate centre line and east of centre line. The dissipation of these excess pore pressures had stabilized at 2019-09-11 02:00 (most of the excess pore pressures dissipated). Thereafter, the pore pressures increased to peak values around 2019-09-15 upon which the pressures again decreased until mid October. From mid October a slight increase followed to the start of November. The pore pressures then remained constant until works with back-filling between the structure and SPWs started in the end of February 2020. These works involved complete drainage of the pit in its lowest levels (in the south) before and in order to place and compact the back-fill material. The back-fill was placed up to level +2.0 which is above the estimated in-situ ground water level, located between level ±0 to +1 in the top most soil layers based on Figure C.3. 2020-04-23 the southern SPW was recovered (pulled up by vibro) and an increase/recovery in pore pressures has been registered thereafter. Ideally the pore pressures should recover to approximately 30-40 kPa if complete recovery is achieved (sensors located at level -3.05).

5.3.3 Effective stresses

The effective stresses were evaluated based on the measurements of total stresses and pore pressures under the concrete working platform and permanent slab. The effective stresses are presented in Figure 5.9. Viewing these results it should be noted that the centre of the membranes of the cells measuring the horizontal stresses are located at level -3.28, and the centre of the cells measuring the vertical stresses at level -2.67. The piezometers are located at level -3.05. The measured pore pressure have been subtracted from the vertical and horizontal total stresses although the piezometer is located in between them. Evaluation of the relation of vertical to horizontal effective stresses can therefore not be made directly from Figure 5.9. Such an evaluation is therefore presented separately in section 5.3.7 relating to K_0.

As seen in Figure 5.9 the vertical and horizontal effective stresses increased between 2019-07-02 (casting of the working platform in the location of the instruments) up until the casting of the concrete slab. This increase is most likely a result of the finalization of the remaining sequential excavation works within the pit (proceeded until the end of July 2019) and the accompanying heave process. Note that the registered pore pressure in the centremost location was negative during this time period, the evaluated effective stresses in this location are therefore overestimated by maximum ca 4 kPa.
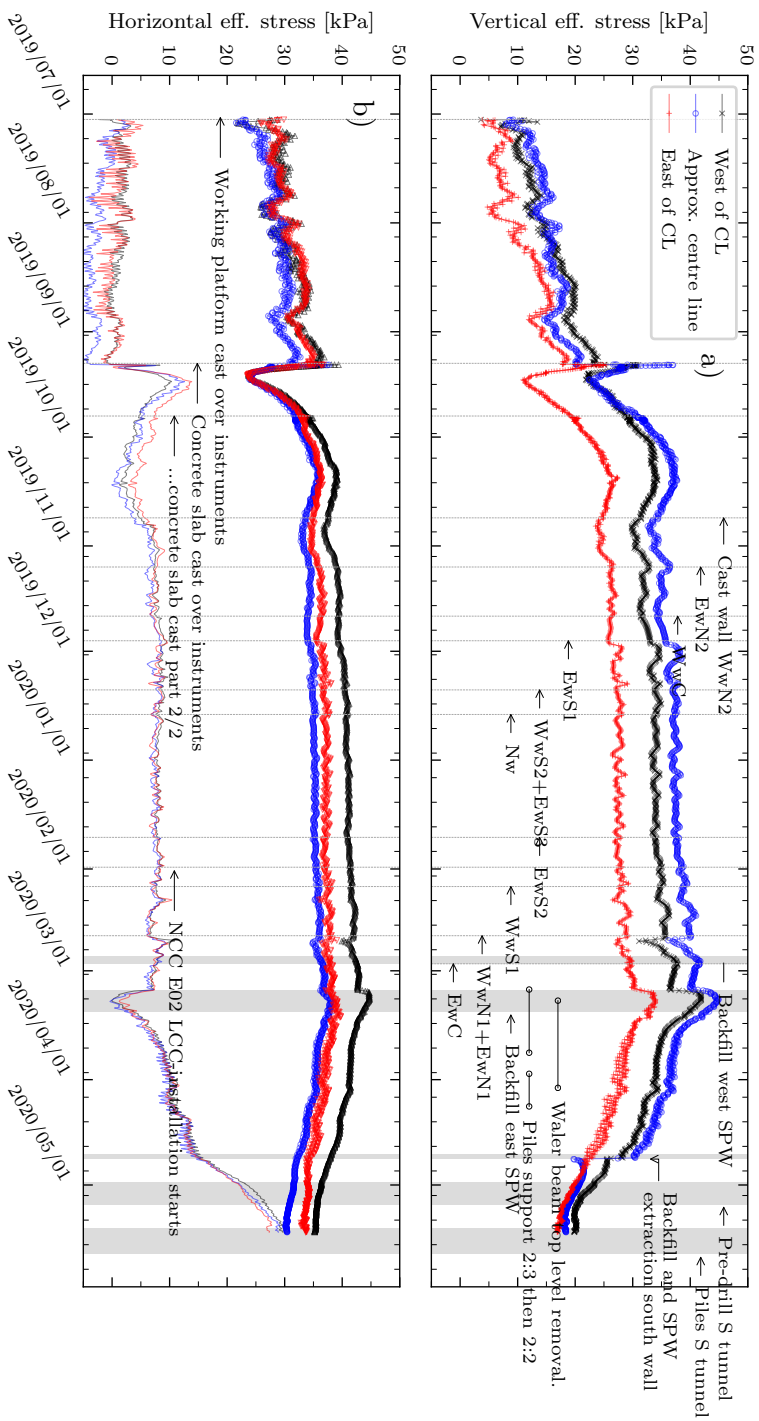
Figure 5.9: *Evaluated effective stresses under concrete slab,* a) *vertical and* b) *horizontal stresses. The occurrence of main construction stages including casting order for the walls of the structure are annotated. Included in* b) *are also pore pressures from Figure 5.8. For layout of wall locations refer to Figure 4.8.*

The casting of the slab resulted in general observations of the response as follows. During casting of the concrete slab on 2019-09-10 the vertical and horizontal effective stresses increased during pouring of the wet concrete (from 07:00 to 14:00) as the immediate increase in total stresses were not compensate for in excess pore pressures. As an example in the immediate vertical effective stress increase in the centremost location was 17 kPa and the horizontal effective stress 6 kPa (the maximum immediate increase in total stresses and pore pressures were offset by 1-2 hours, pore pressure response being delayed). The excess immediate pore pressures increase during this period had almost completely dissipated until 2019-09-11 02:00. Thereafter the pore pressures increased to peak values 2019-09-15 causing the horizontal effective stresses to experience lower stress levels then prior to casting of the slab. This was true also for the vertical effective stress in the location towards the east SPW, see Figure 5.9. From 2019-09-15 the pore pressures decreased until mid October, resulting in an increase in vertical as well as horizontal effective stresses. As the pore pressures from mid October increased slightly until the start of November, the effective stresses decreased. The gain in vertical effective stresses seem to follow an observable trend, being apparently shadowed mainly by changes in pore pressures.

From the start of November the pore pressures remained fairly constant until the end of February 2020 and the effective stresses increased slightly in both vertical and horizontal directions. In the end of February works with back-filling between the structure and SPWs started. As drainage/pumping within the pit ended along with the progress of back-filling, an increase/recovery in pore pressures has been registered and the effective stresses have decreased. The decrease in vertical effective stresses being larger than the decrease in horizontal effective stresses.

It is seen in Figure 5.9 that following cast of the slab the vertical effective stress is greatest in the approximate centerline in the instrumented section. To the west the existing embankment/ramp for the Göta river bridge most likely contributes to higher degree of mobilisation of shear stresses relative to the east. This might be an explanation to the higher vertical uplift stresses in the west part of the slab relative the east part. The horizontal stresses are greater towards the locations of the SPWs and less in the centremost location of the excavation, this is most likely due to mobilisation of passive resistance in front of the SPWs (excavated side).

The net increase in vertical effective stresses that *the slab* experience, is the net gain in effective vertical stress since the slab was cast. This net gain is plotted in Figure 5.10 with reference to 2019-09-10 07:00 (just before the slab was cast). In Figure 5.10 a vertical effective stress range corresponding to $0.2\text{-}0.5 \times \sigma'_v$ is included. The range is based on expected vertical heave pressures from a prestudy to this report (Tornborg 2017). At the level of the cells measuring the total vertical stress (level -2.7) the vertical effective stress in-situ has been estimated to σ'_{v0}=74 kPa. The value of $0.5\sigma'_{v0}$ was suggested in the prestudy as an upper bound for preliminary design purposes for infinitely wide and long excavations. $0.2\text{-}0.3\sigma'_{v0}$ is an estimated value based on FE calculations in the prestudy which included the stiffness and deformation of slab and piles, for details see Tornborg (2017). If the net gain in vertical stresses is solely attributed to effective heave pressures,
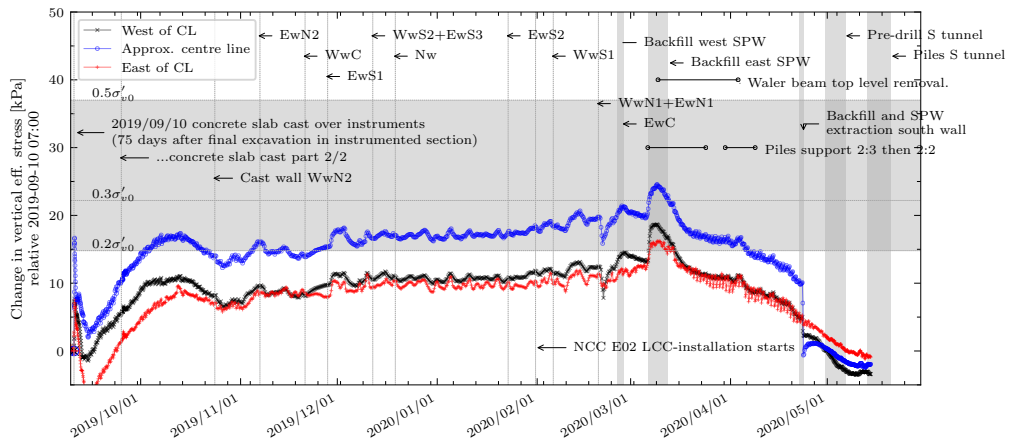
Figure 5.10: *Change in vertical effective stresses under concrete slab relative 2019-09-10 07:00 i.e. just before pouring the wet concrete for the slab.*

the estimate of uplift vertical effective stresses based on 0.2-$0.3\sigma'_{v0}$ agree relatively well with the measured values.

In Section 5.3.7 the measured effective stresses that were presented in Figure 5.9 are evaluated by replotting them in p'-q stress space. In doing so both the vertical total stresses and pore pressures have been adjusted in order to compare the vertical and horizontal effective stresses at a reference level, set at the centre of the cells measuring the horizontal stresses (i.e. level -3.28).

5.3.4   Temperature

The results of measurements temperature under the concrete working platform and permanent slab are presented in Figure 5.11. The temperature readings are taken from the thermistors located in the sensor housings of the piezometers. It is worth noting the after casting of the concrete working platform, an additional $10°C$ temperature increase followed when casting the 1.0 m thick concrete slab. The thermistors in the total earth pressure cells (located in the sensor housing just below the working platform) registered increase of maximum $20°C$ (data presented in figs. C.25-C.27). Since casting of the slab in July 2019 the temperature, as recorded in the piezometers, decreased towards an asymptotic value of $7.5°C$. From April 2020 a small temperature increase is noticeable most likely correlated with the increase in air temperature. Complete measurement data of temperature in all VW sensors (piezometers and earth pressure cells) are presented in Appendix C.1.1 Figures C.25-C.27.
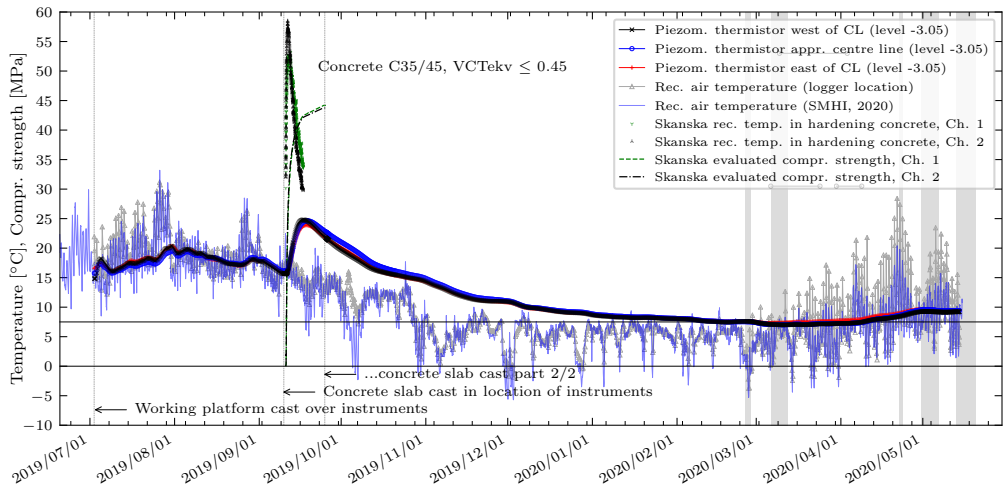
Figure 5.11: *Registered temperature in piezometers under concrete slab as well as recorded temperature in permanent concrete slab during hardening and evaluated compressive strength. Temperature data from SMHI included for comparison of recorded temperature at ground surface within the excavation (location of data logger).*

5.3.5 Vertical deformation in clay-structure interface

The results of measurements of vertical deformation in the VW extensometer cast into the concrete working platform and permanent slab are presented in Figure 5.12 as calculated strain. The centre of the extensometer anchor is located 1.63 m under the bottom of the concrete slab and 1.33 m under the concrete to which the extensometer head was cast into (for details see Appendix C Figure C.21). The strain have been calculated as registered deformation divided by 1.33 m. Immediately after installation of the extensometer, tension was registered up until the casting of the concrete slab, when the mode of deformation was reversed to compression. The maximum registered tension was 2.7 mm, corresponding to 0.20 % strain. After casting of the slab, the extensometer registered compression until ca 1 month after casting and thereafter (from mid October 2019) the mode of deformation has reversed to extension generally (shorter periods of compression, e.g. 2020-03-06–12 during pumping within pit for backfilling along east SPW, appears to be correlated with decrease in pore pressure). The absolute deformation of the slab is unknown since no accurate measurements were made of the slab level after casting. Some indication of absolute movements can however be estimated from bellow-hose measurements carried out after completion of the slab, presented in Figure 5.2, indicating 6 mm settlement in measurements taken the day after and 3 weeks after casting of the slab. Thereafter no or little settlement is estimated based on the bellow-hose readings. In the next section the incremental strain response after casting of the slab is evaluated in combination with evaluated effective stresses.
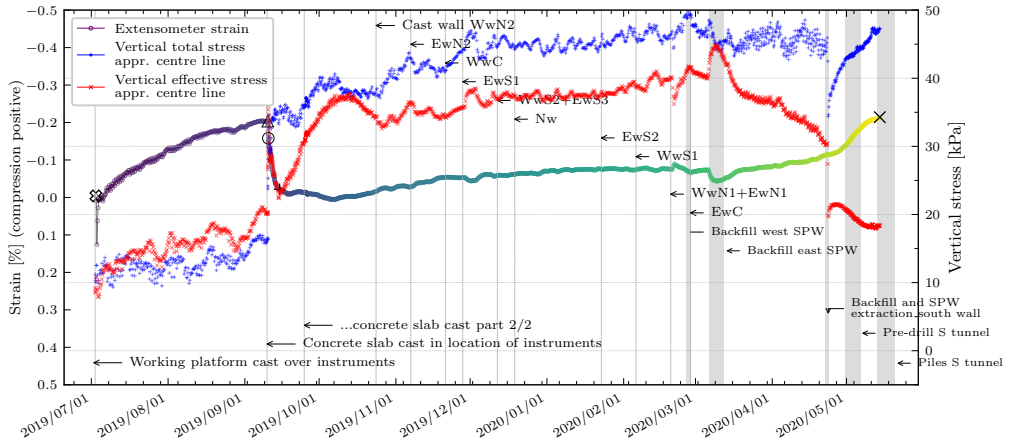
Figure 5.12: *Registered vertical deformations in VW extensometer, presented as strain, under the concrete slab. Included also vertical total and effective stresses (secondary y-axis) evaluated from the vertical total earth pressure cell and piezometer in the centremost location under the slab.*

5.3.6 Evaluation of stress-strain response during reloading (casting of slab)

In Figure 5.13 is included a detailed plot of measurement values during and 2 weeks after the casting of the concrete slab. A "jagged" response is noticeable after casting of the slab, this could be due to a successive load transfer of the weight of the concrete slab from the clay to the piles.

In Figure 5.13 b) two secant values of reloading moduli have been estimated. These moduli are based on the stress-strain response during and immediately after pouring of the wet concrete. The values are calculated based on measured strain in the extensometer and effective stress increase in the sensors in the centremost location of the excavation. The results are also presented as stress-strain response in Figure 5.14.

The values of 37 and 11 MPa secant reloading modulus during casting of the slab were derived over strain increments of 0.05 % and 0.07 % respectively and loading increments from 20 kPa to 37 and 28 kPa respectively. The results can be compared to IL oedometer tests on samples from 7.1 m depth (level -4.2) with secant reloading moduli ranging from approximately 3 to 4 MPa (four separate tests, Figure 4.13) for the load increment from 10 to 35 kPa that initiated load reversal after unloading from σ'_{v0}. The CRS-test on the sample from 6.3 m depth (level -3.4) with a unloading-reloading loop gave an initial reloading modulus of approximately 33 MPa (5 kPa load step starting from 25 kPa, 0.015 % strain) and secant reloading modulus of 7.5 MPa (25 kPa load step, 0.33 % strain).
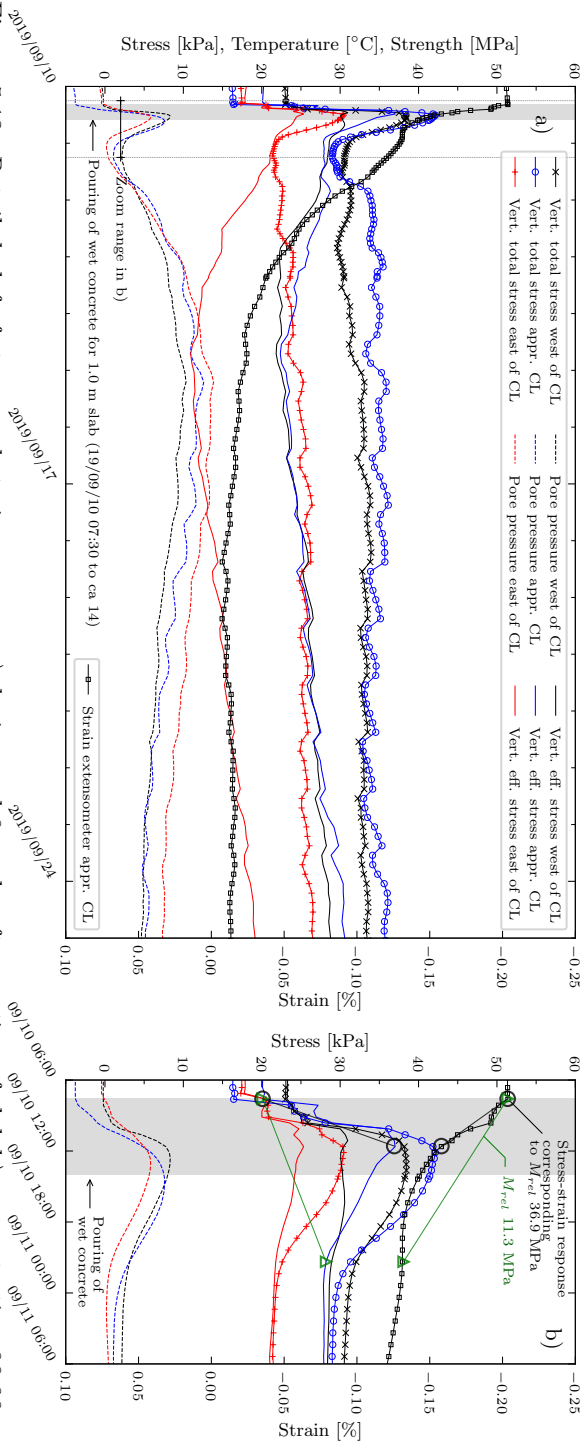
Figure 5.13: *Detailed plot of stress and strain response a) during and 2 weeks after casting of slab b) zoom starting 06:00 on day of casting including evaluation of reloading modulus as two secant values following the pouring of the wet concrete.*
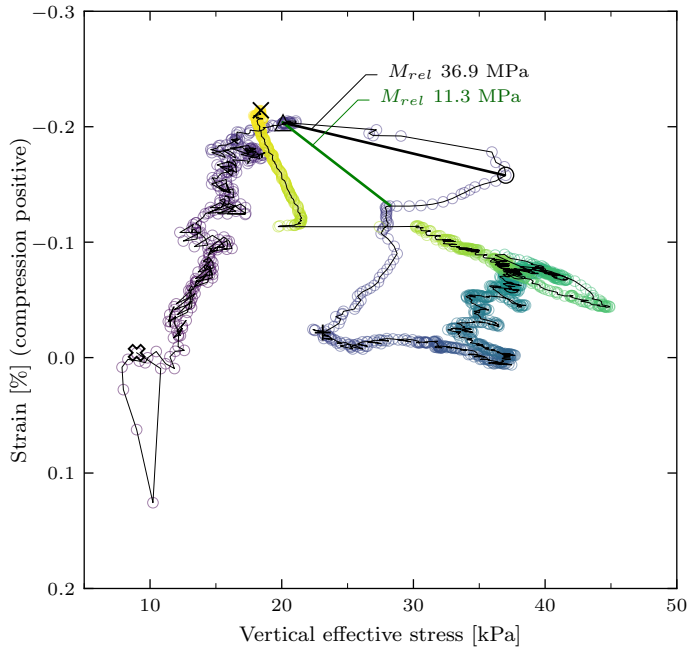
Figure 5.14: *Plot of strain obtained from extensometer readings versus stress response from centremost total vertical earth pressure cell and piezometer. The annotated lines of secant reloading modulus correspond to the lines in Figure 5.13. The gradient colour line and symbols correspond to timesteps in Figure 5.12.*

Based on field measurements of G_0 (Wood 2016) an à-priori best-estimate of M_{reload} would range approximately 20-28 MPa for small-strains (assessed G_0 range 10-15 MPa and ν'_0=0.20). The evaluated field measurement results of initial reloading modulus are therefore considered feasible. However, the CRS and extensometer moduli are derived over increments of small strain and it should be noted that the accuracy of the extensometer (described in Section 4.4.4) is $\pm$0.25% FS i.e. $\pm$0.25 mm and the resolution 0.02% FS i.e. 0.02 mm. The potential error in registered strain increments of 0.05-0.07 % (i.e. 0.7-0.9 mm) is thus $\pm$28-36 %. Furthermore, the measured stress-strain response is affected by the presence of the previously installed piles and concrete working platform. However, during the pouring of the wet concrete the influence of these structures were at a minimum and thereafter increased as the concrete hardened around the pile heads.

5.3.7 Comparison of results to empirical K_0 estimates

Since vertical and effective earth pressures are measured under the structure it is possible to plot the results in triaxial stress space i.e. deviatoric stress, $q=\sigma_a-\sigma_r$, versus mean effective stress, $p'=(\sigma'_a+2\sigma'_r)/3$, or alternatively for plane strain conditions as shear stress, $t=(\sigma_1-\sigma_3)/2$, versus mean effective stress in the plane of shearing, $s'=(\sigma'_1+\sigma'_3)/2$. To plot the measurements in triaxial stress space requires an assumption of the stress in the out of plane direction, since p' in general form is written as $p'=(\sigma'_1+\sigma'_2+\sigma'_3)/3$. In the evaluation of the measurements this has been done by assuming $\sigma'_2=\sigma'_3=\sigma'_h$. The results of measurements in the three locations of the instrumented section are presented in p'-q stress space in Figures 5.15, 5.16 and 5.17. A plot in s'-t stress space is presented in Figure 5.18 for the centremost location. The VW sensors (vertical and horizontal earth pressures cells and piezometers) are not located at the same depth/level. In order to evaluate the measurement results a reference level was therefore set to that of the centre level of the membrane of the cells measuring horizontal earth pressures, i.e. level -3.28. Vertical total stress and pore pressure have thus been adjusted in order to compare vertical to horizontal effective earth pressures.

Included in Figures 5.15, 5.16 and 5.17 are also:

- The development of stresses during excavation based on a K_0-OCR relationship according to Schmidt (1966). Both $K_0^{in-situ}$ as well as K_0 during unloading have been assumed to follow the formula by Schmidt i.e. $K_0 = K_0^{nc}OCR^{1.2sin\phi'}$ with ϕ'=30° and K_0^{nc}=0.53. The value of K_0^{nc}=0.53 is based on previous laboratory tests on Gothenburg clay in which K_0^{nc} range from 0.50-0.55 (Sällfors 1975; Kullingsjö 2007; Olsson 2013). The value of ϕ'=30° was selected based on Swedish empirical estimate of the friction angle corresponding to peak strengths in triaxial compression tests and ranges of friction angles estimated from new triaxial tests carried out with "slow" strain rates as presented in Section 4.3 (see Figure 4.17).
- The normal compression surface (NCS) for the Creep-SCLAY1S model. The surface is drawn based on parameter values in Table 4.2 representing the in-situ conditions before start of excavation i.e. M_c=1.40, M_e=1.02, α_0=0.56, K_0^{nc}=0.43. The model value of K_0^{nc} results from Jaky's formula and a friction angle consistent with that of M_c. As pointed out in the context to figure 2.11, this value of K_0^{nc} is rather low compared to the range of 0.50-0.55 in previous laboratory tests of Gothenburg clay.
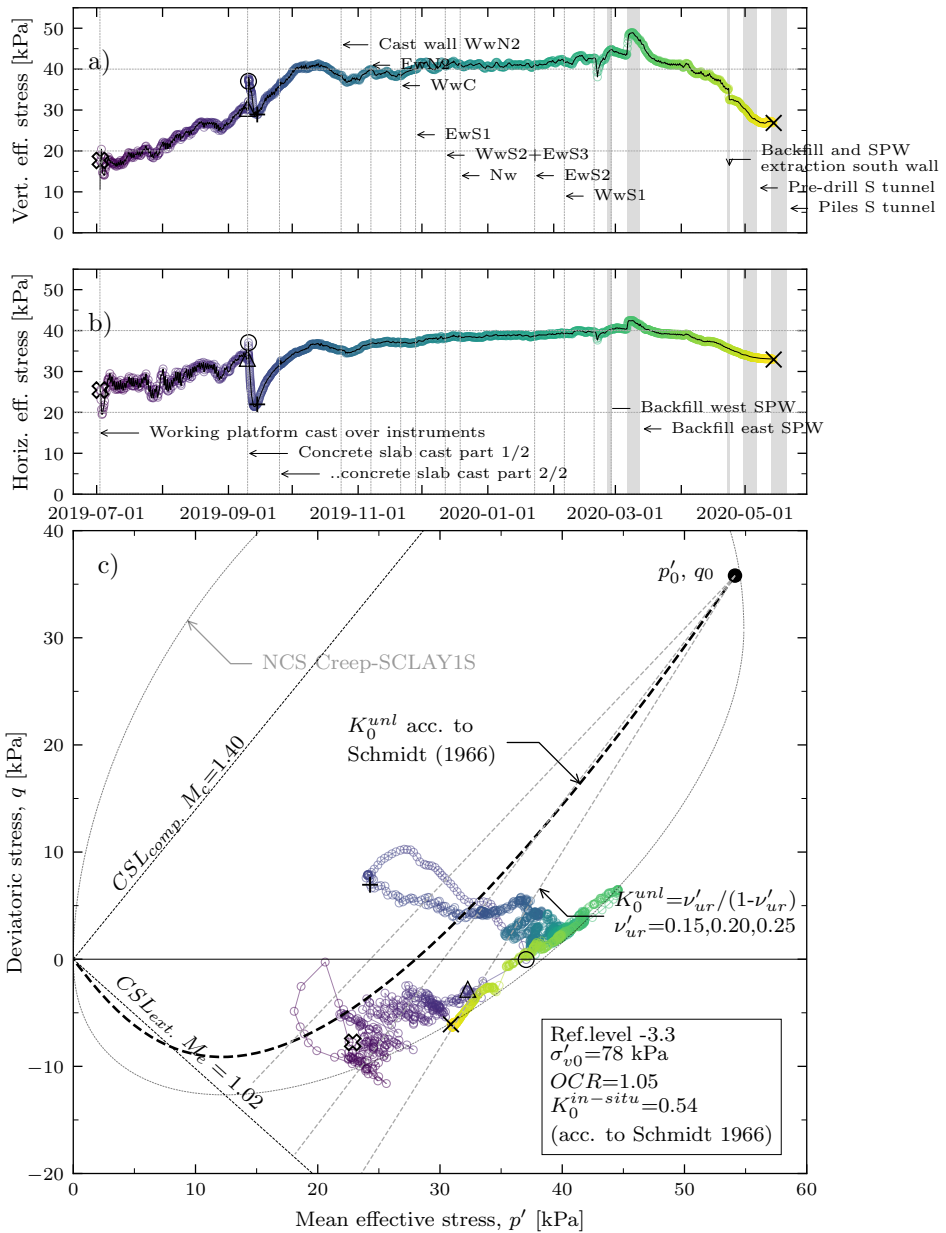
Figure 5.15: *Evaluation of earth pressures with time and plot of corresponding stress path for sensors located towards the **west** sheet pile wall.*
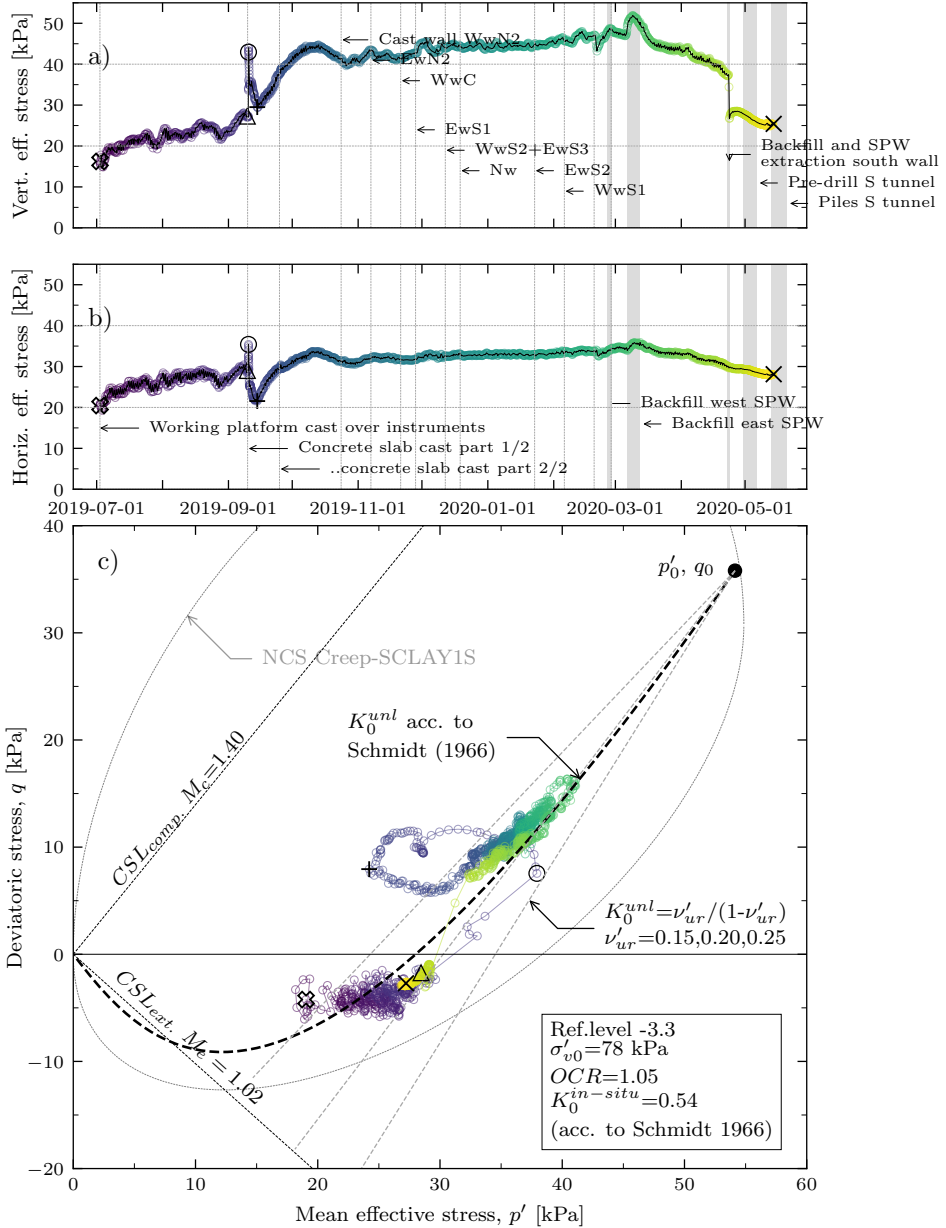
Figure 5.16: *Evaluation of earth pressures with time and plot of corresponding stress path for sensors located **centremost** in the instrumented section. See Fig. 5.18 for plot in s'-t stress space.*
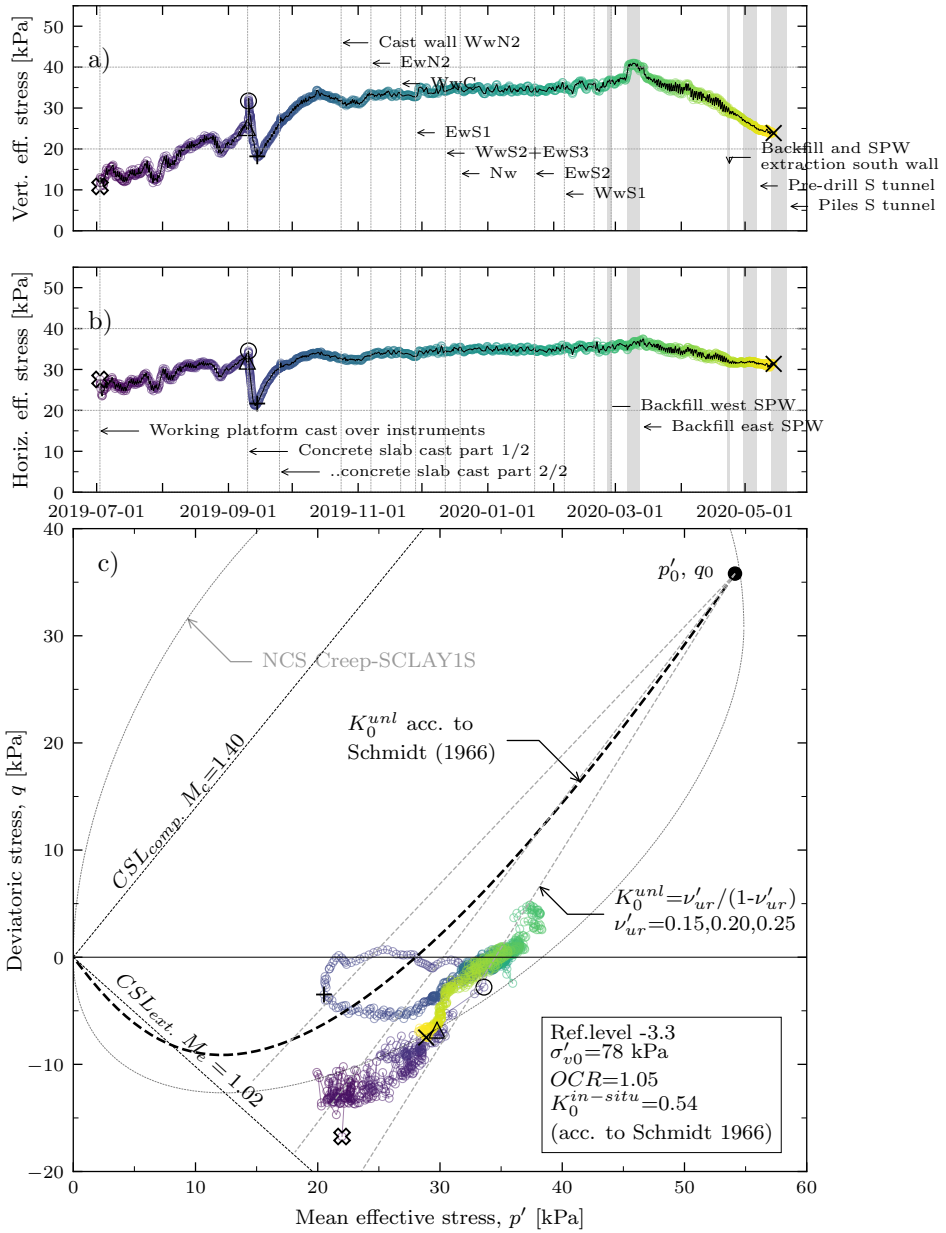
Figure 5.17: *Evaluation of earth pressures with time and plot of corresponding stress path for sensors located towards to the* **east** *sheet pile wall.*
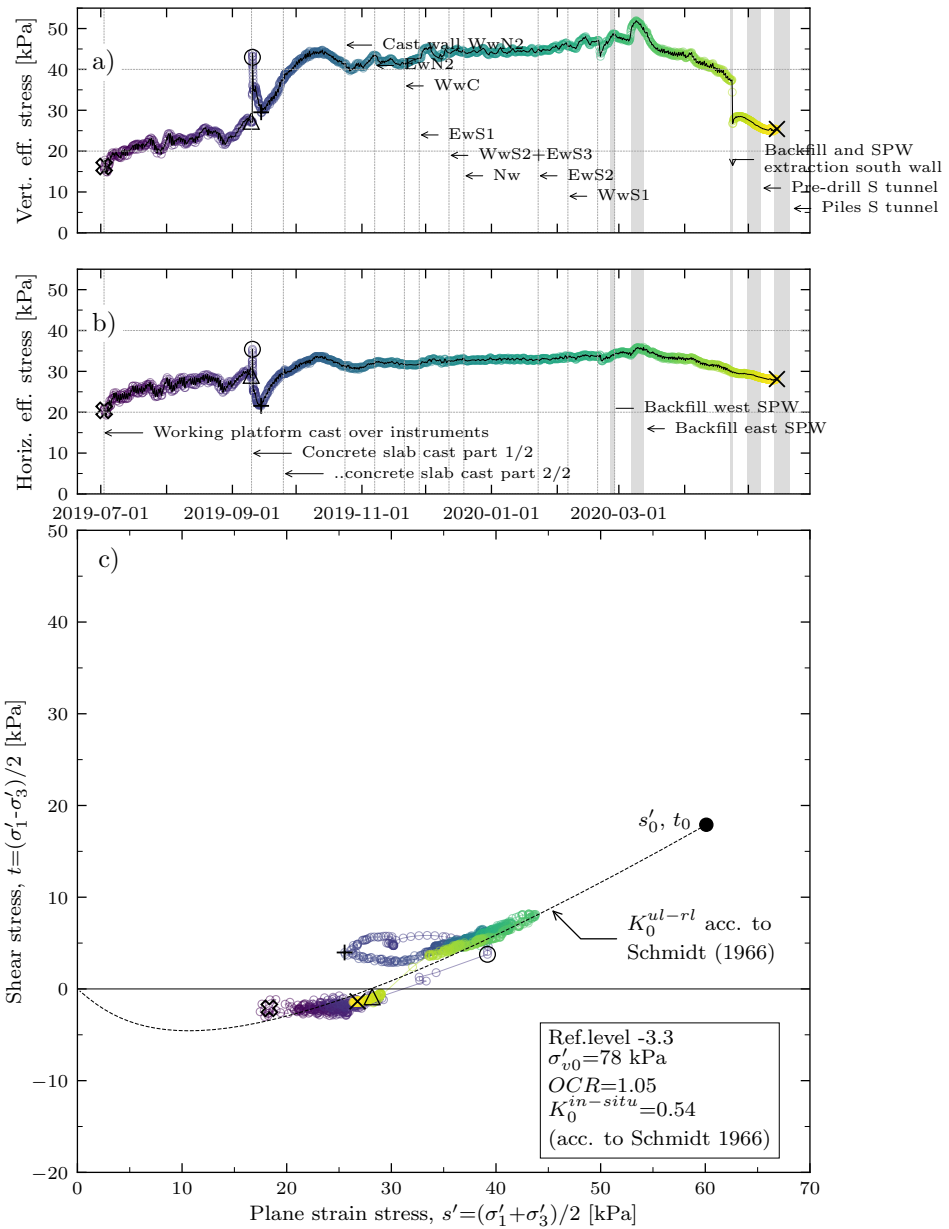
Figure 5.18: *Evaluation of earth pressures with time and plot of corresponding s'-t stress path for sensors located **centremost** in the instrumented section.*

From Figures 5.15-5.18 it can be noted that:

- Studying the result in Figure 5.16 and 5.18 i.e. the centremost location, which is most likely to resemble oedometer conditions, the formula for K_0 during unload-reload according to Schmidt (1966) provide a reasonable approximation of the stress state after excavation and relatively accurately represents the slope of the stress path followed during reloading, i.e. casting of the 1.0 m slab (from triangle symbol to circle)). For locations within the excavation where horizontal strains in the soil differ from zero, as they most likely do close to the SPWs, then comparisons to K_0 relationships derived from oedometer conditions (zero lateral strain) are not feasible.
- The effective stress paths tend to not fall outside the normal compression surface with the assumed parameter set-up for the Creep-SCLAY1S model (except for the initial readings in the east location).
- The deviator stress levels are approximately the same in the locations close to the west and east SPWs. The deviator stress is higher in the centremost location (due to higher vertical stress as well as lower horizontal stress then in the other locations).
- In general in all locations from November 2019 until March 2020 (then the pore pressures started to recover) the vertical effective stresses increased slightly more than the horizontal effective stresses. The higher increase in vertical compared to horizontal effective stresses correspond to a decrease in K_0. The increase in vertical stresses in the slab-clay interface may e.g. be caused by restrained heave and/or the casting of the walls of the structure during this time period.
- As only the east and west locations show stress states located significantly to the "lower right", high horizontal effective stress are attributed mainly to increasing earth pressures in front of the SPWs (due to excavation).
- The installation of piles does not seem to have caused significant increase in horizontal effective stresses as then also the stress state in the centremost location would be shifted to "lower right". This may result from the pre-augering that was carried out to 18 m depth before each pile installation. As seen in Figure 5.1 the pre-augering was effective in minimising the deformations during pile installation. Therefore the horizontal stresses may not have increased as much as they most likely would have done otherwise and most probably did below 18 m depth. Based on such arguments pre-augering may be beneficial in the sense to not only minimise deformations to the surroundings during the pile installation processes but also in order minimise potential increase in long-term earth pressures acting against permanent structures.

5.4 Preliminary comparison of measurements and FEM Class A prognosis

This section briefly present a comparison of an initial Class A prognosis of the excavation versus the measurement data. The comparison is made for vertical effective stresses in the centremost sensor location under the slab. Further comparisons of numerical predictions and measurement results as well as further analyses data will presented based on future work (after the completion of this mid-term report).

An initial Class A prognosis by numerical modelling of the studied excavation was carried out within the framework of a Master thesis work at Chalmers University of Technology (Harlén and Poplasen 2019) supervised by the author. The primary aim of the thesis was to establish a Class A prognosis of the displacements and structural forces developing during the construction phase. The model parameter values for the constitutive soil model, Creep-SCLAY1S, were derived based on laboratory tests presented in 4.3. The model parameter values have been presented in Tables 4.2 and 4.3. The work also included a comparison of the results obtained by the Creep-SCLAY1S model and the NGI-ADP model (used in the design by the contractor).

The numerical model prediction has since been updated by the Author with the actual construction times. The results of measured versus predicted vertical effective stress in the centremost sensor location under the concrete slab are presented in Figure 5.19. The general trend of the vertical effective stress is captured well with the numerical model prediction. The measured vertical effective stress are however unadjusted, they will be slightly offset as the pore pressures have not been corrected (as described earlier in the report; initial negative pore pressure before casting of the slab and piezometer located 0.4 m deeper than vertical stress cell). In conclusion: as in the case study of Göta Tunnel, the preliminary comparison presented in Figure 5.19 is encouraging for future studies of excavation problems in soft clays by use of the Creep-SCLAY1S model.
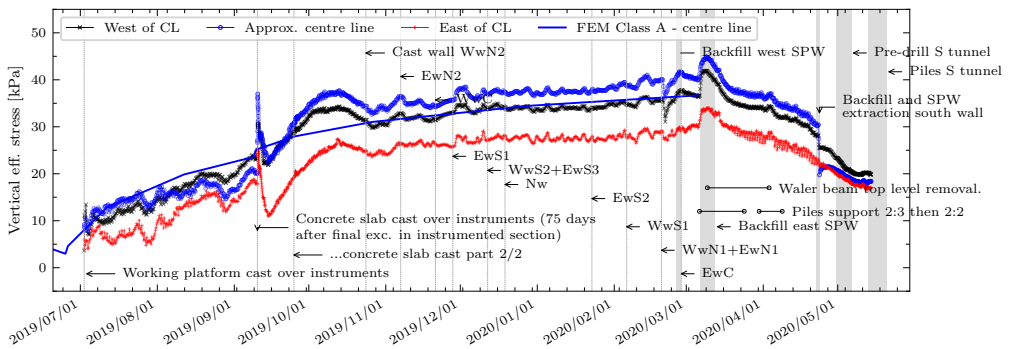
Figure 5.19: *Comparison of measured versus predicted vertical effective stress in centremost location under slab. Predicted stress extracted from model established for FEM Class A prediction as presented by Harlén and Poplasen (2019).*

6 Conclusions and recommendations for future work

6.1 Conclusions

6.1.1 General

This report has focused on instrumentation, and the measurements of deformations and earth pressures within an excavation and underneath an underground structure in soft clay. Additionally, a constitutive soil model for numerical modelling of excavations has been benchmarked on field scale by means of benchmarking against a well instrumented excavation as part of the Göta Tunnel. Summarised below are the main conclusions and recommendations from the literature review, the case study and the monitoring data collected and evaluated so far (measurements are on-going for continued long-term monitoring).

The main conclusions arising from the literature review and studies presented in Chapters 2-5 are presented below.

6.1.2 Retaining structures in soft clay - literature review

- Design of excavations has historically been based on regulations focusing on the Ultimate Limit State. However, for deep excavations on close proximity to existing infrastructure or historic buildings there are strict regulations on allowable deformations. Examples from the literature review points to the fact that limiting the deformations in the short-term, may affect the earth pressures in the long-term: e.g. less deformation on the retained side during construction works leads to higher earth pressures in the long-term, closer to the preconstruction at-rest earth conditions (Carder and Darley 1998; Richards et al. 2007). Accounting for deformations in the short-term may lead to savings, as the design of the permanent structure based on e.g. pre-construction horizontal earth pressures at rest may be associated with overdesign.

- Numerical modelling with rate-dependent effective stress based models offer a way to account for soil-structure interaction and interlinked response both in the short- (construction) and long-term (design lifetime) in soft sensitive clays. By modelling the entire construction chain, and the transition from short- to long-term, optimisation is achieved e.g. by accounting for the effect of allowable deformations on the development of earth pressures.

- The viscous nature of clay affect the earth pressures arising against underground structures in the short and long-term. Examples being the concepts (rheological models) of creep and relaxation influencing the structural response (example from British guidelines given in Figure 2.1). Rate-dependent effective stress based soil models provides the advantage of using one unique model parameter set to account for the viscous behaviour, in predictions of the short-term (construction period,

normally the contractors focus) as well as the transition to the long-term (normally the clients focus).

- Factors affecting the short-term response (and therefore, as stated above also the long-term response) are for example excavation geometry and stiffness of the support system. It would be favourable to expand on previous studies, e.g. generalising undrained pore pressure change to factors such as B/H of the excavation or time the excavation remains open, in order to extract normalised diagrams on e.g long-term (design) earth pressures (see section 6.2 for recommendations on future work).

- There is a scarcity in long-term measurements of horizontal, as well as vertical, earth pressures against permanent underground structures in soft clay. Such measurements, even though site and project specific, are valuable in providing insights of the field-scale (macro) soil response and soil-structure interaction. The data can facilitate benchmarking of numerical model predictions. Furthermore, measurements of earth pressures can aid clients and contractors in the use of the observational method with respect to design of earth pressures.

- As a representative of a 2D stress state in a soil, K_0, the lateral earth pressure at rest, is often used as a starting point for the analyses. For large strains K_0 adopts to an asymptotic value (thus suitable as a model parameter) denoted K_0^{nc}. It should be noted that depending on the stress state it is representing, K_0 can take on values lower than K_0^{nc}. Furthermore, in plastic normally consolidated clays K_0 increase with time, the order of magnitude being ΔK_0=0.04 in average per log cycle for soft Swedish clay (details provided in section 2.2.7).

- In Swedish literature and guidelines there is a mix of definitions regarding K_0. For example, K_0^{nc} (which in international literature is accepted as the asymptotic value of K_0 during primary loading) was used by Larsson (1977) to denote an equation for empirical estimates of $K_0^{in-situ}$. Such misconceptions should be avoided and hopefully section 2.2.7 (covering aspects of K_0) of this report provides some clarification.

6.1.3 Case study the Göta Tunnel

A well instrumented cross section of the Göta Tunnel project, contract J2, section 1/430 was studied in order to benchmark the Creep-SCLAY1S constitutive soil model. The work involved recollection of project log-books and extensive sets of valuable measurement data. The primary conclusions from the case study are outlined below.

- The comparisons of the model predictions versus measurement values of earth pressures, strut forces, pore pressures and deformations indicate satisfactory performance of the Creep-SCLAY1S model and inspires for future use in modelling excavation problems.

- The case study highlights the importance of considering installation effects in modelling. Excess pore pressures and displacements were registered during installation of the SPWs and pre-cast concrete displacement piles. Although adopting a rudi-

mentary approach for modelling of the pre-augering and pile installations, the model predictions of these installation effects were still in general in good agreement with the measured displacements.

- The predicted horizontal total stresses (behind the SPW) and strut force were in good agreement with the measured values. However, the model prediction do not incorporate the impact of temperature variations on strut force (neither due to steel or soil response to temperature change). In addition to the daily variations, the measurement data showed a distinct general decrease in strut force during September-February (cool period) and an increase during March-August (warm period).

- The measurements of earth pressures highlight that short- and long-term earth pressures are dependent on site specific settings (e.g. geometry and stiffness of the support system, construction sequence and methods, stiffness of support system). This supports the need for further studies in order to generalise the impact of such factors on e.g. consolidation rates, long-term (design) earth pressures, wall movements, etc.

- The long-term stress-state around underground structures depend on e.g. induced shearing (rotation of principal stresses) during excavation. Therefore, estimation of design horizontal effective stresses based on empirical estimates of in-situ before construction values of K_0 (e.g. equation 2.31) may lead to overdesign, if horizontal earth pressures are reduced due to effects of e.g. wall installation or excavation and flexibility of the structure.

- The industry practice of using a K_0 value for the estimation of the design long-term earth pressures will assume the interaction of structure and soil being represented by means of independent springs (Muir Wood 2004) and does not include e.g. soil-structure interaction or stiffnesses, excavation geometry, etc. These aspect can be incorporated by numerical modelling. However, design charts would be beneficial for industry in order to account for these effects in the estimation of design long-term earth pressures in project which falls under some sort of standard category (see recommendations for future work section 6.2).

- The value of K_0^{nc} governs the asymptotic (target) K_0 value and is therefore important also for excavation problems, during loading situations such as e.g. placing of backfill material. The adopted K_0^{nc} value for this study (0.43) is rather low compared to previous laboratory test data on Gothenburg clay (range 0.45-0.55 as pointed out in the context to figure 2.11). Underestimation of K_0^{nc} may result in underestimation of the horizontal effective stresses if e.g. backfill works initiate primary loading.

- Continued horizontal and vertical displacements (settlements) were registered up to 9 months after the final dewatering of the excavation. These deformations are considered to be due to the installation effects of vertical anchors (tied to the slab in the studied section) and tie-back anchors in an adjacent part of the project. The anchors were installed by means of ODEX-drilling, most likely resulting in disturbance of the sensitive clay and possibly some volume loss in the frictional material underneath. This highlights the importance of the choice of construction

methods in urban areas, where drilling of anchors or steel piles should be done with utmost care. As in the case of drilled piles, they are often intended/deployed in order to reduce deformations relative that of displacement piles, which this study shows might not always be the case.

6.1.4 Site characterisation - laboratory testing

Triaxial, CRS and IL oedometer tests were carried out for site characterisation. The tests focused on the unloading and intrinsic behaviour of the clay. Additionally, a part of the testing programme comprised supplementary tests to investigate testing methodologies with respect to rate-effects and stress paths adopted for excavation problems. The results and testing methodologies highlight:

- The deformation rate during triaxial and CRS tests can easily be varied by means of computer control. Varying the deformation rate makes it possible to extract additional data on the viscous behaviour of the soil compared to the "standard" tests.

- The incremental loading tests with unload-reload stages in this report support Wood (2014) in using the relationship for unloading modulus as proposed by Karlsrud (2012). For the data presented in Figure 4.15 parameters a=175 and b=0.6 in Karlsrud's equation (Fig. 2.16) provide a reasonable fit with respect to the IL test data. CRS-tests may provide an indication of the unloading modulus, however IL tests are preferable with respect to CRS rate-effects and apparent stresses as discussed in section 4.3.3.1. Analytical estimations of 1D heave with unloading modulus, as estimated from IL-tests only holds for oedometer conditions. Observable heave in the field will depend on boundary conditions, such as for example restraints or lock-in effects due to SPWs, piles or on-going settlements in the adjacent ground. Numerical analysis taking such boundary conditions into account may however use IL tests for element level calibration of model parameters.

- The soil response on the retained side of excavations can be studied by means of drained triaxial tests. These should be conducted by imposing a reduction of the lateral stress under a condition of constant vertical effective stress. The imposed paths in stress space and compression plane are still idealisations of reality, but considered more appropriate for excavation problems in general compared to conventional CADC tests (increasing the vertical stress). However, a constant decrease of the radial stress imposes an increasing vertical strain rate (presented in Appendix C.1.2). For a controlled rate of radial deformation, such tests could be refined by means of a constant increase of radial deformation.

6.1.5 Field monitoring

An excavation for Hisings Bridge was instrumented for monitoring of the excavation process and studying the development of vertical and horizontal earth pressures in the short- and long-term. Conclusions from the instrumentation and field monitoring so far are presented below.

6.1.5.1 Instrumentation

- The installation of the total earth pressure cells for monitoring of vertical and horizontal stresses worked satisfactory due to careful planning, including a number of trial installations of the equipment in the field.

- Hydraulic total earth pressure cells are affected by the temperature change (both the vibrating wire sensors and the hydraulic cell fluid). Temperature correction factors for the vibrating wire sensor itself are generally supplied by the manufacturer. However, the temperature correction factor for the *entire unit* under field boundary conditions needs to be estimated based on a) empirical equations/estimates b) testing in laboratory or c) from periods in the field with constant load and varying temperature. The latter approach was used in this study and is recommended, as it provides indication of the correction factors under the boundary conditions the cell experiences in the field, which is not possible to recreate in laboratory environment.

- The successful installation of sensors and re-routing of the cables throughout the construction phase required close cooperation with the construction site personnel and continuous presence at site. Especially, one needs to be kept informed about, and be present, during crucial construction stages.

6.1.5.2 Monitoring results

- During the pre-augering prior to pile installation settlements were registered in the soil layers down to 18 m depth. This shows that deep pre-augering can cause collapse of the auger hole, which may disturb the clay and affect the subsequent response during excavation. Pre-augering should, therefore, be carried out with care i.e. the method need to be adjusted to the local soil conditions in order to avoid collapse and net volume outtake by excessive augering.

- The pouring of wet concrete for the slab provided a satisfactory verification of the sensor installations and set-up in the field. If such a construction stage, providing a known "test-load", does not occur naturally during the monitoring program, it is recommended to be included for example by means of dead weight loading. This enables to verify the sensor readings under field conditions (potential errors include e.g. arching effects in the surrounding soil).

- During the hardening process of the slab a 10-15°C temperature increase was registered in the piezometers under the slab. This increase was additional to temperatures already in the range of 15-20°C before casting the slab. It highlights that temperature increase that follows casting of concrete slabs, or in-situ cast concrete piles during hardening, can prove to be an "installation effect" which potentially could be exploited in the design of underground structures for geothermal storage and ground heat exchange. This "installation effect" may prove to provide a "free" thermal pre-loading of the soft clay adjacent to the structure.

- The net gain in the vertical effective stresses after casting of the slab corresponded to approximately 0.2-0.3σ'_{v0}. If this increase in vertical effective stresses is attributed to upward effective heave pressures (EHPs) solely, it is in line with estimations of EHPs

as in the pre-study to this report. The pre-study estimated $0.2\sigma'_{v0}$ for infinitely wide and long excavations taking the stiffness of slab and piles into account. At the studied site a number of factors may have contributed to a higher than normal vertical effective stress increase e.g.; the 1.0 m slab can be considered as "inflexible" and the clay layers extend to great depth. A factor that most likely contribute to limiting the increase in uplift stresses after excavation is the relatively narrow width of the excavation (compare to Figure 2.8 were generation of Δu decreases with decreasing ratio of excavation width to wall embedment).

- In light of the point above, it should be noted that the structural response of a slab (also retaining walls) is to the total stress i.e. effective stresses and pore pressures must both be accounted for in design (Gaba, Simpson, et al. 2003). Furthermore, as pointed out in the pre-study to this report, the effective heave pressure can be considered in design of serviceability limit states, since the pressure dissipates if the slab is allowed to deform.

- Studying the results of the instruments located in the centremost location of the excavation (Figure 5.16), which is closest to oedometer conditions, the formula for K_0 during unload according to Schmidt (1966) provide a reasonable approximation of the stress state after excavation. Thus previous laboratory test data on soft clays (Persson 2004; Kullingsjö 2007) have been validated by full scale field measurements. The formula proposed by Schmidt also provides a relatively accurate representation of the slope of the stress path during reloading, i.e. casting of the slab.

- Comparison of the vertical effective stress in the centremost location, and the results of preliminary FEM analyses indicate that the numerical model accurately predicts the trend of increasing vertical effective stresses.

- The measurement data of the vertical and horizontal effective stresses make it possible for further evaluation (benchmarking) of the Creep-SCLAY1S soil model. Overall the Creep-SCLAY1S model provide a tool for refined numerical studies and optimisation of excavation problems. This should be exploited, as e.g. described in the following section *Recommendations for future research*.

6.2   Recommendations for future research

The results presented in this report comprise measurement data from extensively instrumented and documented excavations in soft clays. The field measurement data collected so far at the Hisings Bridge site (Chapter 5 is recommended to be analysed further, and used for further benchmarking of the Creep-SCLAY1S model. Furthermore, the monitoring including documentation of construction activities at the site is recommended to be continued for long-term. Continued monitoring also provides valuable knowledge on the impact of adjacent construction activities on existing structures, most notably the effect of the approximately 15 m deep future excavation for the West Link tunnel will provide information on the effect on stresses under the existing slab.

Field measurements provide valuable input on full scale soil response and soil-structure

interaction. However, results are inherently site specific (e.g. soil properties, geometry and stiffness of the structure). It is therefore recommended to generalise the field measurements by means of numerical modelling. The numerical modelling should be carried out with an effective stress based constitutive soil model that incorporates relevant features of soft clays. Incorporation of e.g. rate-dependence enables to asses the impact of viscous behaviour on short-term loading situations and long-term earth pressures and (creep) deformations. The recommended outline for generalisation of the field measurement results is presented below:

- Benchmarking and calibration of numerical model using the monitoring results from the Hisings Bridge site.

- Identify variables for generalisation and use dimensional analyses to design a programme for numerical experiments.

- Study the effect of governing variables on the development of primarily:

  - The generation of excess pore pressure during excavation and the subsequent consolidation process.
  - Horizontal and vertical stresses (vertical uplift heave pressure). This is recommended as e.g. the current use of K_0 to asses long-term design horizontal earth pressure for underground structures in soft clays is considered rudimentary. Potential savings lies in adding knowledge which can contribute to more nuanced design approaches.

  At this point it is considered relevant to quantify the impact of variables such as e.g.:

  - Geometry of excavation e.g. by means of the stability number, N, as a measure of imposed shear strains due to excavation.
  - Soil stiffness and retaining wall system stiffness.
  - Rate-dependence i.e. the time to complete the excavation process and the time the excavation remains open.
  - Hydraulic conductivity of soil as well as suction limit.

- Multi-objective optimisation to study e.g. optimal ratios of correlated variables such as soil and wall stiffness on the long-term earth pressures.

- Present generalised results in the form of normalised diagrams/charts.

During the process described above it is recommended to study and identify if characteristic stress paths exists. Advanced laboratory testing following/targeting these stress paths enables final refinement of the model parameters.

Additional recommendations for future work are:

- Instrumentation of additional underground structures in soft clay for monitoring of long-term earth pressures. This will provide further knowledge on soil-structure response and evaluation of e.g. generalised results such as outlined above. To speed

up the available knowledge and optimisation, potential test excavations including structures should be considered.

- Include modelling of installation effects in generalised results.

- Develop the Creep-SCLAY1S model to include small-strain stiffness. The impact of including this aspect of soil behaviour in excavation problems could then be studied and quantified in the generalised results. In order to evaluate such an extension of the model, additional laboratory testing should be carried out focusing on measuring small-strain stiffness during both loading and unloading stress paths.

References

Aas, G. (1984). Stability problems in a deep excavation in clay. In *International conference on case histories in geotechnical engineering* (pp. 315–323). St. Louis.

Alén, C., & Jendeby, L. (1996). Hävning vid avschaktning – Ullevi, ett praktikfall. In *Nordic geotechnical meeting* (pp. 353–358). Reykjavik.

Alén, C., & Sällfors, G. (2001). *Utredning rörande svälltryck mot pålad bottenplatta [Investigation regarding heave pressure acting on piled foundation]*. Göteborg: Swedish Transport Administration (Vägverket).

Amavasai, A., Gras, J. P., Sivasithamparam, N., Karstunen, M., & Dijkstra, J. (2017). Towards consistent numerical analyses of embankments on soft soils. *European Journal of Environmental and Civil Engineering*, *8189*, 1–19

Amavasai, A., Sivasithamparam, N., Dijkstra, J., & Karstunen, M. (2018). Consistent Class A & C predictions of the Ballina test embankment. *Computers and Geotechnics*, *93*(2018), 75–86

Augustesen, A., Liingaard, M., & Lade, P. V. (2004). Evaluation of time-dependent behavior of soils. *International Journal of Geomechanics*, *4*(3), 137–156.

BAT. (2020). BAT Groundwater Monitoring System. Retrieved March 10, 2020, from https://www.bat.eu/en-GB

Bear, J., & Verruijt, A. (1987). *Modeling Groundwater Flow and Pollution*

Benz, T. (2007). *Small-strain stiffness of soils and its numerical consequences* (PhD thesis, Universität Stuttgart, Stuttgart).

Benz, T., Berengo, V., Simonini, P., & Leoni, M. (2013). Back analysis of Treporti test embankment with a time dependent small strain stiffness constitutive model. *Springer Series in Geomechanics and Geoengineering*, 89–96.

Bergström, A. (2017). *In-situ testing of floating thermal piles in soft sensitive clay* (Licentiate thesis, Chalmers University of Technology, Gothenburg).

Berntson, J. A. (1983). *Portrycksvariationer i leror i Göteborgsregionen [Pore pressure variations in clays in the Gothenburg region]*. Linköping: Swedish Geotechnical Institute.

Berre, T., & Bjerrum, L. (1973). Shear strength of normally consolidated clays. In *8th international conference on soil mechanics and foundation engineering* (pp. 39–49)

Bertoldo, F., & Callisto, L. (2016). Effect of Consolidation on the Behaviour of Excavations in Fine-grained Soils. *Procedia Engineering*, *158*, 344–349

Biot, M. A. (1941). General theory of three-dimensional consolidation. *Journal of Applied Research*, *12*(2), 155–164.

Biot, M. A. (1955). Theory of Elasticity and Consolidation for a Porous Anisotropic Solid. *Journal of Applied Physics*, *26*(2), 182–185.

Bjerrum, L. (1967). Engineering geology of Norwegian normally-consolidated marine clays as related to settlements of buildings. *Géotechnique*, *17*, 81–118.

Bjerrum, L. (1969). Effect of strain rate on undrained shear strength of soft clays. In *7th international conference soil mechanics and foundation engineering*, Mexico City.

Bjerrum, L. (1973). Problems of soil mechanics and construction on structurally unstable and weak soils. In *8th international conference on soil mechanics and foundation engineering* (pp. 1111–1159). Moscow.

Bjerrum, L., & Andersen, K. H. (1972). In-situ measurement of lateral pressures in clay. In *Fifth european conference on soil mechanics and foundation engineering* (pp. 11–20). Madrid.

Bjerrum, L., & Eide, O. (1956). Stability of strutted excavations in clay. *Géotechnique*, *6*(1), 32–47.

Bjerrum, L., & Holmberg, S. (1971). *Preliminary report on long term consolidation tests with measurements of horizontal stresses on the soft Bangkok Clay*. NGI. Oslo.

Björk-Tocaj, C., & Toller, E. (2017). *Pressure Caused by Restrained Heave* (MSc Thesis, Chalmers University of Technology, Gothenburg).

Brooker, E. W., & Ireland, H. O. (1965). Earth Pressures at Rest Related to Stress History. *Canadian Geotechnical Journal*, *2*(1), 1–15

Burland, J. B. (1990). On the compressibility and shear strength of natural clays. *Géotechnique*, *40*(3), 329–378.

Burland, J. B., & Karla, J. C. (1986). Queen Elizabeth II Conference Centre: geotechnical aspects. *Proceedings of the Institution of Civil Engineers*, *80*(Dec.), 1479–1503.

Callisto, L., & Calabresi, G. (1998). Mechanical behaviour of a natural soft clay. *Géotechnique*, *48*(4), 495–513

Callisto, L., Maltese, F., & Bertoldo, F. (2014). Design of deep excavations in fine-grained soils accounting for changes in pore water pressures. In *8th international symposium on geotechnical aspects of underground construction in soft ground.*

Carder, D. R., & Darley, P. (1998). *The long term performance of embedded retaining walls*. Transport Research Laboratory. Crowthorne.

Chan, D., & Madabhushi, G. (2017). Designing urban deep basements in South East England for future ground movement: Progress and opportunities for experimental simulation of long- term heave. *International Symposia for next generation infrastructure*, 1–10.

Chang, M. F., Moh, Z. C., Liu, H. H., & Viranuvut, S. (1977). A method for determining the in situ K0 coefficient. In *Proceedings of the 10th international conference on soil mechanics and foundation engineering.* (pp. 61–64). Tokyo.

Chen, R. P., Li, Z. C., Chen, Y. M., Ou, C. Y., Hu, Q., & Rao, M. (2015). Failure investigation at a collapsed deep excavation in very sensitive organic soft clay. *Journal of Performance of Constructed Facilities*, *29*(3), 04014078–1—14.

Claesson, P. (2003). *Long term settlements in soft clays* (Doctoral dissertation, Chalmers University of Technology, Gothenburg).

Crawford, C. B. (1964). Interpretation of the consolidation test. *Journal of the Soil Mechanics and Foundations Division*, *90*(5), 87–102.

Daigle, L., & Zhao, J. Q. (2004). The influence of temperature on earth pressure cell readings. *Canadian Geotechnical Journal*, *41*(3), 551–559.

David Suits, L., Sheahan, T., & Talesnick, M. (2005). Measuring Soil Contact Pressure on a Solid Boundary and Quantifying Soil Arching. *Geotechnical Testing Journal*, *28*(2), 12484

DiBiagio, E., & Roti, J. A. (1972). Earth pressure measurements on a braced slurry-trench wall in soft clay. In *Fifth european conference on soil mechanics and foundation engineering* (pp. 51–59). Madrid.

Do, T.-N., Ou, C.-Y., & Chen, R.-P. (2016). A study of failure mechanisms of deep excavations in soft clay using the finite element method. *Computers and Geotechnics*, *73*(2016), 153–163

Eigenbrod, K. D. (1975). Analysis of the Pore Pressure Changes Following the Excavation of a Slope. *Canadian Geotechnical Journal*, *12*(3), 429–440

Faheem, H., Cai, F., & Ugai, K. (2004). Three-dimensional base stability of rectangular excavations in soft soils using FEM. In *Computers and geotechnics* (Vol. 31, *2*, pp. 67–74)

Fang, H.-Y. (Ed.). (1991). *Foundation Engineering Handbook* (2nd ed.)

Fossil Free Sweden. (2020). Roadmaps for fossil free competitiveness. Retrieved June 12, 2020, from http://fossilfritt-sverige.se/in-english/roadmaps-for-fossil-free-competitiveness/

Fredén, C., Samuelsson, L., Häger, K. O., Brusewitz, A. M., Cato, I., Fält, L.-M., & Miller, U. (1981). *Tuveskredet, geologi [The Tuve landslide, geology]*. Linköping: Swedish Geotechnical Institute.

Fredriksson, A., Kullingsjö, A., Ryner, A., & Stille, H. (2018). *Sponthandboken 2018*. Pålkommissionen.

Gaba, A. R., Simpson, B., Beadman, D. R., & Powrie, W. (2003). Embedded retaining walls: Guidance for economic design. *Proceedings of the Institution of Civil Engineers: Geotechnical Engineering*, *156*(1), 13–15.

Gaba, A., Hardy, S., Doughty, L., Powrie, W., & Selemetas, D. (2017). *Guidance on embedded retaining wall design*. London: CIRIA.

Gebreselassie, B. (2003). *Experimental , Analytical and Numerical Investigations of Excavations in Normally Consolidated Soft Soils* (PhD dissertation, Kassel, Kassel).

Goh, A. T. C. (1994). Estimating Basal-Heave Stability for Braced Excavations in Soft Clay. *Journal of Geotechnical Engineering*, *120*(8), 1430–1436

Gothenburg's history and heritage. (2020). Retrieved May 19, 2020, from https://www.goteborg.com/en/gothenburgs-history/

Graham, J., Crooks, J. H., & Bell, A. L. (1983). Time effects on the stress-strain behaviour of natural soft clays. *Geotechnique*, *33*(3), 327–340.

Graham, J., & Houlsby, G. T. (1983). Anisotropic elasticity of natural clay. *Géotechnique*, *33*(2), 165–180

Grammatikopoulou, A., Schroeder, F., Kovacevic, N., & Potts, D. M. (2015). Stiffness anisotropy and its effect on the behaviour of deep excavations. In *16th european conference on soil mechanics and geotechnical engineering* (pp. 3–7). Edinburgh.

Gras, J. P., Sivasithamparam, N., Karstunen, M., & Dijkstra, J. (2017). Strategy for consistent model parameter calibration for soft soils using multi-objective optimisation. *Computers and Geotechnics*, *90*(2017), 164–175

Gras, J. P., Sivasithamparam, N., Karstunen, M., & Dijkstra, J. (2018). Permissible range of model parameters for natural fine-grained materials. *Acta Geotechnica*, *13*(2), 387–398.

Grimstad, G., Degago, S. A., Nordal, S., & Karstunen, M. (2008). Modelling creep and rate effects using the time resistance concept in a model for anisotropy and destructuration. In *15th nordic geotechnical meeting* (pp. 195–202). Sandefjord.

Grimstad, G., Andresen, L., & Jostad, H. P. (2012). NGI-ADP: Anisotropic shear strength model for clay. *International Journal for Numerical and Analytical Methods in Geomechanics*, *36*(4), 483–497

Grimstad, G., Degago, S. A., Nordal, S., & Karstunen, M. (2010). Modeling creep and rate effects in structured anisotropic soft clays. *Acta Geotechnica*, *5*(1), 69–81

Grimstad, G., Haji Ashrafi, M. A., Degago, S. A., Emdal, A., & Nordal, S. (2016). Discussion of 'Soil creep effects on ground lateral deformation and pore water pressure under embankments'. *Geomechanics and Geoengineering*, *11*(1), 86–93

Grimstad, G., & Jostad, H. P. (2012). Stability analyses of quick clay using FEM and an anisotropic strain softening model with internal length scale. In *16th nordic geotechnical meeting*, Copenhagen.

Harlén, M., & Poplasen, G. (2019). *Excavation in soft clay - Class A prediction of excavation in central Gothenburg* (Master thesis, Chalmers University of Technology, Gothenburg).

Hashash, Y. M. A., & Whittle, A. J. (1996). Ground Movement Prediction for Deep Excavations in Soft Clay. *Journal of Geotechnical Engineering I June 1996 I 475*, *122*(6), 474–486

Hung, N. K., & Phienwej, N. (2016). Practice and experience in deep excavations in soft soil of Ho Chi Minh City, Vietnam. *KSCE Journal of Civil Engineering*, *20*(6), 2221–2234.

Huntley, S. A., & Valsangkar, A. J. (2016). Laboratory thermal calibration of contact pressure cells installed on integral bridge abutments. *Canadian Geotechnical Journal*, *53*(6), 1013–1025.

Ingram, P. (2012). Retaining walls as part of complete underground structure. In *Ice manual of geotechnical engineering* (Chap. 67, pp. 1031–1038).

Jaky. (1948). Pressure in silos. In *2nd international conference on soil mechanics and foundation engineering*, Rotterdam.

Jamiolkowski, M., Ladd, C. C., Germaine, J. T., & Lancellotta, R. (1985). New developments in field and laboratory testing of soils. In *Proc. 11th int. conference on soil mechanics and foundation engineering* (pp. 57–153).

Janbu, N. (1972). Earth pressure computations in theory and practice. In *Proc., 5th european conf. on soil mechanics and foundations engineering* (pp. 47–54). Madrid.

Janbu, N., Bjerrum, L., & Kjaernsli, B. (1956). *Veiledning ved løsning av fundamenteringsoppgaver*. NGI. Oslo.

Jendeby, L. (1986). *Friction piled foundations in soft clay - a study of load transfer and settlements* (Doctoral dissertation, Chalmers University of Technology, Gothenburg).

Karlsrud, K. (2012). *Prediction of load-displacement behaviour and capacity of axially loaded piles in clay based on analyses and interpretation of pile load test results* (Doctoral dissertation, NTNU, Trondheim).

Karlsrud, K., & Andresen, L. (2005). Loads on Braced Excavations in Soft Clay. *International Journal of Geomechanics*, *5*(2), 107–113

Karlsrud, K., & Andresen, L. (2008). Design and performance of deep excavations in soft clays. In *6th international conference on case histories in geotechnical engineering*, Arlington.

Karlsrud, K., & Hernandez-Martinez, F. G. (2013). Strength and deformation properties of Norwegian clays from laboratory tests on high-quality block samples. *Canadian Geotechnical Journal*, *50*(12), 1273–1293.

Karstunen, M., & Amavasai, A. (2017). *BEST SOIL: Soft soil modelling and parameter determination*. Chalmers University of Technology. Gothenburg.

Karstunen, M., Krenn, H., Wheeler, S. J., Koskinen, M., & Zentar, R. (2005). Effect of Anisotropy and Destructuration on the Behavior of Murro Test Embankment. *International Journal of Geomechanics*, *5*(2), 87–97

Kempfert, H.G. Gebresellassie, B. (1999). Effect of anchor installation on settlement of nearby structures in soft soils. In *International symposium on geotechnical aspects of underground construction in soft ground* (pp. 665–670).

Kulhawy, F. H., & Mayne, P. W. (1990). *Manual on Estimating Soil Properties for Foundation Design*. New York: Cornell University.

Kullingsjö, A. (2007). *Effects of deep excavations in soft clay on the immediate surroundings* (Phd thesis, Chalmers University of Technology, Gothenburg).

L'Heureux, J. S., Leroueil, S., & Laflamme, J. F. (2009). Evolution of the factor of safety following excavation in clay. *Canadian Geotechnical Journal*, *46*(5), 487–493.

Ladd, C. C. (1991). Stability Evaluation During Staged Construction. *Journal of Geotechnical Engineering*, *117*(4), 540–615.

Ladd, C. C., Foot, R., Ishihara, K., Schlosser, F., & Poulos, H. G. (1977). Stress-Deformation and Strength Characteristics. In *9th international conference on soil mechanics and foundation engineering*, Tokyo.

Lafleur, J., Silvestri, V., Asselin, R., & Soulié, M. (1988a). Behaviour of a test excavation in soft Champlain Sea clay. *Canadian Geotechnical Journal*, *25*(4), 705–715

Lafleur, J., Silvestri, V., Asselin, R., & Soulié, M. (1988b). Behaviour of a test excavation in soft Champlain Sea clay. *Canadian Geotechnical Journal*, *25*(4), 705–715

Lande, E., & Karlsrud, K. (2015). *Feltforsøk stagboring - Dokumentasjon av effekter ved boring i leire*. NGI. Oslo: BegrensSkade, Delrapport nr. 4.1.

Länsivaara, T. (1999). *A study of the mechanical behavior of soft clay* (Phd thesis, Norwegian University of Science and Technology, Trondheim).

Larsson, P.-G. (2018). *Geotechnical site investigation report*. Bohusgeo AB. Uddevalla: Bohusgeo AB.

Larsson, R. (1977). *Basic behaviour of Scandinavian soft clays* (tech. rep. No. 3). Swedish Geotechnical Institute. Linköping.

Larsson, R. (1980). Undrained shear strength in stability calculation of embankments and foundations on soft clays. *Canadian Geotechnical Journal*, *17*, 591–602.

Larsson, R. (1981). *Drained behaviour of Swedish clays*. Swedish Geotechnical Institute. Linköping.

Larsson, R. (1986). *Consolidation of soft soils*. Linköping: Swedish Geotechnical Institute.

Larsson, R. (2008). *Jords egenskaper [Properties of soil]*. Linköping: Swedish Geotechnical Institute.

Larsson, R. (2015). *CPT-sondering, utrustning – utförande – utvärdering [CPT-testing, equipment - execution - evaluation]*. Linköping: Swedish Geotechnical Institute.

Larsson, R., & Sällfors, G. (1981). Hypothetical yield envelope at stress rotation. In *10th international conference on soil mechanics and foundation engineering* (pp. 536–537).

Larsson, R., Sällfors, G., Bengtsson, P., Alén, C., Bergdahl, U., & Eriksson, L. (2007). *Skjuvhållfasthet - utvärdering i kohesionsjord [Shear strength - evaluation in cohesive soil]*. Linköping: Swedish Geotechnical Institute.

Leica. (2020). Leica Viva TS16 Total Station. Retrieved May 27, 2020, from https://leica-geosystems.com/products/total-stations/robotic-total-stations/leica-viva-ts16

Leoni, M., Karstunen, M., & Vermeer, P. A. (2008). Anisotropic creep model for soft soils. *Géotechnique*, *58*(3), 215–226. arXiv: 0812.0143v2

Leroueil, S. (2001). Natural slopes and cuts: Movement and failure mechanisms. *Géotechnique*, *51*(3), 197–243.

Leroueil, S., Bouclin, G., Tavenas, F., Bergeron, L., & La Rochelle, P. (1990). Permeability anisotropy of natural clays as a function of strain. *Canadian Geotechnical Journal*, *27*(5), 568–579.

Leroueil, S., & Hight, D. W. (2003). Behaviour and properties of natural soils and soft rocks. In *Characterization and engineering properties of natural soils* (1, pp. 29–254). Singapore.

Leroueil, S., Kabbaj, M., & Tavenas, F. (1988). Study of the validity of a stress-strain-strain rate model in in situ conditions. *Soils and Foundations*, *28*(3), 13–25.

Leroueil, S., Kabbaj, M., Tavenas, F., & Bouchard, R. (1985). Stress–strain–strain rate relation for the compressibility of sensitive natural clays. *Géotechnique*, *35*(2), 159–180.

Leroueil, S., & Tavenas, F. (1981). Pitfalls o f Back-Analyses. In *10th international conference on soil mechanics and foundation engineering*.

Leroueil, S., Tavenas, F., Samson, L., & Morin, P. (1983). Preconsolidation pressure of Champlain clays. Part II. Laboratory determination. *Canadian Geotechnical Journal*, *20*(4), 803–816.

Leroueil, S., & Vaughan, P. R. (1990). The general and congruent effects of structure in natural soils and weak rocks. *Geotechnique*, *40*(3), 467–488.

Lo, K. Y., & Morin, J. P. (1972). Strength Anisotropy and Time Effects of Two Sensitive Clays. *Canadian Geotechnical Journal*, *9*(3), 261–277

Long, M. (2001). Database for Retaining Wall and Ground Movements due to Deep Excavations. *Journal of Geotechnical and Geoenvironmental Engineering*, *127*(3), 203–224

Lunne, T., & Andersen, K. H. (2007). Soft Clay Shear Strength Parameters for Deepwater Geotechnical Design. *Proceedings 6th International Conference on Offshore Site Investigation and Geotechnics, OSIG, London UK*, (September), 11–13.

Magnus, R., Teh, C. I., & Lau, J. M. (2005). *Report on the incident at the MRT Circle Line worksite that led to the collapse of the Nicoll Highway on 20 April 2004*. Ministry of Manpower. Singapore.

Magnusson, O. (1975). *Deformationer i en schaktbotten av lera*. Statens råd för byggnads-forskning, Rapport R21:1975. Stockholm.

Massarsch, K. R. (1975). New Method for Measurement of Lateral Earth Pressure in Cohesive Soils. *Canadian Geotechnical Journal*, *12*(1), 142–146.

Mayne, P. W. (1982). K0 – OCR relationships in soil. *Journal of the Geotechnical Engineering Division*, 851–869.

Mayne, P. W. (2002). Flow Properties from Piezocone Dissipation Tests. Retrieved April 1, 2020, from http://geosystems.ce.gatech.edu/Faculty/Mayne/papers/PiezoDissipation.pdf

Mayne, P. W., & Swanson, P. G. (1981). The Critical-State Pore Pressure Parameter from Consolidated-Undrained Shear Tests. In *Laboratory shear strength of soil* (pp. 410–410–21)

McRostie, G. C., Morissette, L., & St-Louis, M. W. (1996). Bottom-heave control of a deep sensitive clay excavation in Ottawa, Canada. *Canadian Geotechnical Journal*, *33*(6), 926–936

Mesri, G., & Castro, A. (1987). Cα/Cc Concept and K0 During Secondary Compression. *Journal of Geotechnical Engineering*, *113*(3), 230–247

Mesri, G., Feng, T., Ali, S., & Hayat, T. (1994). Permeability characteristics of soft clays. In *13th international conference on soil mechanics and foundation engineering* (pp. 187–192). New Delhi.

Muir Wood, D. (2004). *Geotechnical Modelling*. London: Spon Press.

Muir Wood, D. (2015). Analysis of consolidation with constant rate of displacement. *Canadian Geotechnical Journal*, *53*(5), 740–752.

O'Brien, A. S., Burland, J. B., & Chapman, T. (2012). Piles and Piled Rafts. In *Ice manual of geotechnical engineering* (Chap. 56, January 2012, pp. 853–885).

Olsson, M. (2013). *On rate-dependency of Gothenburg clay* (Phd thesis, Chalmers University of Technology, Gothenburg).

Peck, R. B. (1943). Earth-pressure measurements in open cuts, Chicago (Ill.) subway. *ASCE*, *108*, 1008–1036.

Peck, R. B. (1969). Deep excavations and tunneling in soft ground. In *Proceedings of the 7th international conference in soil mechanics and foundation engineering* (pp. 225–290). Mexico.

Persson, J. (2004). *The Unloading Modulus of Soft Clay: A Field and Laboratory Study* (Doctoral dissertation, Chalmers University of Technology, Gothenburg).

Petalas, A. L., Karlsson, M., & Karstunen, M. (2019). Modelling of undrained shearing of soft natural clays. *E3S Web of Conferences*, *92*, 15001

Price, G., & Wardle, I. F. (1986). Queen Elizabeth II Conference Centre: Monitoring of Load Sharing Between Piles and Raft. *Proceedings of the Institution of Civil Engineers*, *80*(Dec.), 1505–1518.

Rankine, W. J. M. (1857). On the Stability of Loose Earth. *Philosophical Transactions of the Royal Society of London*, *147*, 9–27.

Richards, D. J., Powrie, W., Roscoe, H., & Clark, J. (2007). Pore water pressure and horizontal stress changes measured during construction of a contiguous bored pile multi-propped retaining wall in Lower Cretaceous clays. *Géotechnique*, *57*(2), 197–205

Rowe, R. K. (Ed.). (2001). *Geotechnical and Geoenvironmental Engineering Handbook*

Ryner, A., Fredriksson, A., & Stille, H. (1996). *Sponthandboken - Handbok för konstruktion och utformning av sponter [Sheet piling handbook - Handbok for design of sheet pile walls]*.

Sahlström, P., & Stille, H. (1979). *Förankrade sponter*. Stockholm: Statens råd för byggnadsforskning.

Sällfors, G. (1975). *Preconsolidation pressure of soft, high-plastic clays* (Doctoral dissertation, Chalmers University of Technology, Gothenburg).

Sällfors, G. (2013). *Geoteknik – Jordmateriallära, jordmekanik* (5th ed.). Göteborg.

Sällfors, G., & Larsson, R. (2016). *Bestämningar av odränerad skjuvhållfasthet med specialiserade metoder i praktiska tillämpningar - Delrapport 3 - Sammanställning av Case records*. Gothenburg: Trafikverket.

Sällfors, G., & Larsson, R. (2017). *Rapport 1:2017. Metodik för bestämning av skjuvhållfasthet i lera [Report 1:2017 Methodology for determination of shear strength in clay]*. Linköping: Swedish Geotechnical Society.

Schmertmann, J. (1983). A simple question about consolidation. *Journal of Geotechnical Engineering, 109*(1), 119–122.

Schmertmann, J. (2012). *New concepts for the mobilization of the components of shear resistance in clay*. Oslo: NGI.

Schmidt, B. (1966). Earth Pressures at Rest Related to Stress History. *Canadian Geotechnical Journal, 3*(4), 239–242.

Schofield, M. A., & Wroth, C. P. (1968). *Critical State of Soil Mechanics*. London: McGraw-Hill.

Silvestri, V., Soulie, M., Touchan, Z., & Fay, B. (1988). Triaxial relaxation tests on a soft clay. In *Advanced triaxial testing of soil and rock* (pp. 321–337). Philadelphia.

Simpson, B. (2018). Effective heave pressures beneath restrained basement slabs. *Proceedings of the Institution of Civil Engineers - Geotechnical Engineering, 171*(1), 28–36

Simpson, B., & Vardanega, P. J. (2014). Results of monitoring at the British Library excavation. *Proceedings of the Institution of Civil Engineers - Geotechnical Engineering, 167*(GE2), 99–116

Sivasithamparam, N. (2012). *Modelling Creep Behaviour of Soft Soils*. PLAXIS B.V. & University of Strathclyde.

Sivasithamparam, N., Karstunen, M., & Bonnier, P. (2015). Modelling creep behaviour of anisotropic soft soils. *Computers and Geotechnics, 69*(2015), 46–57

Skempton, A. W. (1951). Bearing capacities of clays. In *Building research congress* (Vol. 1, pp. 180–189). London.

Skempton, A. W. (1954). The Pore-Pressure Coefficients A and B. *Géotechnique, 4*(4), 143–147

Skempton, A. W. (1984). Slope Stability of Cuttings in Brown London Clay. In *Selected papers on soil mechanics* (pp. 241–250)

Stille, H. (1976). *Behaviour of anchored sheet pile walls* (Phd Thesis, Royal Institute of Technology, Stockholm).

Svahn, P.-O., & Liedberg, S. (2001). *Väg 45 Götatunneln - Järntorget, entreprenad J2, PM Tråg/tunnel 1/160–1/350*. Skanska Sverige AB. Göteborg: Skanska Sverige AB.

Swedish Geotechnical Society. (1993). *Rekommenderad standard för vingförsök i fält. SGF Rapport 2:93*. SGF. Linköping: SGF.

Swedish Meteorological and Hydrological Institute. (2020a). Air temperature recordings. Station "Göteborg A". SMHI. Retrieved from https://www.smhi.se/data/meteorologi/ladda-ner-meteorologiska-observationer

Swedish Meteorological and Hydrological Institute. (2020b). Hydrologiska ord och begrepp. Retrieved June 22, 2020, from https://www.smhi.se/kunskapsbanken/hydrologiska-begrepp-1.29125

Tan, Y., & Wang, D. (2013). Characteristics of a Large-Scale Deep Foundation Pit Excavated by the Central-Island Technique in Shanghai Soft Clay. *Journal of Geotechnical and Geoenvironmental Engineering, 139*(11), 1894–1910.

Tavenas, F., Jean, P., Leblond, P., & Leroueil, S. (1983). The permeability of natural soft clays. Part II: Permeability characteristics. *Canadian Geotechnical Journal, 20*(4), 645–660

Tavenas, F., Leblond, P., Jean, P., & Leroueil, S. (1983). The permeability of natural soft clays. Part I: Methods of laboratory measurement. *Canadian Geotechnical Journal, 20*(4), 629–644

Tavenas, F., & Leroueil, S. (1977). Effects of Stresses and Time on Yielding of Clays. In *9th international conference on soil mechanics and foundation engineering (tokyo)*.

Taylor, D. (1948). *Fundamentals of Soil Mechanics*.

Terzaghi, K. (1936). A fundamental fallacy in earth pressure computations. *Boston Society Civil Engineers Journal, 23*, 71–88.

Terzaghi, K. (1943). *Theoretical soil mechanics*

Terzaghi, K., & Peck, R. B. (1967). *Soil mechanics in engineering practice* (2nd ed.). New York: John Wiley & Sons.

Terzaghi, K., Peck, R. B., & Mesri, G. (1996). *Soil mechanics in engineering practice* (3rd ed.). New York: John Wiley & Sons.

Tesarik, D., Seymour, J., Williams, T., Martin, L., & Jones, F. (n.d.). *Temperature corrections to earth pressure cells embedded in cemented backfill*. National Institute for Occupational Safety and Health. Cincinnati.

Tong, L., Liu, L., Cai, G., & Du, G. (2013). Assessing the coefficient of the earth pressure at rest from shear wave velocity and electrical resistivity measurements. *Engineering Geology, 163*, 122–131

Tornborg, J. (2017). *Svälltryck på grund av avlastning i lös lera [Heave pressure due to unloading in soft clay]*. Skanska Teknik. Göteborg: Development Fund of the Swedish Construction Industry (SBUF).

Tornborg, J., Karlsson, M., & Karstunen, M. (2019). Benchmarking of a contemporary soil model for simulation of deep excavations in soft clay. In *17th european conference on soil mechanics and geotechnical engineering*.

Torstensson, B. (1973). *Friction piles in soft clay - A field-research on model piles* (Phd thesis, Chalmers University of Technology, Gothenburg).

Trafikverket. (2014). Trafikverkets tekniska krav för geokonstruktioner, TK Geo 13, ver 1.0.

Trafikverket. (2016a). Krav Brobyggande, ver 3.0.

Trafikverket. (2016b). Krav Tunnelbyggande, ver.1.0.

Trafikverket. (2016c). Trafikverkets tekniska råd för geokonstruktioner, TR Geo 13, ver 2.0.

Tschebotarioff, G. P. (1951). *Soil Mechanics, Foundations, and Earth Structures* (1st ed.). New York: McGraw-Hill.

UN. (2020). Sustainable Development Goals, Knowledge Platform. Retrieved May 13, 2020, from https://sustainabledevelopment.un.org/topics/sustainabletransport

Vermeer, P., & Neher, H. (1999). A soft soil model that accounts for creep. *In Proceedings of the international symposium "Beyond 2000 in Computational Geotechnics*, 249–261.

Wang, J. H., Xu, Z. H., & Wang, W. D. (2010). Wall and ground movements due to deep excavations in Shanghai soft soils. *Journal of Geotechnical and Geoenvironmental Engineering*, *136*(7), 985–994.

Watabe, Y., Tanaka, M., Tanaka, H., & Tsuchida, T. (2003). K0-consolidation in a triaxial cell and evaluation of in-situ K0 for marine clays with various characteristics. *Soils and Foundations*, *43*(1), 1–20

Westerberg, B. (1999). *Behaviour and Modelling of a Natural Soft Clay* (Doctoral dissertation, Luleå University of Technology, Luleå).

Wheeler, S. J., Näätänen, A., Karstunen, M., & Lojander, M. (2003). An anisotropic elastoplastic model for soft clays. *Canadian Geotechnical Journal*, *40*(2), 403–418

Wood, D. M. (1990). *Soil behaviour and critical state soil mechanics*. Cambridge university press.

Wood, D. M. (2018). Soil modelling (BA8304) - lecture notes. (Chap. Elasticity). Trondheim: NTNU.

Wood, T. (2014). *RegionCity. Phase 3 – Site Characterization and Sensitivity Analysis*. Gothenburg: Chalmers University of Technology.

Wood, T. (2016). *On the small strain stiffness of some Scandinavian soft clays and impact on deep excavations* (Phd thesis, Chalmers University of Technology, Gothenburg).

Zhou, C., Yin, J.-h., Zhu, J.-g., & Cheng, C.-m. (2005). Elastic Anisotropic Viscoplastic Modeling of the Strain-Rate-Dependent Stress–Strain Behavior of K0 -Consolidated Natural Marine Clays in Triaxial Shear Tests. *International Journal of Geomechanics*, *5*(3), 218–232

Züblin. (2015a). *ED1 - Marieholm Tunnel. Geotechnical interpretative report*. Gothenburg: Trafikverket.

Züblin. (2015b). *ED1 - Marieholmstunneln. Försöksrapport - Geotekniska undersökningar [ED1 - Marieholm Tunnel. Report of geotechnical investigations]*. Gothenburg: Trafikverket.